Analysis of the Strength of Deformed Ice Features over Multiple Scales: A Comprehensive Experimental and Numerical Analysis

By

© Soroosh Afzali

A thesis submitted to the School of Graduate Studies

in partial fulfilment of the requirements for the degree of

Doctor of Philosophy Faculty of Engineering and Applied Science

Memorial University of Newfoundland

February 2023

St. John’s, Newfoundland and Labrador

EXTENDED ABSTRACT

Ice ridges are one of the key concerns for the design and operation of ships and structures in ice prone areas. Little information on the flexural behavior of ridges is available. This body of research aimed to develop, calibrate, and validate a numerical tool based on data gathered during the last eight years in the Development of Ice Ridge Keel Strength (DIRKS) and the Mechanics of Ice Rubble (MIR) projects in the Centre for Arctic Resource Development (CARD) to gain a better understanding of the failure mechanism and loads arising during flexural failure of ice ridge.

The flexural failure of an ice ridge is dependent on the failure of its consolidated layer and of its keel. This requires an understanding of not only the properties and modes of failure of these two layers but also the strength of the freeze-bonds between the submerged ice blocks of the keel. A new model for the 3D DEM modeling of ice was developed and implemented in an open-source codes WooDEM and LIGGGHTS. This ice model contains normal, shear, torsional, and flexural springs that operate between neighboring particles which are bonded or that overlap due to compressive stresses. Energy dissipation is accounted for using a hysteretic damping in WooDEM and viscous damping in LIGGGTHS.

This program of research aimed to link physics of underpinning ice bond formation to the flexural failure of ice ridges with engineering simulations tools. This can be used for full-scale applications of intent for engineering design. To this end, this program has been executed in four phases:

A testing method using a new apparatus was developed to examine the tensile strength of freeze-bonds under submerged, confined conditions. The experiments showed that the freeze-bonds exhibited brittle failure, with no degradation prior to failure. The tensile strength increased with

higher confinement pressure during freeze-bond formation. The strength of the freeze-bond decreased by increasing the submersion time from 2 minutes to 3 hours.

The second theme focused on the flexural failure of level ice and was based on in-situ experiments on side loaded ice beam specimen. The results of these tests were used to parameterize a discrete element model that simulates ice fracture under flexural loading. The simulations were carried out using the open-source DEM code WooDEM. Despite the limitations in simulating ice crushing behavior, the simulations captured the main features of beam failure reasonably well

Next, using the newly developed 3D DEM model in the LIGGGHTS code, the strength and failure behavior of ice rubble beams and freeze-bonds were investigated. Rubble specimens were generated and compacted, and bonds between blocks were introduced based on freeze-bond experiments. Simulations of medium-scale freshwater ice rubble punch tests were conducted, considering two types of block shapes. The simulations aligned with experimental results, with empirical block simulations providing a more accurate estimation of the failure force compared to cuboid block simulations.

The last research theme was the modeling of prismatic ice ridges composed of both a consolidated and a partially consolidated keel. Ice rubble blocks were created using spherical DEM particles and imported into the DEM domain with gravity and buoyancy forces. A simplified ice ridge, consisting of a rubble keel with a bonded consolidated layer on top, was modeled. From this study it was found that the freeze-bond strength between the rubble blocks has limited influence on the flexural failure of ice ridges when the keel to consolidated layer thickness ratio is less than around 7 and thickness of the consolidated layer is the main contributor to flexural strength. The DEM model introduced in this study can be used as a valuable tool to estimate the flexural load arising from the interaction of ice ridges and offshore structures in the ice prone area.

Key Words: Discrete Element Modelling, Numerical Modelling, Experiments, Flexural Failure, Tensile Failure, Ice Rubble, Freeze Bonds, Ice Ridges, Level ice, Consolidated Layer

ACKNOWLEDGEMENTS

I would like to express my heartfelt gratitude to my supervisors, Dr. Rocky Taylor and Dr. Robert Sarracino, for their invaluable guidance, unwavering support, and continuous encouragement throughout my thesis journey. Their expertise and insightful feedback greatly enriched my work. I also want to convey my sincere appreciation to Dr. Ian Turnbull for his valuable suggestions and discussions as a member of my supervisory committee.

I am also deeply thankful to my colleague and fellow researcher Dr. Marjan Boroojerdi whose collaboration in sharing her valuable test data and conducting the experiments significantly influenced the direction of my research. I would also like to extend my gratitude to Dr. Baafour Nyantekyi-Kwakye, the ENGI 9211 (Experimental Methods) class of Fall 2019, Mr. Lucas Reid, and the Technical Services department at Memorial University for their invaluable assistance and support in conducting the experiments.

I wish to express my gratitude for the financial assistance provided by the School of Graduate Studies at Memorial University, InnovateNL, Mitacs, the Natural Sciences and Engineering Research Council (NSERC), and Hibernia Management and Development Company Ltd. (HMDC), which enabled the realization of this research.

My deepest appreciation goes to my parents for their unending love, encouragement, and sacrifices. Their unwavering belief in my potential has been the driving force behind my accomplishments.

Lastly, I extend my thanks to all my friends and family members who supported me during this academic pursuit. Your encouragement and positivity were invaluable in keeping me motivated and focused.

TABLE OF CONTENTS

LIST OF FIGURES

LIST OF TABLES

NOMENCLATURE

A	area $[m^2]$
$breakN$	tensile strain to breakage []
C	specific heat capacity $[J.K^{-1}.Kg^{-1}]$
c	cohesion $[Pa]$
$°C$	degree Celsius
cm	centimeters
D	particle diameter $[m, cm]$
distFactor	maximum relative particle separation []
E	elastic modulus $[Pa, GPa]$
F_n	normal force $[N]$
F_t	shear force $[N]$
F_{ij}	bond force between particles i and j $[N]$
h	hour(s)
H_s	sail height $[m]$
k_n	normal spring stiffness $[N/m^{-1}]$
k_t	tangential spring stiffness $[N.m^{-1}]$
K_w	twist spring stiffnesses $[N.m^3]$
K_r	bending spring stiffnesses $[N.m^3]$
l,w,h	length, width, height $[m]$
L	freezing fusion capacity $[J.Kg^{-1}]$
min	minutes(s)
n	normal

$\hat{n}_{ij}$	unit vector from the center of particle *i* to the center of particle *j*
P	load $[N]$
p_c	normal confinement pressure $[Pa]$
r	particle radius $[m, cm]$
R_{LL}	ridge line load $[N.m^{-1}]$
S	salinity $[ppt]$
t	tangential
$\hat{t}_{ij}$	unit normal to $\hat{n}_{ij}$
T	temperature [°C]
T_n	normal torque $[N.m]$
T_t	tangential torque $[N.m]$
T_w	twist torque $[N.m]$
T_r	bending torque $[N.m]$
u_n	normal displacement $[m, cm]$
u_t	shear displacement $[m, cm]$
u_ϕ	angle of twist $[degrees]$
u_θ	angle of bending $[degrees]$
V	volume $[m^3]$
Z	section modulus $[m^3]$

Greek Symbols

β	shear strength to tensile strength
δn_{ij}	normal overlap $[m, cm]$
δt_{ij}	tangential overlap $[m, cm]$
γ_n	normal damping coefficient []
γ_t	tangential damping coefficient []
$v_{n_{ij}}$	normal relative velocity $[m.s^{-1}]$
$v_{t_{ij}}$	tangential relative velocity $[m.s^{-1}]$
ω	angular velocity $[radians.s^{-1}]$
ν	Poisson ratio []
v_b	brine volume $[m^3]$
σ	confinement pressure $[Pa]$
σ_f	flexural strength $[Pa]$
σ_N	normal stress $[Pa]$
σ_T	tensile strength $[Pa]$
ρ	density $[kg.m^{-3}]$
τ	shear stress/strength $[Pa]$
θ	temperature [℃]
ϕ	friction angle []
α	damping coefficient $[N.s.m^{-1}]$
Δr_{ij}	normal overlap $[m, cm]$
Δt_{ij}	tangential overlap $[m, cm]$

Δt	time-step $[s]$

1. INTRODUCTION

1.1. General Introduction

The most common form of sea ice failure in nature is in creation of pressure ridges. The failure of ice against natural and human-made obstacles shows that sea ice tends to fail out of plan, rather than crushing, and form ice rubble. Therefore, as one of the most common ice features in ice prone environments, ice ridges are a key consideration in design (Leppäranta, 2011). In many areas like the west coast of Newfoundland, first-year ridges are an essential consideration in the design load for interaction with offshore structures. In the Baltic Sea, about one-third of the total ice mass consists of ice ridges causing difficulties to operations in the area (Leppäranta and Hakala, 1992). They are also known for being a significant concern for shipping in ice-covered areas. Ice ridges can also scour to the seafloor and are a potential hazard for subsea piping. The internal structure and mechanical behavior of the ice ridges are, however, not well known (Palmer and Croasdale, 2013).

For interactions with sloping structures or ice-class vessels, interactions with the higher and more consolidated layers of ridge keels are of particular interest. As has been discussed by Shayanfar *et al.* (2018), as the strength of the bonds between individual rubble block increases, such regions of a keel tend to behave more like a brittle porous solid and are more prone to fail in flexure rather than shear. The flexural failure of rubble is complex and is highly affected by the shear strength, tensile strength, and compressive strength of the ice blocks and the bonds between them (Mohammadafzali *et al.*, 2016). The availability of direct flexural tests on ice rubble are very limited, and the flexural strength of rubble is often estimated by analytical approaches, such as Mohr Coulomb theory.

Recent studies carried out by the Development of Ice Ridge Keel Strength (DIRKS) and the Mechanics of Ice Rubble (MIR) projects in the Centre for Arctic Resource Development (CARD) provided a unique opportunity to gain a deeper and more accurate insight to the failure of ice rubble. Bailey *et al.* (2015) investigated the change of rubble blocks properties over time and the process of formation of freeze-bond and sintering between ice blocks. Shayanfar (2017) carried out a series of punch box rubble failure experiments under various submersion times, confinement pressures, and initial ice temperatures. These factors were found to highly influence the strength of the freeze-bonds formed between the ice blocks and as a result, change the strength and failure mechanism of the rubble beam. To gain a better understanding of the failure of ice rubble, one needs to account for the effects of the freeze-bonding between the ice blocks (Ettema and Urroz-Aguirre, 1991; Serré *et al.*, 2011; Boroojerdi *et al.*, 2016; Shayanfar *et al.*, 2018). Bailey *et al.* (2012) studied the bond strength formed between pieces of rafted ice and reported two mechanisms of bonding: thermodynamic bonding (weaker) and mechanical bonding (stronger). Boroojerdi *et al.* (2016, 2019b, 2019a) studied the effects of confinement pressure, submersion time, and indentation rate on the shear strength of freeze-bonds.

This study aimed to develop, calibrate, and validate a numerical tool based on data gathered during the last eight years in the DIRKS and MIR projects to gain a better understanding of the failure mechanism and loads arising during flexural failure of ice rubble and ice ridge. To achieve this goal, first the tensile strength of the freeze-bonds as a parameter that significantly affect the flexural failure of ice rubble was investigated. Subsequently, a recently developed Discrete Element Model (DEM) was utilized to simulate the flexural failure of sea ice and ice rubble. These simulations were based on existing data, serving to calibrate and validate the DEM model. Next,

this calibrated model was used to simulate the flexural failure of ice ridge composed of a layer of sea ice (consolidated layer) and a layer of ice rubble (ridge keel).

1.2. Objectives and Scope of Research

In this study, the flexural failure of ice ridges was investigated using a newly developed DEM model. This investigation has been performed in four major phases.

In the first phase, the tensile strength of freshwater freeze-bond was experimentally investigated as a function of confinement pressure and submersion time. Dumbbell-shaped samples of polycrystalline freshwater ice were bonded under submerged confined conditions, and their tensile strength was examined using a newly developed apparatus designed by the author.

The data was then used to aid in the development of the DEM model of ice rubble. The ice model was developed by researchers at C-CORE and implemented into WOODEM and LIGGGHTS DEM codes by the author and other researchers; see Section 1.2.2. This new ice model contains normal, shear, torsional, and flexural springs that operate between neighboring particles that overlap due to compressive stresses or which are bonded. This DEM model was used for simulating the failure of level ice, ice rubble, and ice ridge is described in Section 1.2.2.

The next phase of this study explores the flexural failure of sea ice through DEM simulations, aligning with applications from rubble formation to modeling ice sheet bending against structures. Using in-situ experiments near Storfjorden, Svalbard, the study reproduces load-displacement curve features by adjusting six key parameters. The simulations replicate loading conditions, employing low and high-resolution setups, see Section 1.2.3.

The study then employs DEM simulations to assess the flexural failure of ice rubble based on experiments by Shayanfar (2017). First, cuboid ice blocks were generated, considering size distributions of the experimental block, and contact pressure were calculated analytically. Simulations then used measured block parameters, and a custom MATLAB code to generate DEM rubble blocks. Comparison between the results of these types simulation shows a clear advantage of using imperial blocks.

In the final research phase, the study focused on simulating ice ridge flexural failure using DEM. Investigating bond strength and layer thickness, models for consolidated layers, ice rubble, and freeze-bonds were developed based on experimental data. The simulations in LIGGGHTS comprised a two-layer ice beam representing ridges. The study monitored loads, freeze-bond and solid ice particle failures, and ridge deformation mechanisms during failure, see Section 1.2.5.

In this section more details on the methodology used for each phase and objectives of the study are introduced.

1.2.1. Tensile Strength of Freeze-Bond

The strength of freeze-bonds between ice blocks has been found to significantly affect the strength and failure mechanism of ice rubble and ice ridges (Liferov et al. (2002), Croasdale (2012), Polojärvi and Tukhuri (2013b), Shayanfar (2017), Shayanfar et al. (2018, 2022)). Limited information on the tensile strength of freeze-bond is available at this time. Murdza et al. (2021) conducted four-point bending tests to evaluate flexural strength of freeze-bonds formed between rectangular ice blocks in air. Szabo and Schneebeli (2007) examined bonds formed between micro conical ice samples in sub-second sintering, highlighting freezing of water layer as the main sintering mechanism. The proposed research, studies the bonds formed between ice blocks in submerged condition in a confining pressure range relevant to first-year ice ridges. More details

on the available data on tensile strength of freeze-bonds and the approach of this research can be found in Sections 2.4 and 3.3.

A testing method, as discussed in Section 3.4, has been developed to examine the tensile strength of freeze-bond. A new apparatus was designed and manufactured to conduct the experiments, see Figure 3-2. The mounting system for the apparatus was based on Hawkes and Mellor (1972). However, the inside of the two aluminum end caps were lathed dumbbell shape to minimize the stress concentration around the circumference and in the transition zone (from caps to the gauge).

A Data Acquisition System (DAQ) was used to measure the physical conditions of the experiments and convert the results to digital values that were subsequently analyzed. The components of the DAQ system used in these experiments included the acquisition hardware, Resistance Temperature Detectors (RTD), load cells, and a high-speed camera, which were configured by the Material Testing System (MTS) hydraulic testing apparatus.

The samples used in this study were made of unseeded polycrystalline freshwater ice, frozen at -18°C for a week. The freeze-bonds were formed under confinement and the samples were submerged at freezing temperature, experiments have been conducted at 0°C.

A total of 30 tensile experiments has been conducted to investigate the effect of confinement pressure and submersion time on the tensile strength of freshwater freeze-bond. The formation of the freeze-bonds was under the nominal confinement pressures of 25kPa, 50kPa, 75kPa, and 100kPa, and 5 minutes to 3 hours of submersion time, all at deformation rate of 5mm/s. Experiments were repeated three times to ensure repeatability of the experiments and to reduce the uncertainty of the results. Table 3-1 shows the conditions and strength results for these experiments.

The strength results show a linear relationship between the confinement pressure (σ) during the formation of the freeze-bond and the tensile strength (S) of the freeze-bond in both cases of 0.5 hours and 3 hours submersion. The average tensile strength, however, is 21.4% lower for the submersion time of 3 hours.

The main objective of this work was to investigate the effect of confinement pressure and submersion time on the tensile strength of the unseeded polycrystalline freshwater freeze-bond. To the authors' knowledge, these test results are the first set of uniaxial tensile freeze-bond strength data reported in the literature. These fill an important knowledge and data gaps in ice freeze-bond properties. This information was needed to advance understanding of ice freeze-bond behavior, as well as to aid in the development of numerical models of ice rubble behavior for which freeze-bonds tensile strength is an important model parameter. Details of the experimental procedure and the results are presented in Chapter 3 and has been published in the Journal of Cold Regions Science and Technology under the title "Experimental Investigation on the Tensile Strength of Freshwater Freeze-Bonds"

1.2.2. Development of the DEM Model

The Discrete Element Method (DEM) has had wide success in modelling granular materials and brittle solids, the former through the application of frictional interaction between adjacent particles, and the latter by adding bonds between adjacent particles. By giving the bonds resistance to normal, shear and torsional stresses, and by allowing bonds to fail under tensile, shear and torsional overloading, DEM is well-suited to modelling the initiation and propagation of fractures, as well as post-fracture material response for solid materials. DEM has had wide use in modelling ice and ice-structure interactions for ice rubble and ice ridges.

Numerous DEM models have been employed to understand ice mechanical behavior. Løset (1994a, 1994b) introduced a 2D circular particle-based model for ice failure analysis, considering air drag and Coriolis forces. Paavilainen et al. (2009), Polojärvi and Tuhkuri (2013a, 2013b), and others adopted 2D FEM DEM models to study sea ice fracture against structures, accounting for element elasticity. Lishman and Polojärvi (2015) studied ice-ice friction rate dependency. Lilja (2021) proposed a finite-discrete element hybrid model for sea ice fracture. Berg and Lubbad (2015) used non-smooth DEM for ice rubble. Prasanna and Polojärvi (2023) introduced a particle breakage model enhancing DEM simulations of non-spherical particles' shear failure behavior. A detailed review of the utilization of DEM in ice mechanics applications is available in the next chapters of the thesis.

In this work, a new material model that was developed by researchers at C-CORE, was implemented for the 3D DEM open-source codes WooDEM and LIGGGHTS (please refer to Section 1.3 for more details); this model is also described in the WooDEM documentation. This new ice model contains normal, shear, torsional, and flexural springs that operate between neighboring particles that overlap due to compressive stresses or which are bonded, Figure 1-1 demonstrates the direction of the bonds and springs operating between the particles. The spring stiffnesses can be set independently, but in these simulations, a linearly elastic, isotropic material and corresponding set of relative spring stiffnesses was assumed. In this model, neighboring bonded particles will behave as an ‘equivalent beam’ under tensile, compressive or shear stresses, or flexural or torsional moments.

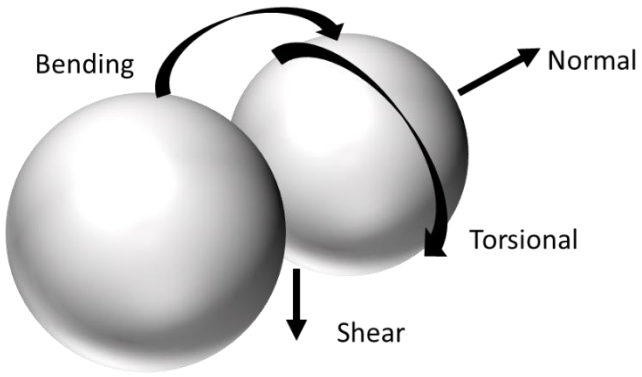

Figure 1-1 Direction of bonds and springs operating between DEM particles

In this DEM model, two spheres can be bonded through any combination of normal, shear, torsional or flexural bonds. When bonds are broken, tensile forces between particles vanish, and the yield values in shear, torsion or flexure between overlapping particles apply. When forces or torques exceed the failure limits, perfectly plastic behavior is assumed, and the forces and torques are limited to the yield values. The model implimentaion in WooDEM uses hysteretic damping rather than viscous damping (see, e.g., Potyondy and Cundall, 2004). That is, particles lose a proportion of their kinetic energy per cycle. Full details of this numerical model including the numerical integration method and formulations can be found in Section 4.6 and Section 5.4

1.2.3. DEM Simulation of the Flexural Failure of Level Ice

An important step in the DEM analysis was an investigation of the flexural failure of ice. Flexural failure of sea ice is of interest in many different applications, ranging from understanding rubble formation processes to modeling bending failure of ice sheets against sloped structures and ship hulls. The top layer of an ice ridge is formed of consolidated pieces of rubble which behaves similarly to a level ice sheet, highlighting the importance of this analysis and calibrating this model for this type of failure.

DEM simulations for this analysis were based on in-situ experiments carried out on side-loaded sea ice beam specimens on the ice fields near Storfjorden, Svalbard, see Section 4.5 for details. The particular experiment modeled in these simulations featured an ice beam of dimensions 2.5 m (length), 0.50 m (width), and 0.55 m (ice depth), loaded to failure by a cylindrical steel platen of diameter 15 cm at a velocity of 1 mm/s. Details of these beam tests may be found in Oshaug et al. (2014).

In this study, there are three main features of the load-displacement curve were aimed to reproduce: the slope of the initial load rise, the peak load, and the displacement between the load peak and immediate post-peak behavior.

Six parameters in the model were found to influence this behavior: E and ν, Young's modulus and Poisson's ratio, respectively; the two strength parameters, i.e., tensile strain to breakage ($\epsilon_b . or\ breakN$) and the ratio of shear strength to tensile strength β; the damping constant α; and the value of the maximum relative particle separation, which in set-up between neighboring particles bonded during the formation phase of the DEM material (distFactor). The slope of the linearly elastic section of the load-displacement curve is determined primarily by the two elastic constants, although, since the aggregate slope up to the load peak is used to determine the effective Young modulus, parameter values affecting bond strength also play a minor role. The load peak and post-peak load decay were found to be influenced by the other four parameters as well, with breakN playing a predominant role.

To simulate the loading conditions used in the field, a vertical cylindrical rod (the platen) was advanced at a constant speed through the mid-point of the ice beam of effective length 2.5 m, width 0.5 m, and vertical height 0.55 m. The DEM beam consisted of a bonded aggregate of spherical particles. The physics engine maintained the platen velocity at a constant value, causing a build-

up of force that eventually causes failure and breakage of the beam. A sample of the simulation setup can be found in Figure 4-4.

In this study, a total of seventy-five low-resolution (1,200 particles) and twelve high-resolution (13,000 particles) simulations were conducted. The overall strategy was to use the low-resolution simulations for the initial phase of the parametric study since this configuration allowed for decreased run-time. In the final phase of the study, a higher resolution 13,000 particle configuration was used to give a more representative, 'smoother' failure process, which was used in the assessment of more refined model parameters. The results of these simulations are presented in Chapter 4 and has been published in the Proceedings of Offshore Technology Conference under the title "Investigation and 3D Discrete Element Modeling of Fracture of Sea Ice Beams".

1.2.4. DEM Simulation of Flexural Failure of Ice Rubble

To examine the capability of DEM in simulating the flexural failure of ice rubble and assess the effect of simulation parameters of the behavior of rubble, a series of simulations based on selected experiments of Shayanfar (2017) were carried out, see Figure 5-6. In this analysis, cuboid ice blocks were first considered and were generated based on the size distribution of the reported rubble beam experiments. for this study the contact pressure between the ice blocks were calculated analytically, details of calculation can be found in Section 5.6.2. Next, simulations were conducted using block size and shape distributions that were based on measured size and area of individual ice blocks extracted from image analysis of pictures of the blocks, which were taken before assembling the ice rubble beams in the experiments, see Section 5.6.3. A custom MATLAB code was written to generate DEM rubble blocks using the shape and size parameters extracted from the image data. In this analysis the contact pressure between the blocks was estimated numerically.

To form an ice rubble beam, these blocks were then rained into a “former” to generate a beam with randomly oriented blocks having the appropriate dimensions. These ice rubble features were then exported to an open-source DEM code WOODEM, to allow for extraction of details of the block-block contact pressures to model the relationship between average applied pressure and average contact pressure between blocks when subjected to hydrostatic pressure.

In this analysis the freeze-bond strength values were set based on Boroojerdi *et al.*, (2019b) and other DEM parameter values were set based on the freeze-bond calibration simulations. To represent the end conditions in the experiments, the two ends of the rubble were fixed to the ends of the box. The indenter plate was then added to the simulation at the mid-point of the rubble beam to allow for simulate loading of the beam until the flexural failure of the rubble beam occurred.

The loads on the platen, between the ice blocks, and on the freeze-bonds were output from the simulations and found to give excellent agreement with the experimental results. Based on these observation, the mode and location of the failure was also identified and compared with the experimental results. The results of these simulations are presented in Chapter 5 of this thesis and has been published in the Journal of Offshore Mechanics and Arctic Engineering under the title “Investigation of the Effect of Block Size, Shape and Freeze Bond Strength on Flexural Failure of Freshwater Ice Rubble Using the Discrete Element Method”.

1.2.5. DEM Simulation of Flexural Failure of Medium Scale Ice Ridges

The last phase of this research focused on the simulation of the flexural failure of an ice ridge using the DEM model. The main purpose of this study was to investigate the effect of bond strength and consolidated layer and ridge keel thickness on the flexural behavior of ice ridges, drawing on the results of the earlier work in this body of research. In this work, the consolidated layer, ice rubble, and freeze-bond models were developed based on experimental data.

The mathematical model used in the DEM simulations of ice ridges, were based on those developed in earlier phase of this work, in the ice were modeled using bonded spherical particles. This mathematical model was implemented in the Open Source DEM Particle Simulation Software, LIGGGHTS, to simulate ice ridges composed of a solid layer of the waterline, representing the consolidated layer, and an assembly of bonded ice blocks, representing the keel.

The consolidated layers of the beam were formed based on the calibrated model of level ice described in Chapter 3. The rubble keels were formed of empirical ice blocks introduced in Chapter 4. The DEM parameters for both layers were based on the properties of unseeded polycrystalline freshwater ice. The bottom layer of the consolidated layers was bonded to the top layer of the rubble to form a single composite beam, representing ice ridges, as shown in Figure 6-3. The ice rubble blocks, made of spherical DEM particles, were generated by a costume MATLAB code and imported to the DEM domain under gravity and buoyancy forces. The consolidated layer was then bonded on the top to create a simplified model of ice ridges as a two-layer ice beam.

The ridge beam underwent the same flexural load that is used to fail the rubble beam in the previous section. The loads on the indenter and ice blocks, the failure of the freeze-bonds and the bonds between the solid ice particles, and the deformation mechanism of the ridge during failure were monitored. Details of the numerical simulations and the results of the study are presented in Chapter 5 are submitted for publication in the Journal of Offshore Mechanics and Arctic Engineering under the title “Discrete Element Modeling of Flexural Failure of Medium Scale Ice Ridges”.

1.3. Summary of Novel Contributions

This section outlines what the author feels to be original insights that push the boundaries of knowledge in the field of Ice Mechanics, bridge existing knowledge with innovative pathways of investigation, and offer fresh perspectives for future exploration.

Various studies have explored the significance of freeze-bond tensile strength in the context of ice rubble behavior and failure. Finite element models by Liferov et al. (2002), Croasdale (2012), and Polojärvi and Tukhuri (2013) and ice rubble beam experiments by Shayanfar (2017), and Shayanfar et al. (2018, 2022) have shown that tension in freeze-bonds plays a critical role in ice rubble failure. Szabo and Schneebeli (2007) examined the tensile strength of bonds formed between micro conical ice samples crafted from degassed clear mountain water, utilizing a standard uniaxial test. Murdza et al. (2021) conducted four-point bending tests on freeze-bonds formed between freshwater ice blocks to measure bond flexural strength.

This study introduces a novel method and apparatus design for creating freeze-bonds between submerged freshwater ice blocks. Subsequent testing of the uniaxial tensile strength of these freeze-bonds yields new experimental data—the first of its kind in existing literature—aimed at addressing significant gaps in our understanding of ice freeze-bond properties. This data is vital for enhancing knowledge of ice freeze-bond behavior and helps the development of numerical models for ice rubble behavior, where freeze-bond tensile strength plays a crucial role.

The Discrete Element Method (DEM), introduced by Cundall and Strack (1979) and subsequently utilized and developed by a number of researchers in the decades since, has proven effective in modeling both granular materials and brittle solids. It accomplishes this by simulating frictional interactions for granular materials and incorporating bonds for brittle solids. These bonds, resistant to various stresses and capable of failing, allow DEM to accurately depict fracture initiation,

propagation, and post-fracture material behavior, making it suitable for ice and ice-structure interaction modeling. In this body of research, a comprehensive material model in DEM was developed and utilized that included springs, bonds, and damping mechanisms – specifically, for damping, a simple hysteritic model and a simple viscous damping model. This work builds on the work of Smilaur (2010), Kloss *et al*. (2012) with contact models further developed and tested at C-CORE by Sarracino, Morgan and the author (see, e.g., Chapter 6 for the latter).

The author was responsible for implementing the bending and torsional components of the model in the LIGGGHTS, modifying normal and shear components of the LIGGGTHS cohesion model to match with ice model introduced in Section 1.2.2, and modifying the LIGGGTHS source code to distinguish between freeze-bond and ice block and bond strength. The methodologies used for generation and testing of cuboid and empirical rubble and ice ridges are also developed by the author.

The significance of sea ice flexural failure spans diverse applications, from understanding rubble formation to modeling ice sheet bending against sloped structures and ship hulls. Valuable in-situ experiments on side-loaded sea ice beams near Storfjorden, Svalbard, have provided valuable data for parameterizing and calibrating the DEM model that replicates ice fracture under flexural loads. The newly developed material model (see Sections 4.6 and 5.4) was integrated into the open-source DEM code WooDEM, and the above experiments were simulated at three resolutions. Despite the complexities introduced by local crushing at platen-ice interface, the simulations effectively captured the key aspects of beam failure with reasonable accuracy. The validation and calibration of the DEM model against level ice was an essential step toward employing this model for more complex simulations, including ice rubble and ice ridge flexural failure simulations.

The DEM code LIGGGHTS was used for simulating medium-scale freshwater ice rubble punch tests. In a novel methodology, rubble samples were created in the simulation by "raining" individual DEM ice pieces onto a rectangular "form" and then compressing the resulting rubble mass to reach the desired porosity level. A two-stage failure mechanism, well-aligned with the observed failure behavior reported in experimental studies, was observed (Chapter 5).

Cuboid ice blocks have been frequently used in ice rubble DEM simulations. Although the rubble failure mechanism generally corresponds with experimental outcomes in these simulations, highlighting the potential of DEM to replicate the overall behavior of ice rubble masses through the mechanics of block-block interactions and calibrated freeze-bond properties, they do, however, often overestimate maximum load before flexural failure of the rubble beam. To improve the simulations, a custom code was developed to generate ice blocks by image processing of actual blocks of broken ice. The resulting simulations using empirically-derived block shapes captured the failure mechanisms, and in addition demonstrated improved agreement with experimental data. This observation highlights the capabilities and advantages of this new method for ice rubble generation in DEM.

The available information on the flexural strength of ridges is limited, and design loads are typically calculated solely using the thickness of the consolidated layer as a basis. In this research the developed DEM model was used to investigate the mode and loads related to flexural failure of ice ridges. Ice rubble blocks made of DEM particles were generated and placed in the LIGGGHTS domain using a custom code similar to the rubble experiments. In a novel approach, a consolidated layer, made of bonded DEM particles, was then compressed and bonded to the top of the blocks, representing a simplified two-layer ice ridge beam.

The simulation results indicated that if the keel to consolidated layer thickness ratio is less than around 7, which covers most of the ice ridges in the nature, the bond strength between rubble blocks in the keel does not play an important role in the flexural failure of the ice ridge. In this case, the main contributor to the flexural strength of ice ridges is consolidated layer thickness, which is in-line with the literature. However, the simulations show that when this ratio is higher than 7, increasing the freeze-bond strength between rubble blocks can significantly increase the ridge strength. This new finding can be an important consideration in design for structures prone to impact these kind of ice ridges.

In summary, this body of work offers a more complete understanding of the strength and failure mechanism of freshwater freeze-bonds, showcasing the efficiency of the developed DEM model in comprehending the flexural behavior of ice ridges. Moreover, it contributes to insights about how ice ridge behavior varies across seasons concerning ice thickness, block distribution, and consolidated layer thickness.

1.4. Supporting Manuscripts

This thesis is organized in a manuscript format. Chapters 3-6 have been published or are in publication progress (refer to Table 1-1), and Chapters 1, 2, and 7 are unpublished.

Table 1-1 Supporting Manuscripts

Chapter / Manuscript Title	**Publication**	**Status as of September 2023**
Chapter 1: Introduction	/NA/	/NA/
Chapter 2: Literature Review	/NA/	/NA/
Chapter 3: Experimental Investigation on the Tensile Strength of Freshwater Freeze-Bonds	Journal of Cold Regions Science and Technology	Published

Chapter 4: Investigation and 3D Discrete Element Modeling of Fracture of Sea Ice Beams	Proceedings of Offshore Technology Conference	Published
Chapter 5: Investigation of the Effect of Block Size, Shape and Freeze Bond Strength on Flexural Failure of Freshwater Ice Rubble Using the Discrete Element Method	Journal of Offshore Mechanics and Arctic Engineering	Published
Chapter 6: Discrete Element Modeling of Flexural Failure of Medium Scale Ice Ridges	Journal of Offshore Mechanics and Arctic Engineering	Submitted
Chapter 7: Conclusion	/NA/	/NA/

1.5. References

Bailey, E., Taylor, R., & Croasdale, K. (2015) 'Mechanics of ice rubble over multiple scales', in *Proceedings of the ASME 2015 34th International Conference on Ocean, Offshore and Arctic Engineering OMAE2015*. St. John's, Canada.

Bailey, E., Sammonds, P. R. and Feltham, D. L. (2012) 'The consolidation and bond strength of rafted sea ice', *Cold Regions Science and Technology*. Elsevier B.V., 83–84, pp. 37–48.

Berg, M. van den and Lubbad, R. (2015) 'The application of a non-smooth discrete element method in ice rubble modeling', in *Proceedings of the 23rd International Conference on Port and Ocean Engineering under Arctic Conditions*.

Boroojerdi, M. T. *et al.* (2016) 'Experimental Study on Shear Strength of Freeze Bonds in Freshwater Ice', in *Proceeding of Arctic Technology Conference 2016*. St. John's, Newfoundland and Labrador, pp. 1–9.

Boroojerdi, M. T., Bailey, E. and Taylor, R. (2019a) 'Experimental Investigation of Rate Dependency of Freeze Bond Strength', *Cold Reg. Sci. Technol.*, Under Revi.

Boroojerdi, M. T., Bailey, E. and Taylor, R. (2019b) ‘Experimental study of the effect of submersion time on the strength development of freeze bonds’, *Cold Reg. Sci. Technol.*, Under Revi.

Croasdale, K. R. (2012) ‘A Simple Model for First-year Ridge Loads on Sloping Structures’, pp. 1–6.

Cundall, P. A. & Strack, O. D. L. (1979). A discrete numerical model for granular assemblies. GeÂotechnique 29, No. 1, 47±65

Ettema, R. and Urroz-Aguirre, G. E. (1991) ‘Friction and cohesion in ice rubble reviewed’, in *Proceedings of the 6th International Speciality Conference Cold Regions Engineering*. Hanover, USA, pp. 316–325.

Hawkes, I. and Mellor, M. (1972) ‘Deformation and Fracture of Ice Under Uniaxial Stress’, *Journal of Glaciology*, 11(61), pp. 103–131.

Kloss, C., Goniva, C., Hager, A., Amberger, S., & Pirker, S. (2012). Models , algorithms and validation for opensource DEM and CFD-DEM Models , algorithms and validation for opensource DEM and CFD-DEM. Progress in Computational Fluid Dynamics, 12(2/3), 140–152. https://doi.org/10.1504/PCFD.2012.047457

Leppäranta, M. and Hakala, R. (1992) ‘The structure and strength of first-year ice ridges in the Baltic Sea’, *Cold Regions Science and Technology*, 20(3), pp. 295–311.

Leppäranta, M. (2011) 'The Drift of Sea Ice. Second Edi.', Springer Science & Business Media.

Liferov, P., Jensen, A., Høyland, K.V., Løset, S., (2002). ‘On analysis of punch tests on ice rubble.’ *Proceedings of the 16th International Symposium on Ice*, Dunedin, New-Zealand, vol. 2, pp. 101-

109.

Lilja, V.P., Polojärvi, A., Tuhkuri, J., Paavilainen, J. (2021), 'Finite-discrete element modelling of sea ice sheet fracture', *International Journal of Solids and Structures*, Volumes 217–218, 2021.

Løset, S. (1994a) ‘Discrete element modelling of a broken ice field - Part I: model development’, *Cold Regions Science and Technology*, 22(4), pp. 339–347.

Løset, S. (1994b) ‘Discrete element modelling of a broken ice field - Part II: simulation of ice loads on a boom’, *Cold Regions Science and Technology*, 22(4), pp. 349–360.

Mohammadafzali, S. *et al.* (2016) ‘Investigation and 3D Discrete Element Modeling of Fracture of Sea Ice Beams’, in *Proceedings of 5th Arctic Technology Conference (ATC2016).* St. John’s, pp. 1–9.

Murdza, A., Polojärvi, A., Schulson, E. M., and Renshaw, C. E. 'The flexural strength of bonded ice' *The Cryosphere*, 15, 2957–2967, https://doi.org/10.5194/tc-15-2957-2021, 2021.

Oshaug, M. *et al.* (2014) *Ice mechanics, loads on structures and instrumentation*.

Palmer, A. and Croasdale, K. (2013) *Arctic offshore engineering*. Singapore: World Scientific Publishing Co. Pte. Ltd.

Paavilainen, J., Tuhkuri, J. and Polojärvi, A. (2009) ‘2D combined finite-discrete element method to model multi-fracture of beam structures’, *Engineering Computations*, 26(2004), pp. 578–598.

Polojärvi, A. and Tuhkuri, J. (2013a) ‘2D FEM-DEM simulations of punch through tests: Effects of partly consolidated rubble deformation’, in *Proceedings of the 22nd International Conference on Port and Ocean Engineering under Arctic Conditions*.

Polojärvi, A. and Tuhkuri, J. (2013b) ‘On modeling cohesive ridge keel punch through tests with

a combined finite-discrete element method', *Cold Regions Science and Technology journal*, 85, pp. 191–205.

Prasanna, M., Polojärvi, A. (2023) 'Breakage in quasi-static discrete element simulations of ice rubble', *International Journal of Mechanical Sciences*, Volume 259, 2023, 108595, ISSN 0020-7403, https://doi.org/10.1016/j.ijmecsci.2023.108595.

Serré, N., Repetto-Llamazares, A. H. V. and Høyland, K. V. (2011) 'Experiements on the relation between freeze-bond and ice rubble strength, Part I: Shear box experiments', in *Proceedings of the International Conference on Port and Ocean Engineering under Arctic Conditions, POAC*.

Shayanfar, H. (2017) *An Experimental Investigation on the Strength and Failure Behavior of Freshwater Ice Rubble*. Memorial University of Newfoundland.

Shayanfar, H. *et al.* (2018) 'The effects of consolidation time on the strength and failure behavior of freshwater ice rubble', *International Journal of Naval Architecture and Ocean Engineering*. Elsevier Ltd, 10(3), pp. 403–412.

Shayanfar, H., Bailey, E., & Taylor, R. (2022). Medium-scale laboratory investigation of the effect of confinement on ice rubble strength and failure behavior. *Cold Regions Science and Technology*, 202, 103629.

Šmilauer, V. Cohesive Particle Model using the Discrete Element Method on the Yade Platform. PhD thesis, Czech Technical University in Prague, Faculty of Civil Engineering & Université Grenoble I – Joseph Fourier, École doctorale I-MEP2, 2010.

Szabo, D. and Schneebeli, M. (2007) 'Subsecond sintering of ice', *Applied Physics Letters*, 90(15), pp. 1–4. doi: 10.1063/1.2721391.

2. LITERATURE REVIEW

In this chapter, the current knowledge on the existence, mechanism of formation, typical geometry, dimensions, and mechanism of failure of ice ridges were overviewed. The flexural failure of an ice ridge is dependent on the failure of its consolidated layer and its keel, so it is important to understand the flexural failure mechanism of these two layers. The properties and modes of failure of these two layers as well as the strength of the freeze-bonds between the submerged ice blocks of the keel were overviewed. A DEM model was employed to simulate the failure of the ridges, so in the last part of this chapter, the DEM models used to simulate the failure of ice are introduced. It is noted that additional literature specific to each literature theme has also been reviewed in each corresponding chapter.

2.1. Ridge Existence, Formation, and Geometry

The amount of ice in ridge form has been reported by several researchers. The existence of ridge is measured either from upper surface data or underwater data, and these data are not merged in most cases. There are many reports on the amount of ice ridge in certain geographical locations. For instance, Kirillov (1957) estimated that 22-39% of ice cover in the Kara Sea consists of ridges and Wittmann and Schule (1966) reported the amount of undersurface ice in ridge form in the Canadian basin is 13% in summer and 18% in winter (Parmerter and Coon, 1972). Most of the current information on ridge profiles are obtained by observation of the upper surface (satellite, radar, air photos, and lasers) or the lower surface (sonars), and there are some limited data obtained by drilling.

Ridges can form through two main mechanisms: shear ridges are shaped by parallel movement of adjacent floes, while pressure ridges are shaped by movement of floes towards each other; pressure ridges are the most prevalent type of deformed ice feature in the Arctic (Parmerter & Coon, 1973). The process of formation of ice ridges is usually driven by environmental forces and is a complex process that involves bending, rafting, buckling, and crushing of sea ice. The ice rubble generated by this process contains blocks of many sizes and shapes. Broken pieces of ice pile up and down to form a ridge that is in hydrostatic equilibrium, so the rubble above the waterline, the sail, and the rubble under the waterline, the keel, form roughly 10 and 90 percent of the total ridge volume respectively. The volume around the waterline is usually refrozen to form a consolidated layer.

The physical basis of the geometric characteristics of a ridge and the relationship between the dimensions is a complex subject, the only available formulas that estimate the geometric properties of the ridges are based on simple curve fitting of available data. The average ratios of keel height to sail height, keel width to keel height, and cross-section area of the keel to cross-section area of the sail for a first-year ridge based analysis of 112 ridges are 4.4, 3.9, and 8.0 respectively (Timco *et al.*, 2000). Figure 2-1 show the typical cross-section of a first year ice ridge.

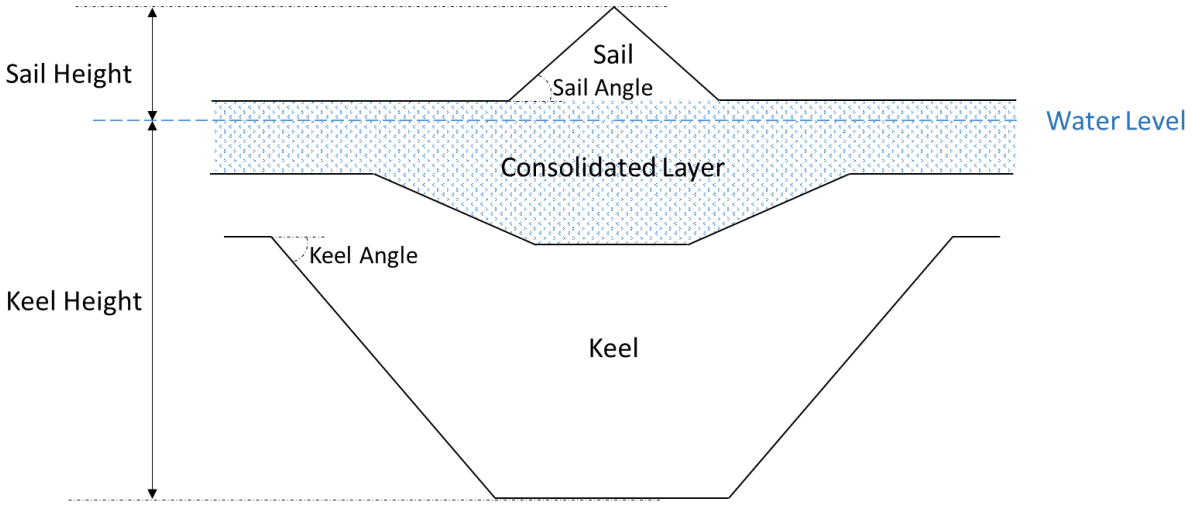

Figure 2-1- Typical cross-section of a first-year ice ridge (after Timco *et al.*, 2000)

As soon as a ridge forms, its mechanical and thermal properties start to change due to various processes. The most significant change happens initially due to the redistribution of heat. Sea ice that forms the ice ridge can be several degrees below freezing point, when ice blocks plunge to the keel, their temperature starts to rise and form new ice and freeze-bonds in the keel. This process changes the average porosity from 0.35 to 0.25 (Timco *et al.*, 2000). If this ice growth happens at the contact points of the blocks, it can contribute to the formation of cohesive bonds between the blocks. After this initial redistribution of energy, the ice rubble and surrounding water will be at thermal equilibrium, so the thermal process will stop changing the ridge. From this point on, pressure consolidation and sintering will change the properties of the keel in the aging procedure (Bruneau, 1996).

Some of the most valuable data available to date on the structure of the sea ice ridges are gathered through a three-year field program (1987-1989) by a joint group of Finnish Institute of Marine Research and the Laboratory of Structural Engineering of the Technical Research Centre of Finland. Freely floating ridges in the Baltic Sea with the total thickness between 4 to 17 meters

were investigated. This study suggests that the thickness of the totally consolidated layer of a ridge can be up to two times of the thickness the surrounding sea ice. An average porosity of 29% for the keel has been reported, and the measured keel shear strength was 1.7-4 kPa (Leppäranta and Hakala, 1992).

2.2. Interaction of Ice Ridges and Offshore Structures

During the interaction of ice ridges and offshore structures, various modes of failure might happen. The force might be limited by the local interaction of ridge and platform (limit stress), by the ridge building force on the interface of the ridge and thin ice behind the ridge (limit force), or by kinetic energy of the ridge (limit momentum/energy). The least among these three defines the design force. In the proposed research in this thesis, the limit stress failure and corresponding forces are of interest. A simplified approach to estimate the load on structures is to assume the consolidated layer fails against the structure in crushing and add this crushing force to the keel failure forces. However, measurements from field interactions show that the consolidated layer, even in vertical structures, often tends to fail out of plane at lower loads than crushing. This is due to the nature of the consolidated layer which is variable in thickness. As a result, even in interaction with vertical structures, the crushing assumption might be over-conservative (Palmer and Croasdale, 2013).

For failure against sloping structures, the flexural strength of the full thickness of ice is the most important parameter. Many studies have been conducted to measure the flexural strength of sea ice (e.g. Weeks and Assur, 1967; Vaudrey, 1977; Timco and Frederking, 1982; Timco and O.'Brien, 1994; Blanchet *et al.*, 1997; Jordaan, 2001; Lu *et al.*, 2016; Aly *et al.*, 2019; Karolina *et al.*, 2019), but very limited data on refrozen ice rubble. There are some valuable data on the full-scale interaction of ice ridges with offshore structures. These data are the most reliable data for developing and validating ridge failure models. The data obtained on the Molikpaq in the Beaufort

Sea during the mid-1980s is the most notable data on full-scale first-year ice ridge available to date. Molikpaq is a gravity-based structure that consists of an octagonal steel caisson annulus and was deployed four times in total. In the last deployments of the Molikpaq in the Beaufort Sea (1987-1990), the platform was set to 10-15m drafts. These low drafts led to impede the ice clearance and resulted in the formation of grounded rubble around the platform. For this reason, the interactions recorded during the 1984-1986 deployment, where the platform was subject to direct ice action in 30m of depth, is of interest (Timco *et al.*, 2000).

The consolidated layer of ice ridges interacted with the almost vertical face of Molikpaq, and the keel moved against a 23° face. Only the largest ridges interacted with the more sloped, deep wall of the platform. The interactions that happened during the deployment of the Molikpaq consisted of mostly small ridges, with sail heights up to 2 meters. Five modes of ridge failure against the platform during the interactions were identified from the recorded videos: spine failures (failure against the central portion of the sail), failing behind (failure in the parent ice behind the ridge), shearing (large cracks perpendicular to the face of the platform), stopping (no initial failure happened, the ridge was stopped for a while, levels of stress increased, subsequent failure happened), and mixed modal (combination of multi modes of failure). A total of 23 ridge interactions with ridge heights from 0.5m to 2.5m were recorded; the global loads from interactions ranged from 30 MN to 89 MN. The following regression line was fitted to the data:

$$R_{LL} = 0.36H_s + 0.25 \tag{2-1}$$

where R_{LL} is the ridge line load and H_s is the sail height. The measured forces and empirical formulas represent the global load on the Molikpaq, and there is only very limited data on the keel load (only of the upper level of the keel) (Timco *et al.*, 2000).

Several studies reported the interactions of ice ridges with the Norströmsgrund lighthouse in the Gulf of Bothnia (Bjerkas *et al.*, 2010; Zvyagin and Ziemer, 2017). Ervik *et al.* (2019) recently studied the interaction of ice ridges with the Norströmsgrund lighthouse and reported on the global force and modes of interaction. A total of 35 interactions with the vertical wall of the lighthouse was reported, resulting global loads up to 6 MN. Three modes of failure were reported in this study: limit-force stalling events, limit-stress ductile events, and limit-stress brittle events. Lemee and Brown (2005) reviewed the ice ridge interactions with the Confederation Bridge and introduced a new model to estimate the ridge loads on vertical walls.

Other observations on the ridge interactions with offshore structures include artificial islands, shallow and deep caissons, Cook Inlet platforms, and lighthouses. Little or no information on the interaction loads is available for these observations, and most of the analysis is qualitative in nature. Several thousands of ridge interaction with the Confederation Bridge has been recorded, but the data remains confidential for the participants.

2.3. Mechanical Properties of Ice Rubble

An ice ridge consists of an above-water sail, a consolidated layer around the water level, and a rubble keel. To understand the flexural failure of an ice ridge, one need to know the mechanical behavior and strength of the consolidated layer and rubble keel layer of the ridge. As stated above, direct measurements on the consolidated layer are rare, but since this layer has a low porosity and pieces of ice are frozen together, it is a reasonable assumption to simplify this layer as a layer of thick level ice.

Shear strength τ of ice rubble is often estimated using soil mechanics concepts that define the strength based on internal friction angle ϕ and cohesion c in Mohr-Coloumb relation (Prodanovic, 1979; Fransson and Sandkvist, 1985; Timco *et al.*, 1992; Løset and Sayed, 1993):

$$\tau = c + \sigma_N \tan \phi \tag{2-2}$$

where σ_N is the normal stress.

It is understandable why ice rubble is, in most cases, considered as a Mohr-Coloumb material; ice rubble has a granular nature, and some of its behavior, e.g., angle of repose, can be represented by this concept. However, ice rubble has some properties that cannot be well described by this concept; for example, the cohesion of the rubble blocks is a function of temperature, geometry, salinity, time, and stress history and varies over the rubble height (Timco *et al.*, 2000). Moreover, contacting pieces of submerged ice can form a freeze-bond even under low confinement pressures (Ettema and Urroz, 1989). The initial failure within the ice rubble is controlled by cohesion, which itself can be highly variable depending on the salinity, geometry, and temperature profiles. After that, the behavior of rubble is mostly controlled by the yielding friction of the rubble that is also highly variable. So it is an oversimplification to consider highly complex behavior of ice rubble as a simple Mohr-Coloumb material with a constant cohesion and friction angle (Weaver, 1995).

Considerable effort has gone into understanding the behavior of ice rubble. The size of full-scale features and the high degree of variability in ice block geometry and conditions throughout a ridge keel pose challenges for conducting representative experiments. The problem is further compounded by the fact that several methods–most notably direct shear box, simple shear box, and biaxial shear –mainly focused only on measuring the shear strength of ice rubble, the study of the flexural behavior of ice rubble has received limited attention.

In situ experiments on ice rubble include:

- Direct shear test: in this method, the consolidated layer of ice is trenched to isolate a rectangular slab. The slab is then pushed horizontally, and corresponding force and displacement are measured. The resulting strength in this method is the shear strength of the bottom layer of the consolidated layer (Croasdale & Associates Ltd., 1997; Smirnov *et al.*, 1999)
- Punch shear test: the consolidated layer of the ice is cut through the underlying rubble. A vertical load pushes the plug downward, and force and displacements are recorded. In this method, the shear strength of the rubble keel is measured (Leppäranta and Hakala, 1992; Croasdale & Associates Ltd., 1996)
- Pull up test: the techniques used in this method is similar to the punch shear test, but the plug is pulled vertically upward to measure the tensile strength of the bond between the consolidated layer and rubble keel.

Figure 2-2 shows a schematic of the most prevalent in-situ experiment on ice ridges.

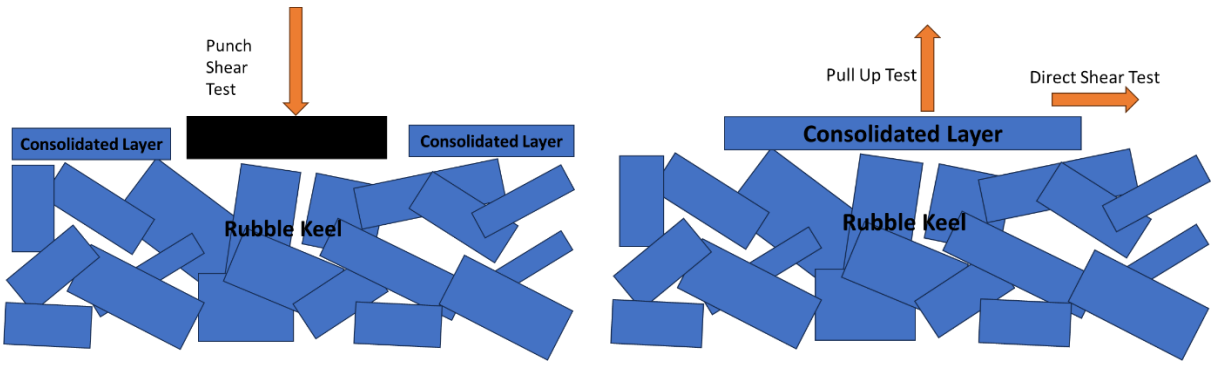

Figure 2-2- Schematic of common in-situ experiment of ice ridges

Azarnejad and Brown (2002) carried a series of laboratory punch tests on freshwater ice rubble to study the failure behavior of ice rubble. This study suggests that the freeze-bonding would affect the frictional behavior of ice rubble. Lemee and Brown (2002) carried out a similar type of experiments and noticed by decreasing the initial ice temperature (before submersion), the freeze-bonding between the blocks, and therefore the rubble strength, increases. Sayed and Frederking (1986), Bruneau (1996), Bailey et al. (2014), Liu et al. (2015), Yulmetov et al. (2017), and Shayanfar *et al.* (2018) also reported on the effect of the block to block freeze-bond strength on overall behavior of ice rubble.

An extensive review of the ice rubble failure experiments can be found in Ettema and Urroz-Aguirre (1991), Timco and Cornett (1999), Liferov and Bonnemaire (2005) and Bailey *et al.* (2015). While these experiments provided valuable insights into the shear failure of ice rubble, Shayanfar (2017) and Shayanfar *et al.* (2018) provided valuable experimental data on the flexural failure of ice rubble. Shayanfar studied the effect of confinement pressure and submersion time on the flexural failure of ice rubble. The numerical simulations proposed for this study are based on these experiments. More details on these experiments are explained in Chapter 3.

2.4. Freeze-Bond and Its Effect on Ice Rubble

When pieces of contacting ice rubble are submerged, they tend to form freeze-bonds (even at low confining pressure). This freeze-bond formation may contribute to the friction angle and so the shear strength of the ice rubble (Ettema and Urroz, 1989), but the mechanism and magnitude of this effect have been an unsolved question for many years. Liferov and Bonnemaire (2005) reviwed the failure behavior and strength of ice rubble based on existing data in an attempt to uncover unsolved questions about the behavior of ice rubble. He suggested that the failure of ice rubble happens in two stages: the primary failure of rubble is dominated by the strength of the

freeze-bonds between the blocks and the secondary failure which is limited by the overall strength of the rubble accumulation provided by the frictional and deformation resistance of the confined body of the rubble. Astrup et al. (2013) also observed this two-stage failure in his laboratory shear box experiments and suggested that the ratio of increasing the freeze-bond stress is comparable with the ratio of increase of the rubble strength. Beyond affecting the strength of ice rubble, freeze-bond strength may also affect the mode of failure; i.e. if the freeze-bond formed between rubble blocks is strong enough, ice failure may happen at the surrounding ice rather than the freeze-bond (Bailey et al., 2015).

Serré et al. (2011) studied the effect of freeze-bonding on the ice rubble strength in shear box experiments. The freeze-bond strength was changed by changing the submersion time in three levels. This study concluded that the failure of rubble starts at the freeze-bonds; as the freeze-bond strength increases, the primary peak of the rubble shear stress during the failure also increases. He also suggested that high strength freeze-bonds would contribute to the formation of large block assemblies. Azarnejad and Brown (2002) carried a series of laboratory punch tests on freshwater ice rubble to study their failure behavior. This study suggests that the freeze-bonding would affect the frictional behavior of ice rubble. Lemee and Brown (2002) carried out a similar type of experiments and noticed by decreasing the initial ice temperature (before submersion), the freeze-bonding between the blocks, and therefore the rubble strength, increases. Bruneau (1996), Bailey et al. (2014), Yulmetov et al. (2017), Liu et al. (2015), and Sayed and Frederking (1986) also reported on the effect of the block to block freeze-bond strength on overall behavior of ice rubble.

While the shear strength of freeze-bond is frequently considered, and studied, as the main contributor to the strength of the ice rubble, Shayanfar (2017) and Shayanfar et al. (2018) observed that a considerable portion of freeze-bonds would fail in tension when rubble is under flexure.

Hence, understanding the strength and failure mechanism of freeze-bond under tension can provide a deeper and more accurate insight into the failure of ice rubble.

Murdza et al. (2021) performed four-point bending tests to assess the flexural strength of freeze-bonds between rectangular ice blocks in air. Freshwater small grain ice with columnar grains was used, bonded at 4 kPa confinement. Increasing the salinity and temperature weakened the freeze-bonds. Freshwater and saline bonds eventually matched parent ice strength at different saturation times. Flexural bond strength ranged from 0 MPa (no bonding) to 1.7 MPa (equaling parent ice). According to Leguillon et al. (2015), the ratio between tensile and flexural strength can vary, particularly for brittle materials, where flexural strength typically falls within 1-2 times their tensile strength. Ashby and Jones (2012) suggested a 1.7 ratio and Murdza et al. (2021) reported freshwater flexural strength exceeding uniaxial tensile strength by about 1.7. While in 3 point and 4 point bending experiments only a small area of the samples experiences the maximum tensile stress, the whole cross-section of the sample experiences the maximum tensile stress in pure tensile testing. This increases the probability of the ice flaws getting exposed to the maximum tensile stress and hence reduce its measured strength. This phenomenon's statistical implications have been discussed further by Jordaan et al. (2007) and Taylor (2010).

Szabo and Schneebeli (2007) investigated the tensile strength of bonds in micro conical ice samples (15 mm long, 3 mm radius), made of degassed clear mountain water, formed in sub-second sintering. In these experiments freezing of the liquid layer between samples was the main sintering mechanism. Ettema and Schaefer (1986) carried out a series of laboratory experiments to determine the effect of confinement, submersion time, bonding area, and salinity on the shear strength of freeze-bond. The confinement of the ice blocks was provided by adding dead weights on top of the blocks, and the shear load was applied by pulling up the top ice block. They noticed

that the strongest freeze-bond forms by submerging the ice blocks in freshwater and the freeze-bond forms in the air (non-submerged) is stronger than the freeze-bond forms in saline water. Repetto et al. (2011a, 2011b) modified this experimental setup and conducted a series of experiments to study the effect of confinement, submersion time, and temperature on the strength of freeze-bond in saline ice.

Shafrova and Høyland (2008), Høyland and Møllegaard (2014), and Bueide and Høyland (2015) used uni-axial and tri-axial compression test techniques to estimate the shear strength of freeze-bond. Shafrova and Høyland (2008) examined the behavior of first-year ridges and laboratory samples and noted that the initial properties of ice, confinement pressure, and block size are the main parameters affecting the bond strength. Høyland and Møllegaard (2014) studied the strength of the laboratory-made freeze-bond as a function of submersion time, initial temperature, and size. Bueide and Høyland (2015) improved this experimental setting and studied the effect of confinement, submersion time, temperature, and salinity.

Boroojerdi *et al.* (2016, 2019a, 2019b) extensively studied the effect of submersion time, initial temperature, deformation rate and confinement pressure on the strength of freshwater freeze-bond. Cylindrical ice samples were confined in an aluminum frame and failed under asymmetrical bending method based on (Frederking and Timco, 1984) and (Bailey et al., 2012). Other studies on the shear strength of freeze-bond include (Møllegaard, 2012) and (Marchenko and Chenot, 2009).

The general effect of the studied parameters on the strength of freeze-bond can be summarised as the followings:

- Temperature: the strength of freeze-bond is highly affected by the initial ice temperature; a lower initial temperature of the ice blocks yields stronger freeze-bonds between the blocks.
- Confinement pressure: the strength of freeze-bond increases proportionally with confinement pressure during the formation of freeze-bond.
- Salinity and porosity: both salinity and porosity of ice blocks have a negative effect on the strength of freeze-bond.
- Submersion time: the strength of freeze-bond initially increases with the submersion time until it reaches a peak at 2-4 minutes. After that, the strength gradually decreases to a minimum at 3-5 hours and starts to slowly increase again and reach its maximum at around seven days.
- Deformation rate: the shear strength of freeze-bond decreases with the increase of deformation rate. The rate dependency under tension is an area of argument; this subject will be discussed further in Chapter 3

2.5. Flexural Failure of Level Ice

As stated, it is a reasonable assumption to consider the mechanical behavior of the consolidated layer of ice as a solid layer of level ice. Many researchers have studied the mechanical properties of sea and freshwater ice and its flexural strength in particular using cantilever and four-point beam experiments in field and in lab (Weeks and Assur, 1967; Vaudrey, 1977; Timco and Frederking, 1982; Timco and O.'Brien, 1994; Blanchet *et al.*, 1997; Jordaan, 2001; Lu *et al.*, 2016; Aly *et al.*, 2019; Karolina *et al.*, 2019). Burton et al. (2022, 2023) utilized machine learning (ML) regression algorithms for predicting the flexural strength of sea ice. This involved compiling an extensive

database encompassing over 2700 records of flexural strength measurements for sea ice beams. While there are many technical challenges and discussions around this topic, only the main results of these studies are review in the following.

Flexural strength of the sea ice is estimated to be around 10-50% of the compressive strength (Vaudrey, 1977). It is suggested that porosity plays the most important role in the flexural failure of sea ice. Vaudrey (1977) defines the flexural strength of sea ice σ_f in kPa as a function of brine volume v_b:

$$\sigma_f = 0.960 - 1.920(v_b^{0.5}) \tag{2-3}$$

Timco and O'Brien (1994) also claims that the brine volume is the main contributor to the flexural strength of sea ice. He used data from approximately 1000 flexural beam test to derive:

$$\sigma_f = 1.76e^{-5.88\sqrt{v_b}} \tag{2-4}$$

where flexural failure is given in MPa, and the brine volume is calculated by:

$$v_b = S\left(\frac{49.185}{|T|} + 0.532\right) \tag{2-5}$$

where *S* is salinity in ppm, and *T* is the temperature in degrees Celsius.

(Aly *et al.*, 2019) studied the scale effect on the flexural strength of sea ice and freshwater ice and suggested that flexural strength of ice decreases with size:

Freshwater Ice $$\sigma_f = 840\left(\frac{V}{V_1}\right)^{-0.13} \tag{2-6}$$

Sea Ice $$\sigma_f = 1324\left(\frac{V}{V_1}\right)^{-0.054} e^{-4.969\sqrt{v_b}} \tag{2-7}$$

where V and V_1 are beam volume and reference volume ($1m^3$), respectively.

2.6. Discrete Element Modeling of Ice

One of the early applications of DEM modelling for simulating the failure of ice was by Løset (1994a, 1994b). This 2D model consisted of circular particles representing pieces of a broken ice field. Each particle was subjected to air and water drag, surface tilt, and Coriolis forces. Particles were contacted to the neighboring particle by visco-elastic-plastic rheology.

A 2D combined FEM DEM model is introduced and used by Paavilainen *et al.* (2009), Paavilainen and Tuhkuri, J. (2013) and Ranta *et al.* (2015) to simulate the multi-fracture of sea ice against sloped structures. In this model, the elements of the beam are elastic FEM components, and each of them works as a DEM particle. This model provides a better understanding of the micro behavior of ice beams during failure in bending but for a high computational cost. The same FEM DEM model was used by Polojärvi and Tuhkuri (2013a, 2013b) for simulating punch through experiments of partially consolidated ice rubble. This study investigates the effect of block size, freeze-bond strength, and block to block friction coefficient on the total load on the indenter. Polojärvi and Tuhkuri (2013a) concluded that the buoyancy force applied to the rubble blocks and moves the broken pieces to the top plays an important role in the failure behavior of ice rubble. This study shows that the peak loads observed during the shear failure of rubble are due to the force chains within the rubble and are limited by buckling of these chains.

Goldstein *et al.* (2013) employed a 2D DEM model to study the pile-up of grounded sea ice against a sloping structure. Based on the simulations results and parametric analysis, Goldstein *et al.* (2013) suggested an equation to estimate the height of grounded ice rubble pile up. Polojärvi *et al.* (2015) introduce another 2D DEM model to simulate direct shear box experiments of ice rubble. The simulations were validated against experiments, and the calibrated model was then used to gain a better understanding of the behavior of ice rubble under shear.

The dynamic friction coefficient of ice is often considered as a constant; however, based on experimental observations, Lishman and Polojärvi (2015) used a 2D DEM model to understand and estimate the rate dependency of the ice-ice friction. The study shows that the dynamic friction coefficient decreases with sliding speed and affects the behavior of ice rubble in shear.

Lilja (2021) proposed a model for fracture analysis of large, cellular, plate-like structures. A method combining finite and discrete elements was presented for studying sea ice sheet fracture with three applications: uniaxial tensile fracture, vertical penetration fracture, and circular hole breakage by a truncated cone.

Sarracino developed a material model in DEM which included normal, tensile, flexural and torsional springs and bonds, and a hysteretic damping model (Sarracino, unpublished work). This novel ice model incorporates normal, shear, torsional, and flexural springs between adjacent particles, either overlapping due to compressive stresses or bonded. While the spring stiffnesses can be configured independently, this simulation assumes a linearly elastic, isotropic material, and sets the relative spring stiffnesses accordingly. In this model, bonded neighboring particles collectively exhibit characteristics akin to an 'equivalent beam' when subjected to tensile, compressive, shear stresses, or flexural, and torsional moments.

This material model was incorporated into the code WooDEM by Smilauer and subsequently utilized in CARD/C-CORE modelling by Liu *et al.* (2015), Mohammadatzali *et al.* (2016), and others (see, e.g., Chapter 4 of this thesis). Later Sarracino and Morgan commissioned Kloss and Goniwe to incorporate a subset of this model into LIGGGHTS (Sarracino, unpublished work), subsequently utilized by Morgan *et al.* (2015) and Afzali *et al.* (2021,2023) (see Chapters 5 and 6, this thesis).

Liu *et al.* (2015) simulated the failure of ice rubble keel during the gouging with sea bed using a 3D DEM model. A Cohesive Frictional Mode (CFM) was used to model the spherical particles. The cohesion model was consisted of normal, shear, and torsion springs, and the sea bed was modeled a rigid body.

Berg and Lubbad (2015) implemented a non-smooth DEM (NDEM) model to simulate the failure of unconsolidated ice rubble in the lab and full scale. NDEM models are faster than smooth models but can induce artificial vibration to the system, especially when larger particles are in use. Moreover, NDEM models neglect the viscoelastic nature of the contact which can play an important role in the energy dissipation of the system.

Bonded 3D DEM models are also used to simulate the interaction of sea ice and conical structures. Yulmetov *et al.* (2017) and Morgan *et al.* (2015) used a bonded 3D DEM model to simulate the interaction of sea ice with the Confederation Bridge. The effect of ice sheet width and length, DEM parameters, and the cone angle on the rubble pile height, shape, volume, and formation mechanisms were studied by Morgan *et al.* (2015). This study suggests that simulating ice in multiple layers results in more accurate simulations but increases the simulation cost significantly.

Prasanna and Polojärvi (2023) present a new particle breakage model for quasi-static DEM simulations, aimed at capturing shear failure in non-spherical particles. Based on experimental observations and advanced modeling, the model's integration into a DEM code enhances simulation precision, especially evident in direct shear box experiments involving ice rubble.

2.7. References

Afzali, S., Taylor, R., Bailey, E., Sarracino, R., & Boroojerdi, M. T. (2021) 'Investigation of the

Effect of Block Size, Shape, and Freeze Bond Strength on Flexural Failure of Freshwater Ice Rubble Using the Discrete Element Method', *Journal of Offshore Mechanics and Arctic Engineering*, 143(5).

Afzali, S., Taylor, R., & Sarracino, R., (2023), in progress.

Aly, M. *et al.* (2019) 'Scale Effect in Ice Flexural Strength', *Journal of Offshore Mechanics and Arctic Engineering*, 141(5), pp. 1–12.

Ashby, M. M. and Jones, D. R. H (2012) 'Engineering Materials 1: An Introduction to Properties, Applications and Design', 4th Edn., Elsevier/Butterworth-Heinemann, Oxford, UK.

Astrup, O. S., Helgøy, H. and Høyland, K. V (2013) 'Laboratory work on freeze-bonds in ice rubble, Part III: Shear box experiments', *Proceedings of the International Conference on Port and Ocean Engineering under Arctic Conditions, POAC*.

Azarnejad, A. and Brown, T. G. (2001) 'Ice rubble behavior in punch tests', *Journal of Cold Regions Engineering*, 15(3), pp. 135–153.

Bailey, E. *et al.* (2014) 'An Overview of the Development of Ice Ridge Keel Strengths Test Program', in *Society of Petroleum Engineers - Arctic Technology Conference 2014*.

Bailey, E., Taylor, R., & Croasdale, K. (2015) 'Mechanics of ice rubble over multiple scales', in *Proceedings of the ASME 2015 34th International Conference on Ocean, Offshore and Arctic Engineering OMAE2015*. St. John's, Canada.

Bailey, E., Sammonds, P. R. and Feltham, D. L. (2012) 'The consolidation and bond strength of rafted sea ice', *Cold Regions Science and Technology*. Elsevier B.V., 83–84, pp. 37–48.

Berg, M. van den and Lubbad, R. (2015) 'The application of a non-smooth discrete element

method in ice rubble modeling', in *Proceedings of the 23rd International Conference on Port and Ocean Engineering under Arctic Conditions*.

Bjerkas, M., Albrektsen, A. and Guntner, A. (2010) 'Static And Dynamic Ice Actions In The Light Of New Design Codes', in *Proceedings of the ASME 29th International gf Conference on Ocean, Offshore and Arctic Engineering, 2010, vol 4*. Three Park Avenue, New York, NY 10016-5990 USA: Ameican Society of Mechanical Engineers, pp. 733–739.

Blanchet, D., Abdelnour, R. and Comfort, G. (1997) 'Mechanical properties of first-year sea ice at Tarsiut Island', *Journal of Cold Regions Engineering*, 11(1), pp. 59–83.

Boroojerdi, M. T. *et al.* (2016) 'Experimental Study on Shear Strength of Freeze Bonds in Freshwater Ice', in *Proceeding of Arctic Technology Conference 2016*. St. John's, Newfoundland and Labrador, pp. 1–9.

Boroojerdi, M. T., Bailey, E. and Taylor, R. (2019a) 'Experimental Investigation of Rate Dependency of Freeze Bond Strength', *Cold Reg. Sci. Technol.*, Under Revi.

Boroojerdi, M. T., Bailey, E. and Taylor, R. (2019b) 'Experimental study of the effect of submersion time on the strength development of freeze bonds', *Cold Reg. Sci. Technol.*, Under Revi.

Bruneau, S. E. (1996) *Development of a first year ridge keel model, Doctor of Philosophy*. Memorial University of Newfoundland.

Bueide, I. M. and Høyland, K. V. (2015) 'Confined compression tests on saline and fresh freeze-bonds', in *Proceedings of the International Conference on Port and Ocean Engineering under Arctic Conditions, POAC*. Trondheim, Norway.

Burton, R., Yulmetov, R., and Taylor, R. (2022) ‘Estimating Freshwater Level Ice Loads on Sloping Structures Using Machine Learning-Derived Flexural Strength’, in *Proceedings of the 26th IAHR International Symposium on Ice*. Montreal, Canada.

Burton, R., Yulmetov, R., and Taylor, R. (2023) ‘Estimating Level Sea Ice Loads on Sloping Structures Using Machine Learning-Derived Flexural Strength’, in *Proceedings of the International Conference on Port and Ocean Engineering under Arctic Conditions, POAC*. Glasgow, United Kingdom.

Croasdale, K. R. (2012) ‘A Simple Model for First-year Ridge Loads on Sloping Structures’, pp. 1–6.

Ervik, Å. *et al.* (2019) ‘Ice-ridge interactions with the Norströmsgrund lighthouse: Global forces and interaction modes’, *Cold Regions Science and Technology*. Elsevier, 158(February 2018), pp. 195–220.

Ettema, R. and Schaefer, J. A. (1986) ‘Experiments on freeze-bonding between ice blocks in floating ice rubble’, *Journal of Glaciology*, 32(112), pp. 397–403.

Ettema, R. and Urroz-Aguirre, G. E. (1991) ‘Friction and cohesion in ice rubble reviewed’, in *Proceedings of the 6th International Speciality Conference Cold Regions Engineering*. Hanover, USA, pp. 316–325.

Ettema, R. and Urroz, G. E. (1989) ‘On internal friction and cohesion in unconsolidated ice rubble’, *Cold Regions Science and Technology*, 16(3), pp. 237–247.

Fransson, L. and Sandkvist, J. (1985) ‘Brash ice properties—laboratory tests’, in *Proc. of the 8th Int. Conf. on Port and Ocean Engineering under Arctic Conditions Narssarssuaq*, pp. 75–87.

Frederking, R. M. W. and Timco, G. W. (1984) ‘Measurement of shear strength of granular/discontinuous-columnar sea ice’, *Cold Regions Science and Technology*, 9(3), pp. 215–220.

Goldstein, R. *et al.* (2013) ‘Grounded ice pile-up. 2D dem simulation’, in *Proceedings of the 22nd International Conference on Port and Ocean Engineering under Arctic Conditions*.

Hawkes, I. and Mellor, M. (1972) ‘Deformation and Fracture of Ice Under Uniaxial Stress’, *Journal of Glaciology*, 11(61), pp. 103–131.

Høyland, K. V and Møllegaard, A. (2014) ‘Mechanical behaviour of laboratory made freeze-bonds as a function of submersion time, initial ice temperature and sample size’, in *22nd IAHR International Symposium on Ice*. Singapore, pp. 265–273.

In Situ Ridge Strength Measurements – 1997. A study sponsored by NRC (PERD) and Exxon Production Research Co. (Proprietary until December 2000). (1997).

In situ strength measurements of first year pressure ridges and rubble fields. A study for the National Energy Board, supported by PERD. (1996).

Jordaan, I. J. (2001) ‘Mechanics of ice - structure interaction’, *Engineering Fracture Mechanics*, 68, pp. 1923–1960.

Jordaan, I. J., Taylor, R., & Reid, S. (2007). 'Fracture, probabilistic averaging and the scale effect in ice-structure interaction.' *In Proceedings of the International Conference on Port and Ocean Engineering under Arctic Conditions*, Dalian, China, June 27-30.

Karulina, M. *et al.* (2019) ‘Full-scale flexural strength of sea ice and freshwater ice in Spitsbergen Fjords and North-West Barents Sea’, *Applied Ocean Research*. Elsevier, 90(April), p. 101853.

Kirillov, A. A. (1957) ‘Calculation of hummockness in determining ice volume’, *Problems of the Arctic,* 2, pp. 53–58.

Leguillon, D., Martin, E., Lafarie-Frenot, M. C. 'Flexural vs. tensile strength in brittle materials', *Comptes Rendus Mécanique*, Volume 343, Issue 4, 2015, Pages 275-281, ISSN 1631-0721, https://doi.org/10.1016/j.crme.2015.02.003.

Lemee, E. and Brown, T. (2002) ‘Small-scale plane strain punch tests’, *Ice in the Environment: Proc. of the 16th IAHR International Symposium on Ice*, 2, pp. 1–7.

Lemee, E. and Brown, T. (2005) ‘Review of ridge failure against the confederation bridge’, *Cold Regions Science and Technology*, 42(1), pp. 1–15.

Leppäranta, M. and Hakala, R. (1992) ‘The structure and strength of first-year ice ridges in the Baltic Sea’, *Cold Regions Science and Technology*, 20(3), pp. 295–311.

Liferov, P. and Bonnemaire, B. (2005) ‘Ice rubble behaviour and strength: Part I. Review of testing and interpretation of results’, *Cold Regions Science and Technology*, 41(2), pp. 135–151.

Lilja, V.P., Polojärvi, A., Tuhkuri, J., Paavilainen, J. (2021), 'Finite-discrete element modelling of sea ice sheet fracture', *International Journal of Solids and Structures*, Volumes 217–218, 2021, Pages 228-258, ISSN 0020-7683, https://doi.org/10.1016/j.ijsolstr.2020.11.028.

Lishman, B. and Polojärvi, A. (2015) ‘2D DEM of ice rubble: The effect of rate-dependent friction’, in *Proceedings of the 23rd International Conference on Port and Ocean Engineering under Arctic Conditions*.

Liu, L. *et al.* (2015) ‘Numerical Simulation of Ice Ridge Gouging’, in *ASME 34th Int. Conf. on Ocean, Offshore and Arct. Eng.At: St. John’s, Canada*.

Løset, S. (1994a) ‘Discrete element modelling of a broken ice field - Part I: model development’, *Cold Regions Science and Technology*, 22(4), pp. 339–347.

Løset, S. (1994b) ‘Discrete element modelling of a broken ice field - Part II: simulation of ice loads on a boom’, *Cold Regions Science and Technology*, 22(4), pp. 349–360.

Løset, S. and Sayed, M. (1993) ‘Proportional strain tests of fresh-water ice rubble’, *J. Cold Reg. Eng.*, 7, pp. 44–61.

Lu, W. *et al.* (2016) ‘Fracture of an ice floe : Local out-of-plane flexural failures versus global in-plane splitting failure’, *Cold Regions Science and Technology*. Elsevier B.V., 123, pp. 1–13.

Marchenko, A. and Chenot, C. (2009) ‘Regelation of ice blocks in the water and on the air’, in *Proceedings of the International Conference on Port and Ocean Engineering under Arctic Conditions, POAC*. Luleå, Sweden, pp. 543–554.

Mohammadafzali, S. *et al.* (2016) ‘Investigation and 3D Discrete Element Modeling of Fracture of Sea Ice Beams’, in *Proceedings of 5th Arctic Technology Conference (ATC2016).* St. John’s, pp. 1–9.

Møllegaard, A. (2012) ‘Experimental study on freeze-bonds in laboratory made saline ice.’

Morgan, D. *et al.* (2015) ‘Simulations of Ice Rubbling Against Conical Structures Using 3D DEM’, in *Proceedings of the 23rd International Conference on Port and Ocean Engineering under Arctic Conditions*.

Murdza, A., Polojärvi, A., Schulson, E. M., and Renshaw, C. E. 'The flexural strength of bonded ice' *The Cryosphere*, 15, 2957–2967, https://doi.org/10.5194/tc-15-2957-2021, 2021.

Oshaug, M. *et al.* (2014) *Ice mechanics, loads on structures and instrumentation*.

Paavilainen, J., Tuhkuri, J. and Polojärvi, A. (2009) ‘2D combined finite-discrete element method to model multi-fracture of beam structures’, *Engineering Computations*, 26(2004), pp. 578–598.

Paavilainen, J., Tuhkuri, J. (2013) 'Pressure distributions and force chains during simulated ice rubbling against sloped structures', *Cold Regions Science and Technology*, Volume 85, 2013, Pages 157-174, ISSN 0165-232X, https://doi.org/10.1016/j.coldregions.2012.09.005.

Palmer, A. and Croasdale, K. (2013) *Arctic offshore engineering*. Singapore: World Scientific Publishing Co. Pte. Ltd.

Parmerter, R. R. and Coon, M. D. (1972) ‘Model of pressure ridge formation in sea ice’, *Journal of Geophysical Research*, 77(33), pp. 6565–6575.

Parmerter, R. R. and Coon, M. D. (1973) *Mechanical models of ridging in arctic sea ice cover*.

Polojärvi, A. and Tuhkuri, J. (2013a) ‘2D FEM-DEM simulations of punch through tests: Effects of partly consolidated rubble deformation’, in *Proceedings of the 22nd International Conference on Port and Ocean Engineering under Arctic Conditions*.

Polojärvi, A. and Tuhkuri, J. (2013b) ‘On modeling cohesive ridge keel punch through tests with a combined finite-discrete element method’, *Cold Regions Science and Technology journal*, 85, pp. 191–205.

Polojärvi, A., Tuhkuri, J. and Pustogvar, A. (2015) ‘DEM simulations of direct shear box experiments of ice rubble: Force chains and peak loads’, *Cold Regions Science and Technology*. Elsevier B.V., 116, pp. 12–23.

Prasanna, M., Polojärvi, A. (2023) 'Breakage in quasi-static discrete element simulations of ice rubble', *International Journal of Mechanical Sciences*, Volume 259, 2023, 108595, ISSN 0020-

7403, https://doi.org/10.1016/j.ijmecsci.2023.108595.

Prodanovic, A. (1979) ‘Model Tests of Ice Rubble Strength’, in *Proceedings of the 5th International Conference on Port and Ocean Engineering under Arctic Conditions, POAC*, pp. 89–105.

Ranta, J., Polojärvi, A. and Tuhkuri, J. (2015) ‘Ice load estimation through combined finite-discrete element simulations’, in *Proceedings of the 23rd International Conference on Port and Ocean Engineering under Arctic Conditions*.

Repetto-Llamazares, A. H. V., Høyland, K. V. and Kim, E. (2011) ‘Experimental studies on shear failure of freeze-bonds in saline ice:. Part II: Ice-ice friction after failure and failure energy’, *Cold Regions Science and Technology*. Elsevier B.V., 65(3), pp. 298–307.

Repetto-Llamazares, A. H. V., Høyland, K. V and Evers, K. U. (2011) ‘Experimental studies on shear failure of freeze-bonds in saline ice: Part I. Set-up, failure mode and freeze-bond strength’, *Cold Regions Science and Technology*. Elsevier B.V., 65(3), pp. 286–297.

Sayed, M. and Frederking, R. (1986) ‘On Modelling of Ice Ridge Formation’, in *lAHR Ice Symposium 1986*. lowa City, USA, pp. 603–614.

Serré, N., Repetto-Llamazares, A. H. V. and Høyland, K. V. (2011) ‘Experiements on the relation between freeze-bond and ice rubble strength, Part I: Shear box experiments’, in *Proceedings of the International Conference on Port and Ocean Engineering under Arctic Conditions, POAC*.

Shafrova, S. and Høyland, K. V (2008) ‘The freeze-bond strength in first-year ice ridges. Small-scale field and laboratory experiments’, *Cold Regions Science and Technology*, 54(1), pp. 54–71.

Shayanfar, H. (2017) *An Experimental Investigation on the Strength and Failure Behavior of*

Freshwater Ice Rubble. Memorial University of Newfoundland.

Shayanfar, H. *et al.* (2018) 'The effects of consolidation time on the strength and failure behavior of freshwater ice rubble', *International Journal of Naval Architecture and Ocean Engineering*. Elsevier Ltd, 10(3), pp. 403–412.

Shayanfar, H., Bailey, E., & Taylor, R. (2022). Medium-scale laboratory investigation of the effect of confinement on ice rubble strength and failure behavior. *Cold Regions Science and Technology,* 202, 103629.

Smirnov, V. *et al.* (1999) 'Large Scale Strength Measurements of Ice Ridges: Sakhalin, 1998.', in *RAO Conference, St. Petersburg*.

Szabo, D. and Schneebeli, M. (2007) 'Subsecond sintering of ice', *Applied Physics Letters*, 90(15), pp. 1–4. doi: 10.1063/1.2721391.

Taylor, R. S. (2010). 'Analysis of scale effect in compressive ice failure and implications for design.' Doctoral dissertation, Memorial University of Newfoundland.

Timco, G., Croasdale, K. R. and Wright, B. (2000) *An overview of first-year sea ice ridges*. National Research Council of Canada, Technical Report HYD-TR-047.

Timco, G. W. *et al.* (1992) 'A laboratory apparatus to measure the behaviour of ice rubble', in *Proc. of Offshore Mechanics and Arctic Engineering Conf*. Calgary, Canada, pp. 369–375.

Timco, G. W. and Cornett, A. M. (1999) 'Is φ a constant for broken ice rubble?', in *Proc. of the 10th Workshop on River Ice Management with a Changing Climate.*, pp. 318–331.

Timco, G. W. and Frederking, R. M. W. (1982) 'Comparative strengths of fresh water ice', *Cold Regions Science and Technology*, 6(1), pp. 21–27.

Timco, G. W. and O.'Brien, S. (1994) 'Flexural strength equation for sea ice', *Cold Regions Science and Technology*, 22(3), pp. 285–298.

Vaudrey, K. D. (1977) 'Ice Engineering: Study of Related Properties of Floating Sea-Ice Sheets and Summary of Elastic and Viscoelastic Analyses', *Naval Facilities engineering Command*, pp. 1–85.

Weaver (1995) *Ice Load Models for First Year Pressure Ridges and Rubble Fields – Phase 1 Report*. Canada.

Weeks, W. and Assur, A. (1967) *MECHANICAL PROPERTIES OF SEA ICE, COLD REGIONS SCIENCE AND ENGINEERING*. Hanover, NH.

Wittmann, W. and Schule, J. J. (1966) 'Comments on the mass budget of Arctic pack ice', in *Proceedings of the Symposium on the Arctic Heat Budget and Atmospheric Circulation*, pp. 215–246.

Yulmetov, R., Bailey, E. and Ralph, F. (2017) 'A Discrete Element Model of Ice Ridge Interaction with a Conical Structure', in *Proceedings of the 24th International Conference on Port and Ocean Engineering under Arctic Conditions*. Busan, Korea.

Zvyagin, P. and Ziemer, G. (2017) 'Study Of Local Ice Loads Measured At Norströmsgrund Lighthouse', in *Proceedings Of The Asme 36th International Conference On Ocean, Offshore And Arctic Engineering, 2017, VOL 8*. Three Park Avenue, New York, Ny 10016-5990 Usa: Amer Soc Mechanical Engineers.

3. EXPERIMENTAL INVESTIGATION ON THE TENSILE STRENGTH OF FRESHWATER FREEZE-BONDS

3.1. Preface

This chapter of this thesis is based on a manuscript titled “Experimental Investigation on the Tensile Strength of Freshwater Freeze-Bonds” published in the journal of Cold Regions Science and Technology. I was the primary author of this manuscript and Dr. Robert Sarracino and Dr. Rocky Taylor co-authored the manuscript. The primary author of the manuscript was in charge of conducting all the experiments, drafting the manuscript, and revising the paper based on the feedback from the co-authors and reviewers. The co-authors helped the primary author with the design of experiments and simulations, providing financial and logistic needs of performing the study, analysing the results, reviewing and revising the manuscript.

3.2. Abstract

The strength of the freeze-bonds between ice blocks has been found to significantly affect the strength and failure mechanism of ice rubble and ice ridges. Limited information on the tensile strength of freeze-bonds is presently available. A new testing apparatus and method has been developed to study the tensile strength of freeze-bonds under submerged, confined conditions as expected in natural ice ridges and rubble. A total of 30 experiments have been carried out to study the effect of normal confinement pressure and submersion time on the tensile strength of freshwater freeze-bonds. The confinement pressures ranged from 25 kPa to 100 kPa and freeze-bonds formed in 5 minutes to 3 hours of submersion. The strength of freeze-bonds has been found to increase with the increase of the confinement pressure. The development of the tensile strength of freeze-bonds by submersion time was found to be similar to the development of the freeze-bond

shear strength. Empirical equations for estimation of the freeze-bond strength as a function of confinement pressure is presented.

3.3. Introduction

Pressure ridges are the most prevalent type of deformed ice feature in the Arctic environment, covering 10-40% of the total volume of drift ice (Leppäranta, 2011). In many ice-covered waters, ridge keels are a dominant feature that play a significant role in the calculation of design loads for offshore structures. They are also a major concern for shipping in ice-covered areas, and can be a danger to underwater infrastructure in shallow water (Timco et al., 2000). As discussed by Croasdale (1996, 1997, 1998), Liferov et al. (2002), Liferov and Bonnemaire (2005), Palmer and Croasdale (2012), Croasdale (2012), Polojärvi and Tuhkuri (2013), Shayanfar (2017), and Afzali *et al*. (2021), the failure of ice rubble is largely controlled by the shear and tensile strength, which is ultimately governed by the strength of freeze-bonds between rubble blocks. The shear strength of the freeze-bond has been investigated by several researchers, but presently, there is limited information on the strength and failure of freeze-bonds under pure tension. This study is aimed to help fill this gap.

When pieces of contacting ice rubble are submerged, they tend to form freeze-bonds (even at low confining pressure). This freeze-bond formation contributes to the shear strength of the ice rubble (Ettema and Urroz, 1989), but uncertainties remain regarding the mechanism and magnitude of this effect. Liferov and Bonnemaire (2005) reviewed failure behavior and strength of ice rubble in existing data to help better understand overall properties and behavior of ice rubble. Liferov suggested that the failure of ice rubble happens in two stages: the primary failure of rubble is dominated by the strength the freeze-bonds between the blocks and the secondary failure which is limited by the overall strength of the rubble accumulation provided by the friction and deformation

resistance of the confined body of rubble. Astrup et al. (2013) also observed this two-stage failure in laboratory shear box experiments, highlighting the role of freeze-bonds in aggregate ice rubble strength. Beyond affecting the strength of ice rubble, freeze-bond strength also can affect the mode of failure. As discussed by Bailey et al. (2015) and Murdza et al. (2021), when freeze-bonds are weak, failure is concentrated at the bond interface, while stronger freeze-bonds can result in failure of the ice blocks themselves rather than at the freeze-bond.

Serré et al. (2011) studied the effect of freeze-bonding on the ice rubble strength in shear box experiments. This study concluded that the failure of rubble starts with freeze-bond failure and as the freeze-bond strength increases, the primary peak of the rubble shear stress during the failure also increases. Serré also suggested that the high strength freeze-bonds would contribute to the formation of large block assemblies. Azarnejad and Brown (2002) carried out a series of laboratory punch tests on freshwater ice rubble, from which the authors concluded that freeze-bonding may also affect the frictional behavior of ice rubble. Lemee and Brown (2002) carried out a similar type of experiments and noticed by decreasing the initial ice temperature (before submersion), the freeze-bonding between the blocks, and therefore the rubble strength, increases. Bruneau (1996), Bailey et al. (2014), Yulmetov et al. (2017), Liu et al. (2015), and Sayed and Frederking (1986) also reported on the effect of the block to block freeze-bond strength on overall behavior of ice rubble.

As discussed by Croasdale (1996, 1997, 1998) and Palmer and Croasdale (2012), the strength of ice rubble under shear and tensile loading is an important consideration in the design of structures for ice. While the shear strength of freeze-bonds has been frequently studied as the main contributor to the strength of the ice rubble, the tensile strength of freeze-bonds has received relatively less attention. Finite element modeling of ice rubble punch tests by Liferov et al. (2002)

highlighted that the lower part of the rubble goes under tension during failure and the tensile strength of the bonds can significantly affect the strength of the rubble. Similarly the model of Croasdale (2012) highlighted that tensile failure was likely to play an important role in ice ridge failure. Subsequently, Polojärvi and Tukhuri (2013) reported from their finite-discrete element simulations that freeze-bonds were observed to fail in tension rather than shear within deforming rubble when modelling ridge keel punch tests. Similar observations were reported from ice rubble beam experiments by Shayanfar (2017), and Shayanfar et al. (2018, 2022) who observed that a considerable portion of freeze-bonds would fail in tension when rubble is subject to flexure.

Murdza et al (2021) used a four-point bending tests to determine the flexural strength of freeze-bonds formed between rectangular ice blocks in air. The parent material in this study was freshwater S2 columnar grained ice and the bonds were formed under 4 kPa of confinement. It was found that the increase in the salinity of the bond material and temperature decreased the strength of the freeze-bond. Both freshwater and saline bonds eventually reached the strength of the intact ice of the same salinity and temperature at different saturation times. In this work the flexural strength of the bond varied between 0 MPa (no bond formed) and 1.7 MPa (strength of the parent ice).

As discussed by Leguillon et al., (2015) the ratio between tensile and flexural strength can vary, with the flexural strength of brittle material typically being between 1-2 times its tensile strength. Ashby and Jones (2012) also suggested that the ratio between tensile and flexural strength of brittle material is around 1.7. Murdza et al (2021) reported that their freshwater flexural strength values were measured to be greater than uniaxial tensile strength values reported in the literature by a factor of about 1.7. This is expected, since the flexural failure of ice is directly governed by local tensile stresses, but only in a small region of the material (under the center indenter in 3-point

testing and between the center indenters in 4 point testing), that carry the maximum tensile stress during flexural loading. In uniaxial tensile tests the entire cross-section of the specimen is loaded. Given that ice is an anisotropic material, this increases the likelihood that the stressed volume will contact larger flaws that can trigger failure at lower nominal stress values than expected for flexural loading; such statistical effects in ice strength have been discussed further by Jordaan et al. (2007) and Taylor (2010).

Szabo and Schneebeli (2007) studied the tensile strength of the bond formed between micro conical ice samples (15 mm in length with a 3 mm radius), made of degassed clear mountain water, in sub-second sintering. The main sintering mechanism in this time scale is freezing of the liquid layer between the two samples. In the current study, focus has been placed on the tensile strength of freeze-bonds formed under submerged conditions for a range of confining pressure of relevance for first-year ice ridges.

To help understand the general behavior of freeze-bonds and the parameters that affect the formation and failure of freeze-bonds, a brief review of available data on the shear strength of freeze-bonds is discussed below.

Ettema and Schaefer (1986) carried out a series of laboratory experiments to determine the effect of confinement, submersion time, bonding area, and salinity on the shear strength of freeze-bonds. They reported that the strongest freeze-bond forms for the zero salinity case (e.g. freshwater ice) and freeze-bonds formed in air (non-submerged) are stronger than the freeze-bonds formed in saline water. Repetto et al. (2011a, 2011b) modified this experimental setup and found that the strength of the freeze-bond declines after 20 minutes of submergence.

Shafrova and Høyland (2008), Høyland and Møllegaard (2014), and Bueide and Høyland (2015) used uniaxial and tri-axial compression test techniques to estimate the shear strength of freeze-bonds. Shafrova and Høyland (2008) noted that the initial properties of ice, confinement pressure, and block size are the main parameters affecting the bond strength. Høyland and Møllegaard (2014) studied the shear strength of the laboratory-made freeze-bond as a function of submersion time, initial temperature, and size. Bueide and Høyland (2015) extended this work to include the effect of confinement, submersion time, temperature, and salinity.

Boroojerdi *et al.*, (2016, 2019a, 2019b) extensively studied the effect of submersion time, initial temperature, deformation rate and confinement pressure on the shear strength of freshwater freeze-bonds. Cylindrical ice samples were confined in an aluminum frame and failed under asymmetrical bending method based on (Frederking and Timco, 1984) and (Bailey et al., 2012). Other studies on the shear strength of freeze-bonds include Møllegaard (2012) and Marchenko and Chenot (2009).

From the studies noted above, the general effect of the studied parameters on the strength of freeze-bonds can be summarised as the followings:

- **Temperature.** The strength of the freeze-bond is highly affected by the initial ice temperature; a lower initial temperature of the ice blocks yields stronger freeze-bonds.
- **Confinement pressure.** The strength of the freeze-bond increases proportionally with confinement pressure during the formation of freeze-bonds.
- **Salinity and porosity.** Increasing both salinity and porosity of ice blocks decrease the strength of freeze-bonds.
- **Submersion time.** The strength of freshwater freeze-bonds initially increases with the submersion time until it reaches an initial peak (about 2-4 minutes). After that, the strength

gradually decreases to a minimum (typically around 3-5 hours) and starts to slowly increase again until it approaches the strength of the parent ice after around a week. The time to reach these different stages also depends on the size and initial temperature of the ice blocks.

- **Strain rate.** The shear strength of freeze-bonds decrease with increasing strain rate. The rate dependency under tension is an area of controversy; it was widely believed that the uniaxial strength of ice would increase with strain-rate, reaching a maximum at a critical value of strain rate and start to decrease afterward (Butkovich, 1954; Gold, 1958). This behavior is regarded as the transition from ductile to brittle behavior (Korzhavin and Ptukhin, 1966). However, Hawkes and Mellor (1972) claim that this decrease would disappear by improving testing techniques.

A review of methods and equipment for testing of ice under tension is provided here. Although none of these methods are specifically designed to test freeze-bonds under tension, this review was needed to understand the benefits and limitations of different approaches to tensile testing of ice, to help inform the design of freeze-bond tests.

To minimize stress concentrations in the vicinity of connectors during uniaxial testing and ensure ice sample fails in the mid-section Peyton (1966) proposed using specimens with reduced central cross-section. This approach was employed by Dykins (1966) who studied the effect of temperature and orientation of grains on the tensile strength of laboratory grown S2 type, columnar-grained ice (mimicking natural sea ice). Tests were conducted by gripping these specimens in matching metal grips and loaded to failure in uniaxial tension.

Hawkes and Mellor (1972) made granular polycrystalline freshwater ice specimens using crushed and sieved ice grains that were placed in a mold and flooded with water. Prior to testing, end caps

were frozen to cylindrical and dumbbell-shaped ice specimens by adding water at freezing point, and specimens were then tested in uniaxial tension. This method was standardized by Schwarz *et al.* (1981) and subsequently used by several researchers for measuring the tensile stress and strain of ice (e.g. Cox and Richter Menge, 1985; Sammonds et al., 1998). Prior to these experiments, it was believed that the tensile strength of ice would decease at high strain rates, but Hawkes and Mellor (1972) indicate that this effect was eliminated by improving the test techniques.

Cole et al. (1985) introduced a new system for mounting the ice in the end caps based on (Mellor et al., 1984). In this method, a fabric-based phenolic material, which develops a strong bond with ice, was used at the contacting surface of the end caps. This fabric-based phenolic material was machined with concentric grooves to increase the exposed fabric area. The fabric-based phenolic material was then soaked in distilled water at freezing temperature and mounted on the saline ice specimen to form a strong bond. Lee (1986) documented this method and recommended it as the standard testing method for measuring the stress and strain of the ice samples during tensile loading. Kuehn et al. (1987) and Richter-Menge and Jones (1993) employed this method for investigating the tensile strength of first-year sea ice.

Sinha (1989) introduced a closed-loop tensile testing system for the testing of multi-year sea ice. In this method, a uniform ice sample was used in the gauge section. Two cylindrical or prismatic built up columnar-grained ice specimens were frozen to the two ends of the sample to form a uniform dog-bone or dumbbell-shaped sample, see Figure 3-1. The two ends of the samples were then pinned to the tensile testing machine to perform experiments.

Figure 3-1 shows 3D and wireframe views of the mounting systems of the methods mentioned above.

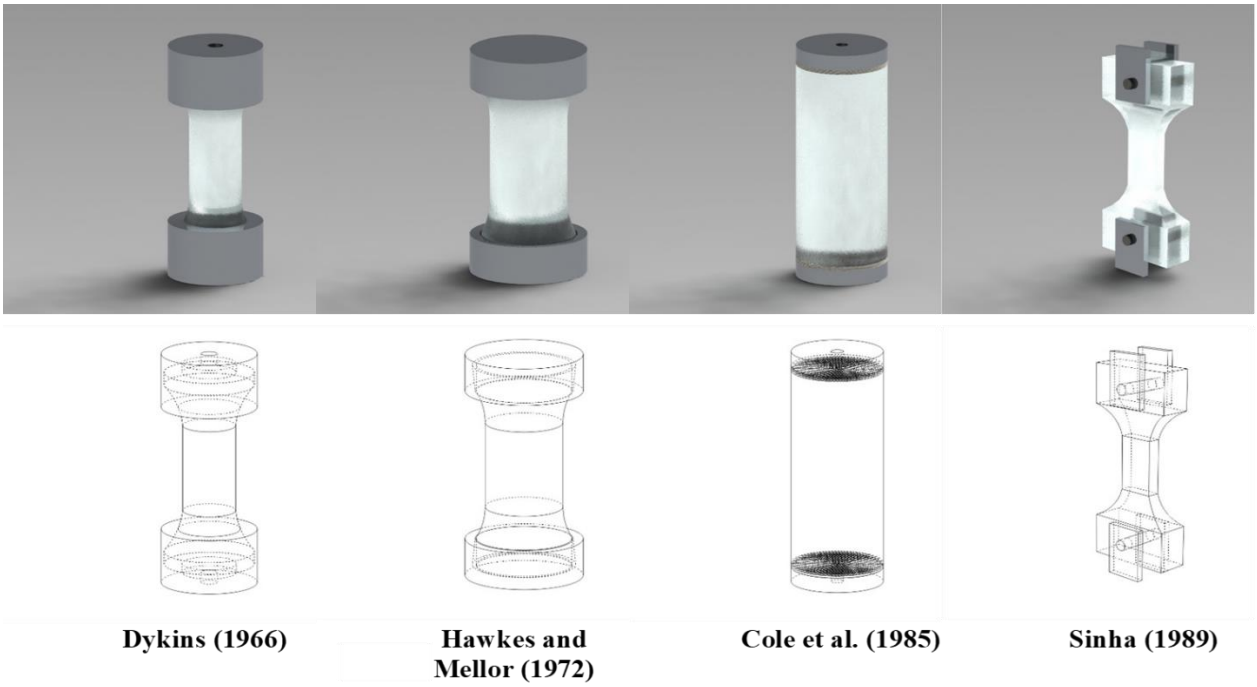

Figure 3-1- CAD models of the current mounting methods for tensile testing of ice

While designs that utilize dumbbell shape specimens and mounting caps present more challenges in terms of apparatus design and sample creation, these types of specimens have proved to be more effective in providing a uniform stress distribution in the cross-section of the samples, with maximum stress occurring in the gauge area.

In this research, a new apparatus and procedure for forming freeze-bonds between two submerged freshwater, polycrystalline ice blocks under confinement and subsequently testing the uniaxial tensile strength of that freeze-bonds are presented, along with a novel set of experimental results obtained using this apparatus. To the authors' knowledge, these test results are the first set of uniaxial tensile freeze-bond strength data reported in the literature. These are intended to fill important knowledge and data gaps in ice freeze-bond properties. This information is needed to advance understanding of ice freeze-bond behaviour, as well as to aid in the development of

numerical models of ice rubble behaviour for which freeze-bonds tensile strength is an important model parameter.

3.4. Methodology and experimental procedure

In this section, the tensile apparatus design, equipment selection, implementation, data acquisition, and test matrix used for the tensile testing of freeze-bonds are summarized.

3.4.1. Tensile apparatus design

This apparatus was designed with end caps inspired by (Hawkes and Mellor, 1972), while also accounting for the need to mount specimens in a confinement frame that can be submerged during the freeze-bonding process. The inside of the two aluminum end caps were lathed into dumbbell shapes to minimize the stress concentration around the circumference of the caps and in the transition zone (from caps to the gauge section). The bottom cap was bolted to an aluminum flange after mounting the ice specimen and connected to the bottom arm of the tensile testing system using a threaded adaptor, as shown in Figure 3-2.

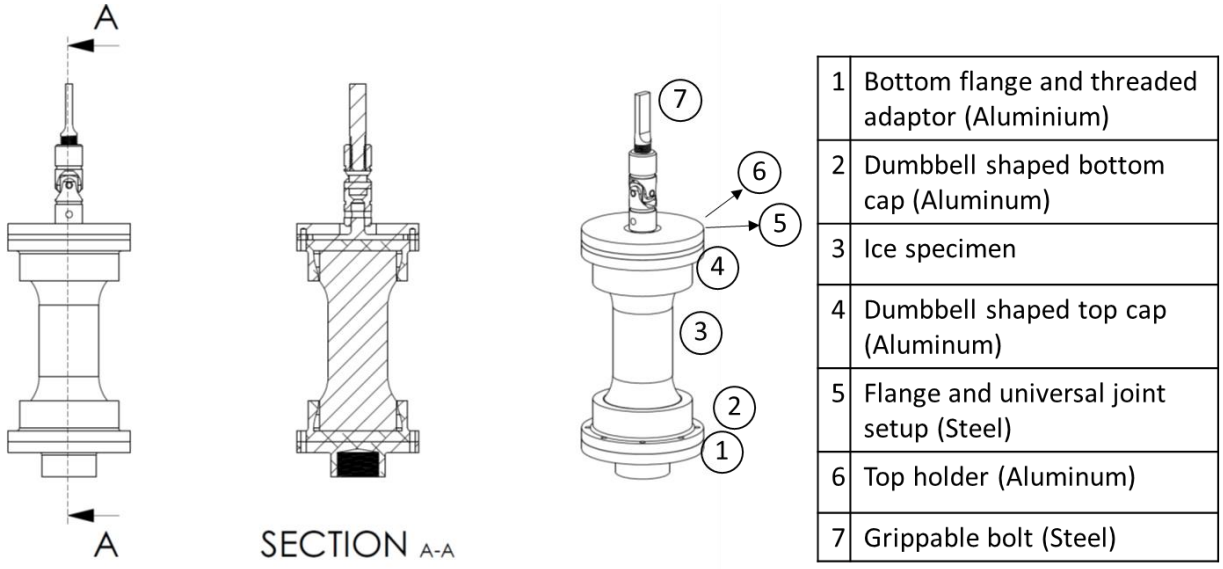

1	Bottom flange and threaded adaptor (Aluminium)
2	Dumbbell shaped bottom cap (Aluminum)
3	Ice specimen
4	Dumbbell shaped top cap (Aluminum)
5	Flange and universal joint setup (Steel)
6	Top holder (Aluminum)
7	Grippable bolt (Steel)

Figure 3-2- Schematic view of the tensile testing apparatus

The top cap was bolted to a stainless-steel flange that had a universal joint welded on the top. The top flange and the universal joint setting were free to move horizontally in an aluminum cup that was holding them vertically. The purpose of using the universal joint, flange and cup setting was to correct possible axial and/or rotational misalignment between two caps and hydraulic rams and to make sure that the tensile force was applied in a direction parallel with the longitudinal axis of the ice sample. The universal joint was connected to a mechanical grip shown in Figure 3-2 using a steel bolt with flats machined on it. Tensile loading was applied through the mechanical grip on the top ram of the hydraulic powered Materials Testing System (MTS).

3.4.2. Data acquisition system

A Data Acquisition System (DAQ) was used to collect measurements of the physical conditions during the experiments and convert the results to digital values that are stored and processed on a computer. The components of the DAQ system used in these experiments include the following:

- Analog-to-Digital Converter and Signal Amplifier: Sensors were connected to an 8 channel HBM Universal Measuring Amplifier, where the output voltages and currents from the sensors were transformed into digital input, amplified and exported to the computer for collection and processing.
- Resistance Temperature Detectors (RTDs): During the experiments, four RTDs were used to measure the temperature of the cold room and freezing water bath precisely, to ensure the prescribed thermal conditions were maintained. The RTDs used in these experiments were wire-wound RTDs with operating temperature range of $-50℃ - 200℃$ and accuracy of $0.3℃$ at freezing temperature.
- Load Cells: Three 900 N Compression Load Button load cells with 0.9 N accuracy were used to measure the confinement force on the ice specimens in the confinement frames. An

MTS machine load-cell was used to measure the uniaxial force applied to the samples during the failure. The calibration of the MTS load cell was verified against known dead loads at 0°C which covered a range of magnitudes similar to those measured during the experiments. From these sensitivity tests the MTS load cell was verified to have an acceptable maximum measurement error of ~1% for the lowest range of freeze-bond strengths.

- Materials Testing System (MTS): The tensile testing of the freeze-bonds was done using the MTS servo-hydraulic testing machine, where the freeze-bond tensile strength was measured. One end of the apparatus was bolted onto the bottom plane of the MTS, and the other end was fastened onto the mechanical grip of the MTS. The upper arm of the MTS moved vertically upward to break the ice samples by inducing tensile stress using a hydraulic system. The displacement data was measured by the internal Linear-variable Displacement Transducers (LVDT) of the MTS system.
- High-speed Camera: A high-speed camera was used to record the freeze-bond failure and the resulting video was played back in slow motion to gain a better understanding of the mode of failure.

3.4.3. Sample preparation

In the preparation of the ice samples, the same ice making approach as Boroojerdi et al., (2016, 2019a, 2019b) has been used. In this method, freshwater unseeded ice samples are frozen in 1 m rectangular steel trays at −18°C. The ice is then cut to smaller pieces and lathed to from cylindrical samples. Readers are referred to these references for additional detail about ice properties. It is noted that this ice making approach was used instead of standard laboratory polycrystalline ice preparation techniques in order to provide consistency with ice making used in earlier large-scale

ice rubble tests carried out by the team (e.g. Bailey et al, 2014) in which industrial-scale volumes of freshwater ice needed to be produced for the near full-scale keel experiments. Following this process, fresh tap water was first poured into a tray with dimensions of 1m × 1m × 0.12m then kept in a freezer at -18°C for a week. Segments of clear, defect free ice were cut from each tray, which were then roughly cut into cuboid shapes of dimensions 12cm × 12cm × 40cm. A band saw was used to reduce the ice samples again to a cuboid shape with dimensions 11cm × 11cm × 30cm. A c-bracket was then used to hold the ice sample and cut off the edges with the band saw to form octagonal prisms. Once the ice samples were in an octagonal prism shape, it was easier to lathe them into a cylindrical shape. The ice samples were mounted in the lathe and turned into cylinders with a diameter of 9.00 (±0.002) cm. Finally a milling machine was used to cut off the ends of the ice specimens giving a final length of 21.00 (±0.002) cm. All the machining steps were performed in a cold-room at -18°C.

The cylindrical sample preparation method, dimensions, and equipment are based on Boroojerdi et al. (2019a, 2019b) to make their experimental results comparable with shear experiments on the freeze-bonds of the same dimensions. Samples used in this study and the Boroojerdi et al. (2019a, 2019b) study are unseeded freshwater polycrystalline ice. The ice samples were mounted back onto the lathe machine, and a custom-made blade was used to lathe the ice sample into a dumbbell shape. Dumbbell shaped samples reduce the stress concentration around the circumference of caps and in the transition zone (around the edge of the aluminum caps) and provide a central gauge section in the middle of the specimen that increases the chances of failure at the freeze-bond. Figure 3-3 shows a schematic view of the dumbbell shape and cylindrical samples used in this study. The actual diameter and length of the gauge section vary by sample, as a manual lathing machine was used to reduce the samples.

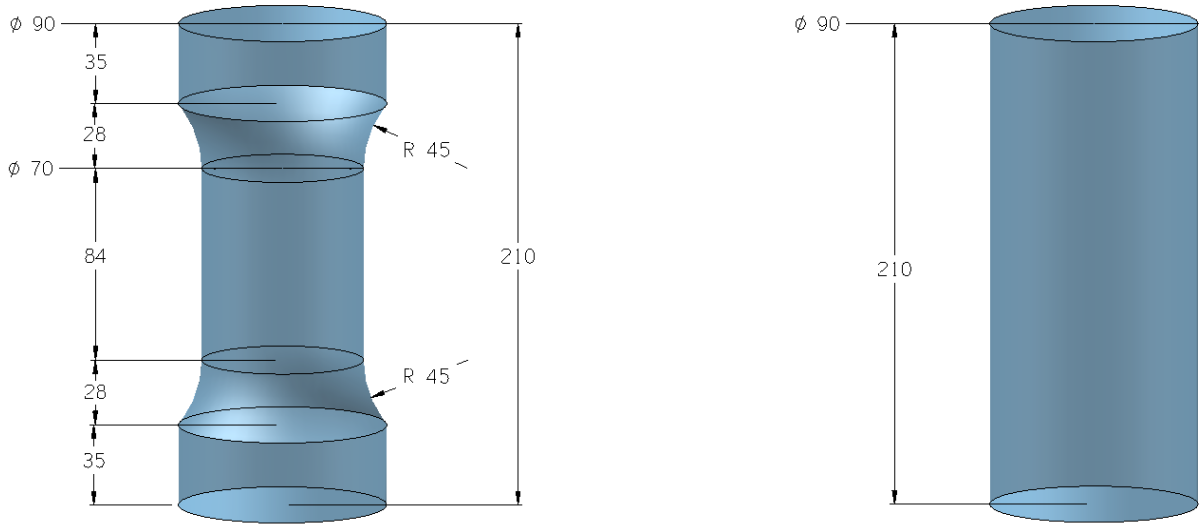

Figure 3-3- Schematic view of the dumbbell shape (left) and cylindrical (right) ice specimen, all dimensions are in millimeters

3.4.4. Experimental procedure

In conducting the experiments, dumbbell shaped specimens were the primary type of specimen used. In the 5, 10, 15, and 30 minutes submersion experiments, dumbbell shaped specimens were used to help ensure the samples failed at the freeze-bond. It was noted during the first few experiments for the 3-hour submersion tests that samples with reduced cross sections (the dumbbell-shaped samples) were prone to damage or failure during mounting, due to the fragility of the freeze-bonds at this submersion time. Only Test 19 was successfully mounted with no damage for the 3 hour submersion time. Consequently, for the remaining tests done at these long submersion times, the cross sections were not reduced

In all cases, the samples were mounted on dumbbell shaped end caps, which helped avoid stress concentration on the ends. Since the strength of the freeze-bonds in the 3-hour submersion time experiments were lower than other submersion times, all the samples failed at the freeze-bond.

To mount the samples, first, each ice specimen was cut into two equal parts using a band saw and a custom-made jig. Each half of the specimen was then mounted into a dumbbell shaped end cap by adding freshwater at freezing temperature around the ice. Two specially designed plastic vertical holders were used (Figure 3-4) during the mounting of the samples to ensure that the specimens are mounted perfectly at the center of the caps. The mounted specimens were then put in a freezer at -18°C for 24 hours.

An aluminium confinement frame was used to apply normal pressure to the two ends of the ice specimen through six linear springs, as shown in Figure 3-4, which were used to achieve the desired confinement pressure during submersion. The normal confinement load was measured using an inline loadcell. Load was applied on the specimen using a manual screw adjustment mechanism.

The two end caps were mounted onto the confinement frame, as shown in Figure 3-4, where a set normal confinement force was applied to them. Two support wedges were used during the confinement and submersion to ensure the two ends were aligned. The confinement frames were submerged in a freshwater bath at freezing temperature for a set duration. No visible thermal cracking of the ice specimens were noticed after submersion. When the desired time was reached, the confinement frames were taken out of the bath, and the ice samples were removed from the frame. Next, the two end-caps holding the ice specimen were bolted onto the MTS. The top arm of the MTS was fixed during the experiments while the bottom arm moved at the constant vertical rate of 5mm/s. The experiments were conducted in a temperature controlled cold-room at 0°C. The diameter of the samples grew by 1 to 5 mm during the submersion, depending on the sample shape and submersion time. The final diameter of the samples were used for calculating the cross-sectional area.

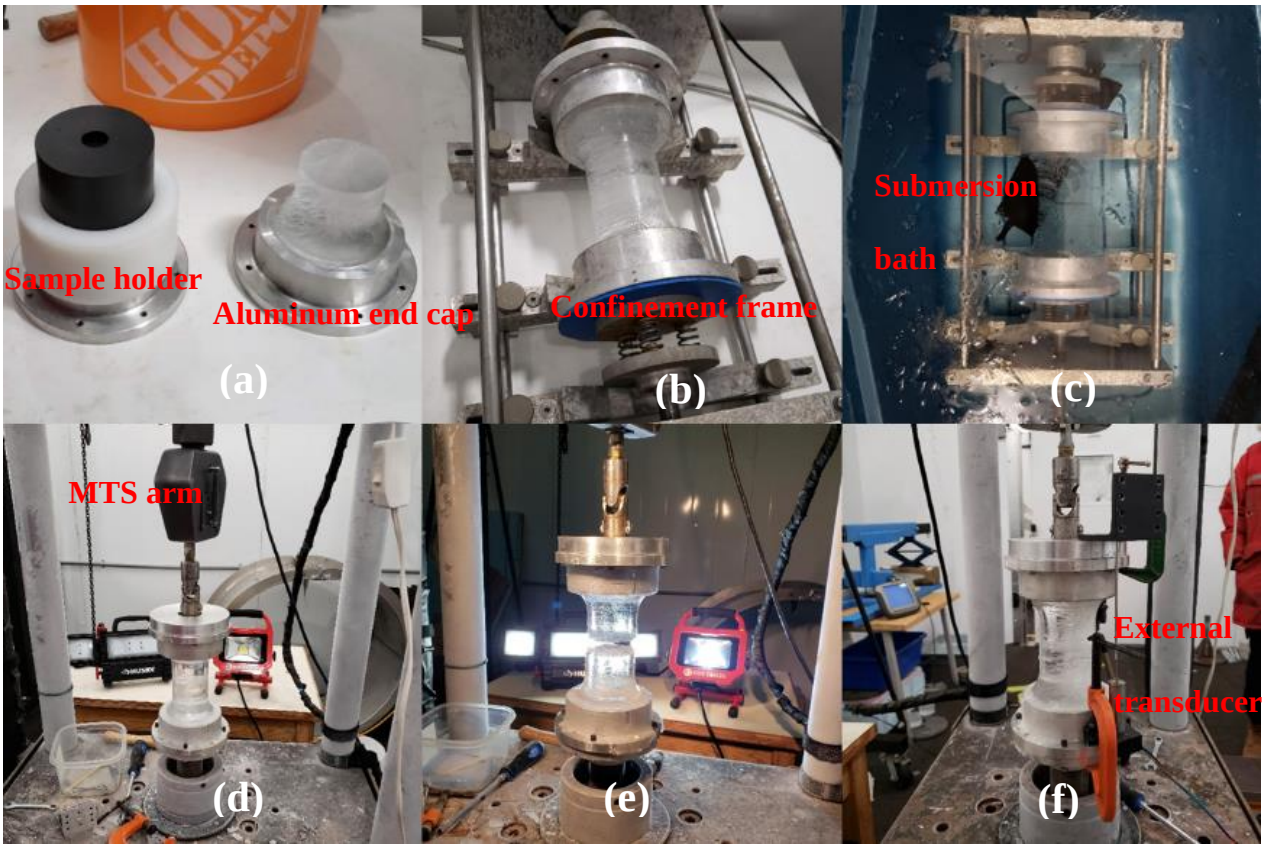

Figure 3-4- Experimental procedure, a: mounting the specimens using plastic holders, b: confinement, c: submersion, d: specimen before failure, e: specimen after failure, f: installation of an external transducer for verification of strain

The MTS load-cell was used to measure the tensile load, and the internal displacement transducer of the MTS was used to measure the displacement during the tests. To ensure the readings of the displacement were purely due to the displacement of the sample, the thickness and material selection for the components of the tensile testing apparatus were set to minimize the deformation on the apparatus components. For narrow cross-section components Aluminum was replaced by stainless steel. The cross-sections and Young's modulus of the components were compared to the ones from ice to ensure that the deformation of the components was negligible compared to ice. To provide additional verification, deformation measurements were taken in three experiments using a displacement transducer mounted on the end caps (Figure 3-4). In all three cases, the

measurements from the internal transducer were within 3% of the readings from the external transducer.

3.5. Results and Discussion

The results of 30 tensile experiments are presented in this section, as summarized in Table 1. The experiments focused on investigating the effects of confinement pressure and submersion time on the tensile strength of freshwater freeze-bond. This series of tests included studying the formation of the freeze-bonds for nominal confinement pressures of 25 kPa, 50 kPa, 75 kPa, and 100 kPa, and submersion times of 5 minutes, 10 minutes, 15 minutes, 30 minutes and 3 hours; the deformation rate was 5mm/s for all tests. The corresponding strain rates were $3.6 \times 10^{-2}\ s^{-1}$ for cylindrical samples and $6 \times 10^{-2}\ s^{-1}$ for dumbbell samples. Experiments were repeated three times to assess repeatability and help quantify uncertainty in the results. Experiments 28 was repeated only two times and experiment 30 was not repeated. This was due to the logistical impacts at the beginning of the COVID 19 pandemic. These experiments were the last experiments in the program, and with the limitations introduced during this time, the author was not able to repeat these experiments.

The temperature of the cold room, the temperature of the freezing water baths, normal confinement load during the submersion, and stress and deformation of the specimen during tension have been monitored and recorded during all experiments. Moreover, a high-speed camera was used to record selected experiments at frame rates between 2000 to 4000 fps. These slow-motion videos were helpful in providing additional insight into failure modes that occurred during the experiments. Table 3-1 shows the test matrix and strength results of the experiments and Figure 3-5 shows typical outputs of the test results.

Table 3-1- Freeze-bond tensile test matrix, deformation rate is 5 mm/s for all tests

Test #	Submersion Time (minutes)	Nominal Confinement Pressure (kPa)	Actual Confinement Pressure (kPa) (Average of the Time Averaged Pressures)	Number of Repeats	Average Strength (kPa)	Repeat 1 Strength (kPa)	Repeat 2 Strength (kPa)	Repeat 3 Strength (kPa)	Standard Deviation	Coefficient of Variation
1-3	30	25	25.2	3	117	65	151	135	37	32%
4-6		50	50.8		264	221	340	232	54	20%
7-9		75	73.9		289	292	242	334	38	13%
10-12		100	98.2		381	391	440	313	52	14%
13-15	180	25	24.8	3	68	70	74	60	6	9%
16-18		50	49.1		156	122	197	149	31	20%
19-21		75	75		270	169	327	314	72	27%
21-24		100	97.2		333	333	240	425	76	23%
25-27	5	25	25.1	3	347	213	430	397	95	28%
28-29	10	25	24.9	2	296	308	284	NA	12	4%
30	15	25	25.1	1	183	183	NA	NA	NA	NA

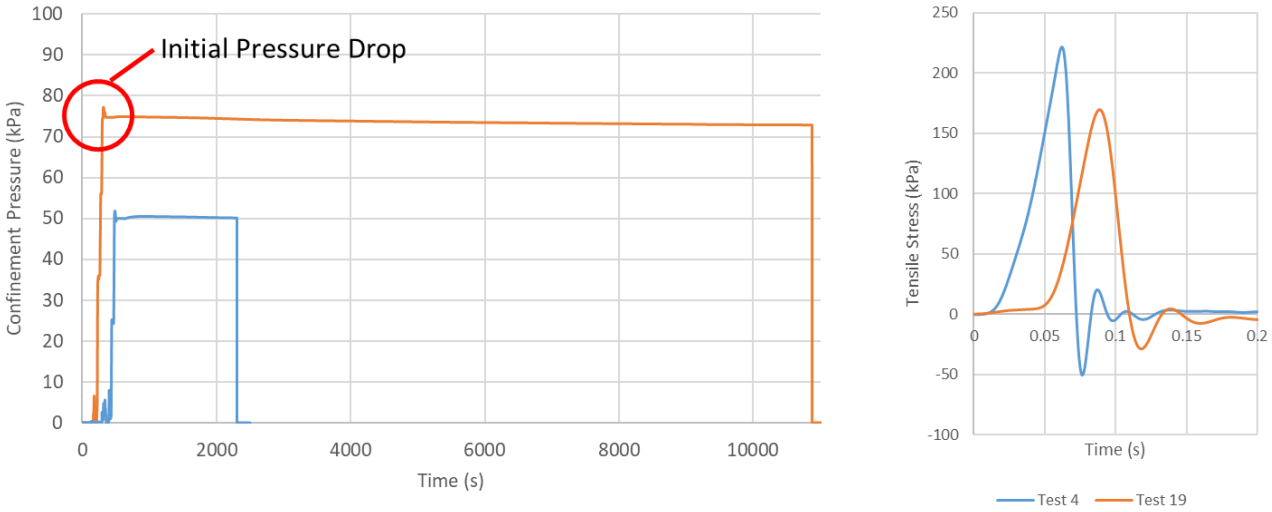

Figure 3-5- Normal confinement pressure during submersion (left), and tensile stress during failure (right) for two typical experiments

It is noted that the actual confinement pressures are slightly different than the nominal values. As illustrated in Figure 3-5, the confinement pressure dropped slightly after submersion. This effect was shown to be due to creep of the ice under pressure and corresponding relaxation of the springs (Boroojerdi et al., 2020b). Consequently, slightly higher confinement pressures were applied initially to compensate this effect. It is also noted that the effect of spring relaxation was more pronounced for higher confinement pressures and higher submersion times and correspondingly the pressure drop was not fully compensated in these experiments. The temperature of the water bath remained close to the freezing temperature and fluctuates between 0°C and 0.2°C for all experiments.

The strength results show a linear relationship between the confinement pressure (p_c) during the formation of the freeze-bond and the tensile strength (σ_T) of the freeze-bond in both cases of 30 minutes and 3 hours submersion. The average tensile strength, however, is 21.4% lower for the submersion time of 3 hours, see Figure 3-7 and Equation 1-2 in Section 3.5.2.

Several measures were taken to minimize the uncertainty in the experimental results. Experiments were repeated, in most cases, three times; this reduces uncertainty by providing more data points, increasing statistical reliability, and allowing for a better understanding of variability and potential outliers. Deformation of the sample gauge was measured using an internal and an external transducer to ensure reliability. The two ends of the ice samples were milled to minimize the effect of eccentricity on pure tensile behavior and the temperature of the freezer and water bath, as well as the confinement pressure during submersion, were continuously monitored and controlled.

However, as shown in Table 3-1, coefficient of variation between 4% and 32% were observed for the experiments. Many factors may contribute to this uncertainty. The freshwater source for ice making and freezing baths was tap water. The presence of impurities such as dirt, debris, water

treatment chemicals or entrained air, if present within the ice could introduce uncertainties on its mechanical properties. Inclusions can create weak points or affect the overall structural integrity. Moreover, the size and orientation of ice grains of the polycrystalline ice samples may vary between the samples taken from different parts of the ice trays. Additionally, the process of cutting the ice samples in the middle with a band saw, could introduce a randomly variable roughness into the surface of the ice and hence affect the effective contact area, and subsequently tensile strength, of the samples.

3.5.1. Mode of failure

Brittle failure is typically characterized by suddenly and unstable failure with no permanent deformation, whereas ductile fracture tends to remain stable and only grow if the load is further increased, with observed necking down of the area typically observed around the failure zone.

For all experiments in this test program, failure was brittle in nature and exhibited characteristic sharp and sudden drops in measured tensile force, see Figure 3-5 (right) with no evidence of permanent deformation as shown in Figure 3-6.

Figure 3-6- Photo of a reduced (dumbbell shape) sample after failure

For solid freshwater ice under tension, Hawkes and Mellor (1972), Schulson (1979), and Kuehn *et al.* (1987) reported that the mode of failure would change from ductile to brittle at strain rates of around $10^{-3}\ s^{-1}$. As the tensile strain rates used in this study were $3.6 \times 10^{-2}\ s^{-1}$ (for cylindrical samples) and $6 \times 10^{-2}\ s^{-1}$ (for dumbbell samples) the observation of brittle failure of the freeze-bond is consistent with the findings of Hawkes and Mellor (1972), Schulson (1979), and Kuehn *et al.* (1987).

3.5.2. Effect of confinement

The results show that the tensile strength of freeze-bonds increases proportionally with the confinement pressure during the formation of the freeze-bond. In this section, the possible mechanisms behind this behavior are discussed.

Sintering is the "formation of bonds between particles close to their melting point." At the contact points of submerged ice blocks at the melting temperature, sintering can play an important role even in very short periods of time. While many mechanisms of sintering such as vapor diffusion,

surface diffusion, surface flow, volume diffusion, plastic flow, and grain boundary diffusion are rather slow, the melting and re-freezing of a liquid layer between ice blocks at contact points can result in fast bonding (Szabo and Schneebeli, 2007).

When two ice particles collide, highly localized deformations may generate heat, which can result in local melting of ice. If this heat is eventually conducted away from the melted layer, it will freeze again (Szabo and Schneebeli, 2007). In the current experiments, since no collision happens between the two blocks, this mechanism cannot be considered a contributor to sintering for the conditions considered in this study. However, pressure melting and the liquid layer on the surface of the ice, can both contribute to sintering at very short times. When two pieces of contacting ice are confined, localized pressure melting may occur due to roughness of the ice surface, especially at asperities. The newly melted ice can refreeze rapidly, especially when the temperature of the blocks are low, and form a bond between the two ice pieces (Ettema and Schaefer, 1986; Kingery, 1960). Thomson (1862) indicates that “any” stress can change the form of ice submerged in freezing water and cause melting and regeneration of new ice. Higher confinement between the blocks increases the amount of melted ice and hence can contribute to formation of a stronger bond. Moreover, high confinement pressures may squeeze the sandwiched film of water between the two pieces and lead to rapid development of a stronger freeze-bond (Ettema and Schaefer, 1986).

Another mechanism that can contribute to the influence of confinement pressure on the strength of freeze-bonds is the crushing of the ice asperities. The real contact area of the two adjacent pieces of ice is much smaller than the nominal contact area since contact actually happens at the contacting asperities of the neighboring ice blocks, not over the entire contact surface (Schulson, 2015). Increasing the normal confinement pressure may result in creep and crushing of these

asperities and hence increase the contact area between the two blocks. Greater contact area would increase the total freeze-bond area and so the total strength of the freeze-bond. Moreover, the compacted ice particles resulting from crushing of the asperities may nucleate new crystals of ice and strengthen the bond between the blocks. Figure 3-7 shows the increase of freeze-bond tensile strength by increasing the confinement pressure for 30 minutes and 3 hours of submersion.

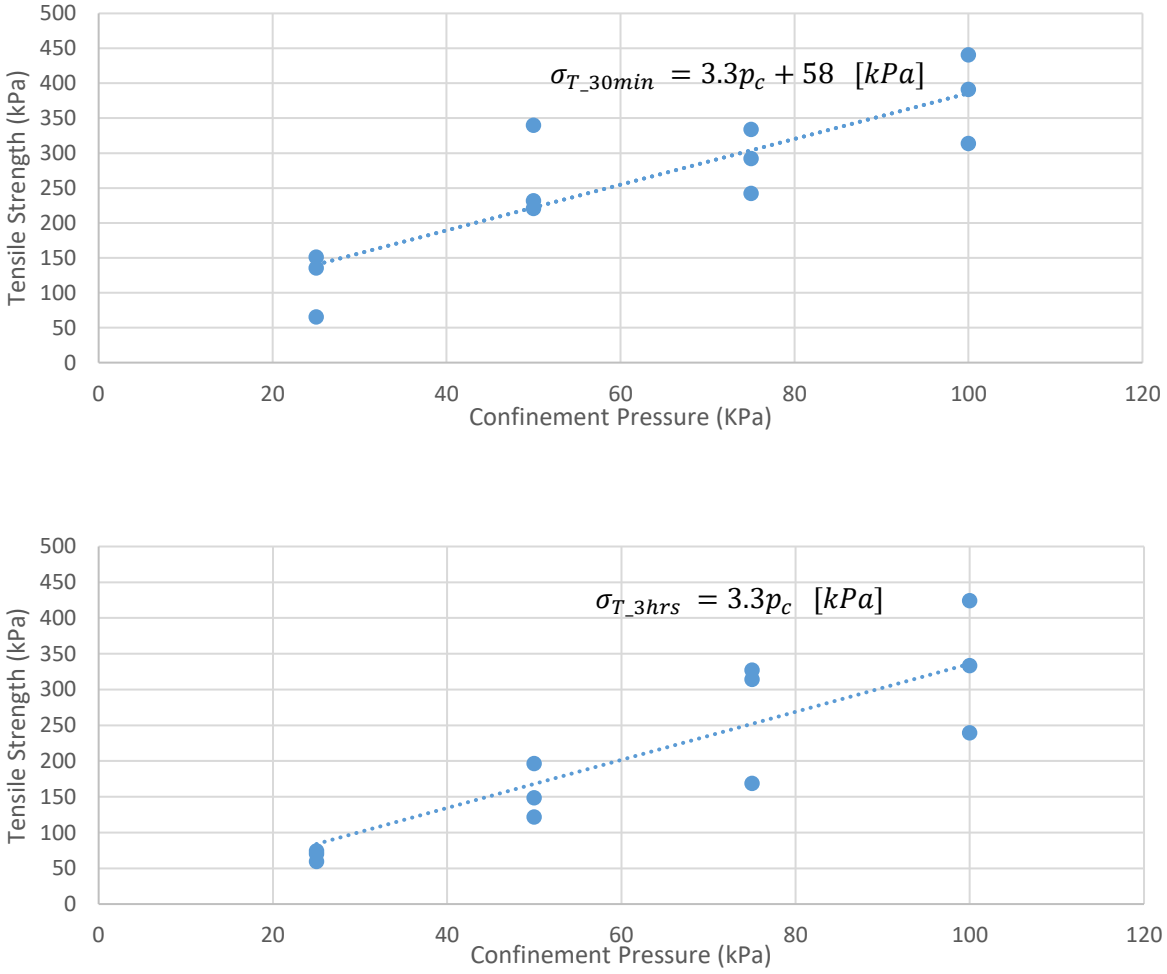

Figure 3-7-Tensile strength vs. normal confinement pressure for 30 minutes (top) and 3 hours (bottom) of submersion

The linear relationship between the normal confinement pressure p_c and tensile strength of the freeze-bond σ_T for the freshwater ice with initial temperature of -18°C is:

$$\sigma_{T\_30min} = 3.3p_c + 58 \quad [kPa] \qquad (3\text{-}1)$$

$$\sigma_{T\_3hrs} = 3.3p_c \quad [kPa] \qquad (3\text{-}2)$$

The R-squared values for the fitted lines are 0.75 and 0.76, respectively. As expected, (see Section 3.5.3 for detailed discussion around effect of submersion time), the freeze-bond strength that resulted from 30 minutes of submersion is higher than the tensile strength for the 3-hour submersion times. It is noted that while the effect of confinement on the tensile strength of freeze-bonds seems to be the same for 30 minutes and 3-hour submersion times (i.e. bonds under all confining pressures weakened at the same rate during submersion), additional tests are recommended to determine if similar trends are observed for submersion times shorter or longer than those considered here, and to determine the submersion time required for the freeze-bond tensile strength to approach that of the parent ice.

Ettema and Schaefer (1986), Serré et al. (2011), Bueide and Høyland (2015), and Bailey et al. (2012) reported an increase of the freeze-bond shear strength by increasing the confinement pressure during the formation of freeze-bonds. Similar trends of increasing freeze-bond shear strength with increasing confinement were reported by Boroojerdi (2020) who measured the shear strength of freeze-bonds subjected to the same level of confinement under which the bonds were formed.

Since Boroojerdi (2020) considered the same range of confinements as has been used in the present work, the ratio between the freeze-bond shear strength τ and tensile strength σ_T as a function of confinement may be calculated. As may be seen in Figure 3-8, the average τ / σ_T ratio for

confinements between 25 kPa and 100 kPa was found to be between 0.4 and 0.9. While this ratio tend to be higher for the 25 kPa confinement cases, no clear trend is evident for pressures above 50 kPa.

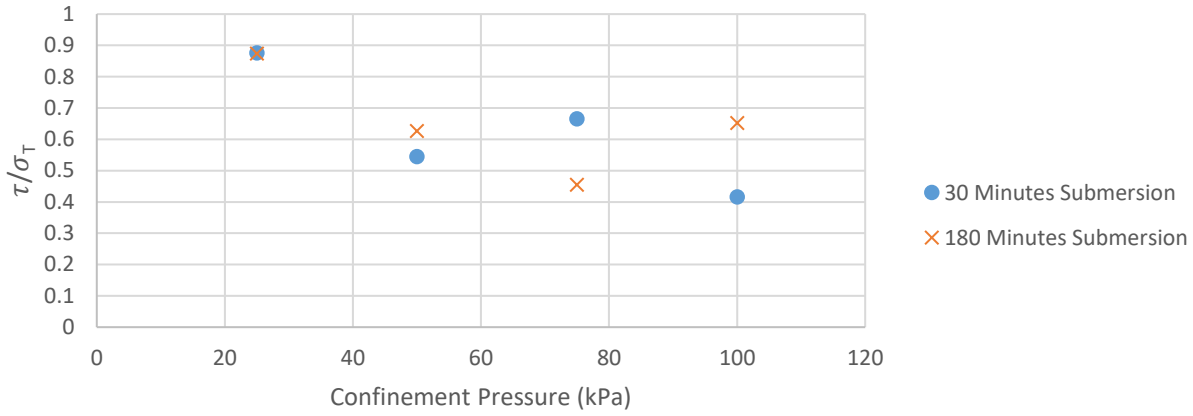

Figure 3-8- Confinement pressure vs shear strength to tensile strength ratio

3.5.3. Effect of submersion time

The experimental results show that the tensile strength of freeze-bonds decreases as the submersion time for the formation of the freeze-bond increases from 5 minutes to 3 hours. Previous studies by Boroojerdi et al. (2020b), Høyland and Møllegaard (2014), Bailey, Sammonds and Feltham (2012), and Shafrova and Høyland (2008) showed similar behavior for the shear strength of the freeze-bond. Boroojerdi et al. (2020b) state that the shear strength of freeze-bonds increases rapidly at the beginning of submersion and reaches a maximum at around 2 to 4 minutes of submersion and gradually decreases to its minimum at 3 to 5 hours. Høyland and Møllegaard (2014) also reported a sharp increase in the strength of freeze-bonds at the first few minutes of submersion and reduction of the strength after this peak value.

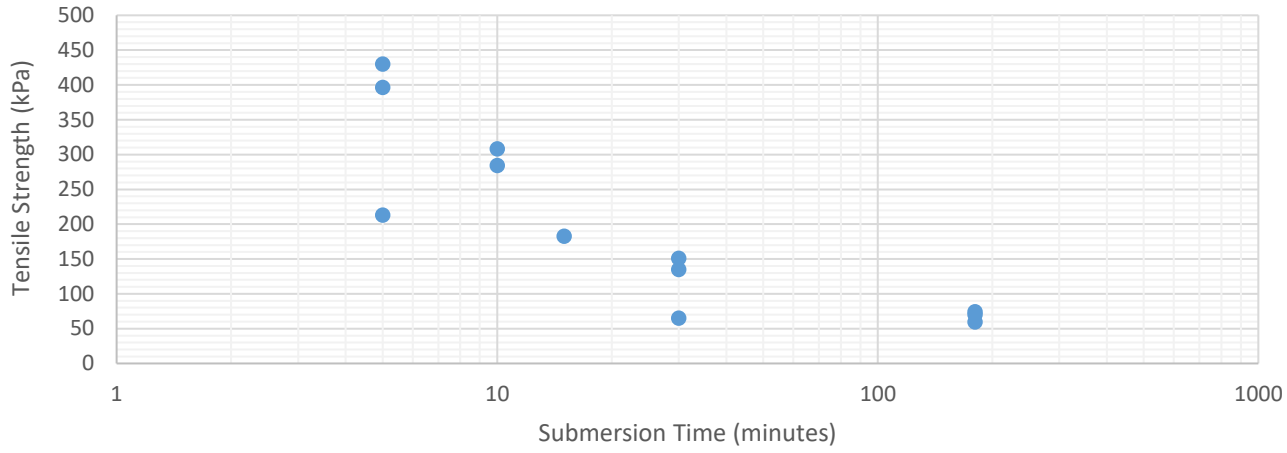

Figure 3-9- Tensile strength of freeze-bonds vs submersion time at 25 kPa confinement pressure

Immediately following submersion, the development of the freeze-bond is dominated by thermal processes. Since the initial temperature of the ice blocks (-18°C) is significantly lower than the surrounding water bath (0°C), heat transfer from water to the ice blocks results in the formation of new ice between and around the ice blocks. Based on temperature measurements by Boroojerdi et al. (2020b), it is apparent that the ice remains quite close to its initial temperature for the first few minutes of freeze-bond formation and it is expected that the freeze-bond itself will quickly equilibrate with the temperature of the surrounding ice. As time proceeds, the entire ice specimen (and correspondingly the freeze-bond) will warm up as heat is transferred from the surrounding water to the ice specimen. As a result, it is expected that the strength of the freeze-bond formed from thermal processes will reach its peak early in this process. As the freeze-bond between the blocks gets warmer, the strength of the bond decreases and in the case of shear strength (see Boroojerdi et al., 2020b) reaches its minimum in 3 to 5 hours, see Figure 3-9. Similarly, Repetto et al. (2011b) tested the shear strength of freeze-bonds formed between saline columnar grained ice under confinement and found that the maximum freeze-bond strength (30 kPa) was measured

for short submersion times (1-20 minutes), the freeze-bond strength reaching a minimum after around 5 hour when ice and water bath reached a thermal equilibrium at the freezing temperature. For longer submergence times (up to 1 week) Boroojerdi et al., (2020b) reported that sintering and creep processes are believed to play a more dominant role, resulting in internal microstructural modifications that reduce local stress concentrations and processes that strengthen the freeze-bond. It would be of high interest to extending the work of Repetto et al. (2011b) to longer submersion to verify if similar effects for saline ice freeze-bond occur as those observed for freshwater ice reported by Boroojerdi et al., (2020b).

The strength of the freeze-bond in shear direction, slowly increases after reaching its minimum and meets the strength of the parent ice several days after submersion, this time depends on the initial conditions and confinement pressure (Boroojerdi et al., 2020b). It is expected that the strength of the freeze-bond in tensile direction also follow the same behavior. Conducting long-time submersion experiments to verify this assumption would be highly beneficial for future work.

Temperature measurements by Boroojerdi et al. (2020b) at the centers of samples with the same dimensions, properties, initial temperatures, and water bath temperatures as this study have shown the temperatures of the ice cores at 0, 5, 10, and 50 minutes after submersion to be -18°C, -10°C, -4°C, and 0°C respectively, with the temperatures remaining at 0°C (bath temperature) beyond 50 minutes. Such observation help explain why the tensile strength of freeze-bonds would not change notably after 30 minutes of submersion and before the effects of sintering become significant.

Considering the results of shear experiments by Boroojerdi et al. (2020b) it can be seen that the submersion time effect on the freeze-bond shear strength is similar to as observed for freeze-bond tensile strength. A peak strength at 5 minutes of submersion time is observed in both modes of failure, followed by a decline in strength up to 3 hours of submersion. Based on these results the

ratio of shear strength to tensile strength for unseeded polycrystalline freshwater ice may be calculated as being between 0.5 and 0.9 over the range of submersion times. As shown in Figure 3-10 for this range of submersion time, the shear strength to tensile strength ratio tends to increase with increasing submersion time. Additional experiments covering a wider of submersion times is recommended in the future.

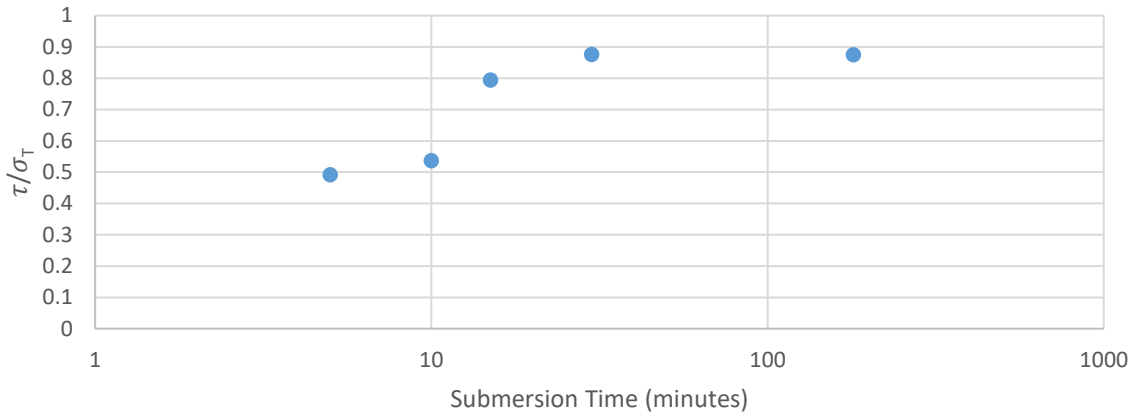

Figure 3-10- Submersion time vs shear strength to tensile strength ratio at 25 kPa confinement pressure

This is an important finding since the development of the shear strength of freeze-bonds by submersion time is well studied by Boroojerdi et al. (2020b) and relating the shear strength to the tensile strength of freeze-bonds provides valuable insight and an approach for estimating the tensile strength development in terms of shear strength values, which is of particular interest for numerical modelling approaches such as those in Afzali et al. (2021) in which the ratio of shear to tensile strength of bonds between DEM particles is a model input parameter. The data obtained here allows for such model inputs to be based on measured data, and allows for future development of confinement dependent DEM bond strength models, since the degree of confinement in a

simulated keel will depend on the size of the keel and the location, size and contact geometry between the ice rubble blocks within the ice ridge.

3.6. Summary and Conclusion

The tensile strength of freeze-bonds is a critical mechanical property of ice that significantly influences the strength and failure mechanism of ice ridges and ice rubble. Little information on the pure tensile strength of ice freeze-bonds, particularly for the states of confinement of interest for natural deformed ice features, is presently available. A testing method has been developed to examine the tensile strength of freeze-bonds under submerged, confined conditions using a new apparatus. A total of 30 experiments have been carried out to study the effect of normal confinement pressure and submersion time on the tensile strength of freshwater freeze-bonds. The confinement pressure ranged from 25 kPa to 100 kPa, with freeze-bonds forming between 5 minutes and 3 hours of submersion.

The results of the experiments indicate that the mode of failure in all conducted experiments at strain rates of $3.6 \times 10^{-2}\, s^{-1}$ and $6 \times 10^{-2}\, s^{-1}$ was brittle failure. No degradation of the specimen gauge section was observed prior to failure and the specimens failed immediately after reaching the maximum force.

The tensile strength of freeze-bonds was observed to increase proportionally with an increase of confinement pressure during the formation of freeze-bond. The tensile strength of freeze-bonds decreases by around 21% by increasing the submersion time from 30 minutes to 3 hours. The weakening of the freeze-bond over this timeframe is believed to be due to the increase of the freeze-bond temperature around the center of the blocks, as well as potential effects on the freeze-bond microstructure. Future experiments to study such details are recommended.

In the initial stages of the development of freeze-bond tensile strength, the same mechanisms will dominate as those that were noted to contribute to the development of the shear strength of freeze-bonds. Following submergence of a confined specimen, thermal bonding is initially expected to be the dominate mechanism of freeze-bond development, which may also be enhanced by localized crushing, as well as pressure-melting and refreezing of asperities due to combined confining pressure effects. Results from the present experiments, as well as experiments by Boroojerdi et al. (2020b) are consistent with this rationale. For tensile strength testing, additional experiments covering a wider range of submersion times are recommended in the future to further quantify these time-dependent aspects of behaviour. Tensile and shear strength of freeze-bonds notably increase with an increase of confinement pressure, but the slope of this increase is higher for the tensile strength.

Comparing with the data from Boroojerdi (2020), the shear strength to tensile strength ratio for freeze-bonds in unseeded freshwater polycrystalline ice was calculated to range between 0.4 and 0.9 for the conditions considered in this program. Additional experiments covering a wider range of submersion times and confinement pressure is recommended in the future. Further investigation on the effect of strain rate on the tensile strength of freeze-bonds is also recommended for future work.

3.7. Refrences

Afzali, S., Taylor, R., Bailey, E., Sarracino, R., & Boroojerdi, M. T. (2021) 'Investigation of the Effect of Block Size, Shape, and Freeze Bond Strength on Flexural Failure of Freshwater Ice

Rubble Using the Discrete Element Method', *Journal of Offshore Mechanics and Arctic Engineering*, 143(5).

Ashby, M. M. and Jones, D. R. H (2012) 'Engineering Materials 1: An Introduction to Properties, Applications and Design', 4th Edn., Elsevier/Butterworth-Heinemann, Oxford, UK.

Astrup, O. S., Helgøy, H. and Høyland, K. V (2013). 'Laboratory work on freeze-bonds in ice rubble, Part III: Shear box experiments', *Proceedings of the International Conference on Port and Ocean Engineering under Arctic Conditions, POAC*.

Azarnejad, A. and Brown, T. G. (2001) 'Ice rubble behavior in punch tests', *Journal of Cold Regions Engineering*, 15(3), pp. 135–153. doi: 10.1061/(ASCE)0887-381X(2001)15:3(135).

Bailey, E. *et al.* (2014) 'An Overview of the Development of Ice Ridge Keel Strengths Test Program', in *Society of Petroleum Engineers - Arctic Technology Conference 2014*. doi: 10.4043/24553-MS.

Bailey, E., Taylor, R., & Croasdale, K. (2015) 'Mechanics of ice rubble over multiple scales', in *Proceedings of the ASME 2015 34th International Conference on Ocean, Offshore and Arctic Engineering OMAE2015*. St. John's, Canada.

Bailey, E., Sammonds, P. R. and Feltham, D. L. (2012) 'The consolidation and bond strength of rafted sea ice', *Cold Regions Science and Technology*. Elsevier B.V., 83–84, pp. 37–48. doi: 10.1016/j.coldregions.2012.06.002.

Boroojerdi, M. T. *et al.* (2016) 'Experimental Study on Shear Strength of Freeze Bonds in Freshwater Ice', in *Proceeding of Arctic Technology Conference 2016*. St. John's, Newfoundland and Labrador, pp. 1–9.

Boroojerdi, M. T., Bailey, E. and Taylor, R. (2020a) ‘Experimental Investigation of Rate Dependency of Freeze Bond Strength’, *Cold Regions Science and Technology*, 178, 103120.

Boroojerdi, M. T., Bailey, E. and Taylor, R. (2020b) ‘Experimental study of the effect of submersion time on the strength development of freeze bonds’, *Cold Regions Science and Technology*, 172, 102986.

Boroojerdi, M. T. (2020) ' Investigation of the Role of Freeze Bonds on the Development of Ice Rubble Strength', Doctoral dissertation, Memorial University of Newfoundland.

Bruneau, S. E. (1996) 'Development of a first year ridge keel model', Doctoral dissertation, Memorial University of Newfoundland.

Bueide, I. M. and Høyland, K. V. (2015) ‘Confined compression tests on saline and fresh freeze-bonds’, in *Proceedings of the International Conference on Port and Ocean Engineering under Arctic Conditions, POAC*. Trondheim, Norway.

Butkovich, T . R . 1954. 'Ultimate strength of ice.' *U.S. Snow, Ice and Permafrost Research Establishment*. Research Paper 11

Campbell, F. C. (2012) 'Fatigue and fracture : understanding the basics.' Materials Park, Ohio, ASM International.

Cole, B. D. M., Gould, L. D. and Burch, W. B. (1985) ‘A system for mounting end caps on ice specimens’, *Journal of Glaciology*, 31(109), 362-365.

Croasdale, K.R. (1996) 'In-situ strength measurements of first year pressure ridges and rubble fields.' National Research Council of Canada PERD Report.

Croasdale, K.R. (1997) 'In-situ ridge strength measurements - 1997', National Research Council

of Canada PERD Report.

Croasdale, K.R. (1997) 'In-situ ridge strength measurements - 1998', National Research Council of Canada PERD Report.

Cox, G. F. N. and Richter Menge, J. A. (1985) ‘Tensile strength of multi-year pressure ridge sea ice samples’, *Journal of Energy Resources Technology, Transactions of the ASME*, 107(3), pp. 375–380.

Croasdale, K. R. (2012). 'A simple model for first-year ridge loads on sloping structures.' *In SNAME 10th International Conf. and Exhibition on Performance of Ships and Structures in Ice.*

Dykins, J. E. (1966) ‘Tensile Properties of Sea Ice Grown in a Confined System’, in *International Conference on Low Temperature Science. I. Conference on Physics of Snow and Ice, II. Conference on Cryobiology*. Sapporo, Japan, pp. 523–537.

Ettema, R. and Schaefer, J. A. (1986) ‘Experiments on freeze-bonding between ice blocks in floating ice rubble’, *Journal of Glaciology*, 32(112), pp. 397–403.

Ettema, R. and Urroz, G. E. (1989) ‘On internal friction and cohesion in unconsolidated ice rubble’, *Cold Regions Science and Technology*, 16(3), pp. 237–247. doi: 10.1016/0165-232X(89)90025-6.

Ettema, R. and Urroz-Aguirre, G. E. (1991) ‘Friction and cohesion in ice rubble reviewed’, in *Proceedings of the 6th International Speciality Conference Cold Regions Engineering*. Hanover, USA, pp. 316–325.

Frederking, R. M. W. and Timco, G. W. (1984) ‘Measurement of shear strength of granular/discontinuous-columnar sea ice’, *Cold Regions Science and Technology*, 9(3), pp. 215–

220. doi: 10.1016/0165-232X(84)90068-5.

Gold, L. W. 1958. 'Some observations on the dependence of strain on stress for ice.' *Canadian Journal of Physics*, Vol. 36, No. 10, p. 1265- 75

Hawkes, I. and Mellor, M. (1972) 'Deformation and Fracture of Ice Under Uniaxial Stress', *Journal of Glaciology*, 11(61), pp. 103–131. doi: 10.3189/s002214300002253x.

Høyland, K. V and Møllegaard, A. (2014) 'Mechanical behaviour of laboratory made freeze-bonds as a function of submersion time, initial ice temperature and sample size', in *22nd IAHR International Symposium on Ice*. Singapore, pp. 265–273. doi: 10.3850/978-981-09-0750-1.

Jordaan, I. J., Taylor, R., & Reid, S. (2007). 'Fracture, probabilistic averaging and the scale effect in ice-structure interaction.' *In Proceedings of the International Conference on Port and Ocean Engineering under Arctic Conditions*, Dalian, China, June 27-30.

Kingery, W. D. (1960) 'Regelation, surface diffusion, and ice sintering', *Journal of Applied Physics*, 833(5), pp. 833–838. doi: 10.1063/1.1735704.

Korzhavin, K. and Ptukhin, F. (1966) 'Evaluation of the compressive strength of ice under short-term rapidly increasing load', *Materialy VIII*, Tom 5.

Kuehn, G. A. *et al.* (1987) 'The Structure and Tensile Behavior of First Year Sea Ice and Laboratory-Grown Saline Ice by', in *Proceedings of the Seventh International Conference on Offshore Mechanics and Arctic Engineering*. New York, USA.

Lee, R. W. (1986) 'A Procedure for Testing Cored Ice Under Uniaxial Tension', *Journal of Glaciology*, 32(112), pp. 540–541. doi: 10.3189/s0022143000012284.

Leguillon, D., Martin, E., Lafarie-Frenot, M. C. 'Flexural vs. tensile strength in brittle materials',

Comptes Rendus Mécanique, Volume 343, Issue 4, 2015, Pages 275-281, ISSN 1631-0721, https://doi.org/10.1016/j.crme.2015.02.003.

Lemee, E. and Brown, T. (2002) 'Small-scale plane strain punch tests', *Ice in the Environment: Proc. of the 16th IAHR International Symposium on Ice*, 2, pp. 1–7.

Leppäranta, M. (2011) 'The Drift of Sea Ice. Second Edi.', Springer Science & Business Media.

Liferov, P., Jensen, A., Høyland, K.V., Løset, S., (2002). 'On analysis of punch tests on ice rubble.' *Proceedings of the 16th International Symposium on Ice*, Dunedin, New-Zealand, vol. 2, pp. 101-109.

Liferov, P. and Bonnemaire, B. (2005) 'Ice rubble behaviour and strength: Part I. Review of testing and interpretation of results', *Cold Regions Science and Technology*, 41(2), pp. 135–151. doi: 10.1016/j.coldregions.2004.10.001.

Liu, L. *et al.* (2015) 'Numerical Simulation of Ice Ridge Gouging', in *ASME 34th Int. Conf. on Ocean, Offshore and Arct. Eng.*At: St. John's, Canada. doi: 10.1115/OMAE2015-41886.

Marchenko, A. and Chenot, C. (2009) 'Regelation of ice blocks in the water and on the air', in *Proceedings of the International Conference on Port and Ocean Engineering under Arctic Conditions, POAC*. Luleå, Sweden, pp. 543–554.

Mellor, M., Cox, G. F. N. and Bosworth, H. (1984) 'Mechanical Properties of Multi-Year Sea Ice Testing Techniques.', *CRREL Report (US Army Cold Regions Research and Engineering Laboratory)*.

Møllegaard, A. (2012) 'Experimental study on freeze-bonds in laboratory made saline ice.'

Murdza, A., Polojärvi, A., Schulson, E. M., and Renshaw, C. E. 'The flexural strength of bonded

ice' *The Cryosphere*, 15, 2957–2967, https://doi.org/10.5194/tc-15-2957-2021, 2021.

Palmer, A., & Croasdale, K. (2012). Arctic Offshore Engineering. Published by World Scientific Publishing Co. Pte.

Peyton, H. R. (1966) 'Sea ice strength.' Fairbanks, AK, University of Alaska. Geophysical Institute. (Report UAG-R-182.).

Polojärvi, A. and Tuhkuri, J. (2013) 'On modeling cohesive ridge keel punch through tests with a combined finite-discrete element method', *Cold Reg. Sci. Technol.*, 85, 191–205, https://doi.org/10.1016/j.coldregions.2012.09.013, 2013

Repetto-Llamazares, A. H. V., Høyland, K. V. and Kim, E. (2011) 'Experimental studies on shear failure of freeze-bonds in saline ice:. Part II: Ice-ice friction after failure and failure energy', *Cold Regions Science and Technology*. Elsevier B.V., 65(3), pp. 298–307. doi: 10.1016/j.coldregions.2010.12.002.

Repetto-Llamazares, A. H. V., Høyland, K. V and Evers, K. U. (2011) 'Experimental studies on shear failure of freeze-bonds in saline ice: Part I. Set-up, failure mode and freeze-bond strength', *Cold Regions Science and Technology*. Elsevier B.V., 65(3), pp. 286–297. doi: 10.1016/j.coldregions.2010.12.001.

Richter-Menge, J. A. and Jones, K. F. (1993) 'The tensile strength of first-year sea ice', 39(133), pp. 609–618.

Sammonds, P. R., Murrell, S. A. F. and Rist, M. A. (1998) 'Fracture of multiyear sea ice', *Journal of Geophysical Research: Oceans*, 103(C10), pp. 21795–21815. doi: 10.1029/98JC01260.

Sayed, M. and Frederking, R. (1986) 'On Modelling of Ice Ridge Formation', in *lAHR Ice*

Symposium 1986. lowa City, USA, pp. 603–614.

Schulson, E. M. (1979) Schulson, E. M. (1979). 'An analysis of the brittle to ductile transition in polycrystalline ice under tension.' *Cold Regions Science and Technology*, 1(2), 87-91.

Schulson, E. M. (2015) 'Kinetic friction of ice sliding slowly over itself: Physical mechanisms', in *Proceedings of the International Conference on Port and Ocean Engineering under Arctic Conditions, POAC*. Trondheim, Norway.

Schwarz, J. *et al.* (1981) 'Standardized Testing Methods for Measuring Mechanical Properties ff Ice', *Cold Regions Science and Technology*, 4, pp. 245–253.

Serré, N., Repetto-Llamazares, A. H. V. and Høyland, K. V. (2011) 'Experiements on the relation between freeze-bond and ice rubble strength, Part I: Shear box experiments', in *Proceedings of the International Conference on Port and Ocean Engineering under Arctic Conditions, POAC*.

Shafrova, S. and Høyland, K. V (2008) 'The freeze-bond strength in first-year ice ridges. Small-scale field and laboratory experiments', *Cold Regions Science and Technology*, 54(1), pp. 54–71. doi: 10.1016/j.coldregions.2007.11.005.

Shayanfar, H. (2017) 'An Experimental Investigation on the Strength and Failure Behavior of Freshwater Ice Rubble.' Master's thesis, Memorial University of Newfoundland.

Shayanfar, H., Bailey, E., Pritchett, R., & Taylor, R. (2018). The effects of consolidation time on the strength and failure behavior of freshwater ice rubble. *International Journal of Naval Architecture and Ocean Engineering*, 10(3), 403-412.

Shayanfar, H., Bailey, E., & Taylor, R. (2022). Medium-scale laboratory investigation of the effect of confinement on ice rubble strength and failure behavior. *Cold Regions Science and Technology*,

202, 103629.

Sinha, N. K. (1989) ‘Closed-loop controlled tensile strength testing method for multi-year sea ice’, in *Proceedings of Eighth International Conference on Offshore Mechanics and Arctic Engineering*. The Hague, pp. 1–6.

Szabo, D. and Schneebeli, M. (2007) ‘Subsecond sintering of ice’, *Applied Physics Letters*, 90(15), pp. 1–4. doi: 10.1063/1.2721391.

Taylor, R. S. (2010). 'Analysis of scale effect in compressive ice failure and implications for design.' Doctoral dissertation, Memorial University of Newfoundland.

Thomson, J. (1862) ‘On crystallization and liquefaction, as influenced by stresses tending to change of form in the crystals’, *Proceedings of the Royal Society of London*, 11, pp. 472–481. doi: 10.1098/rspl.1860.0101.

Timco, G., Croasdale, K. R. and Wright, B. (2000) 'An overview of first-year sea ice ridges.' National Research Council of Canada, Technical Report HYD-TR-047.

Yulmetov, R., Bailey, E. and Ralph, F. (2017) ‘A Discrete Element Model of Ice Ridge Interaction with a Conical Structure’, in *Proceedings of the 24th International Conference on Port and Ocean Engineering under Arctic Conditions*. Busan, Korea.

4. INVESTIGATION AND 3D DISCRETE ELEMENT MODELING OF FRACTURE OF SEA ICE BEAMS

4.1. Preface

This chapter of this thesis is based on a manuscript titled “Investigation and 3D Discrete Element Modeling of Fracture of Sea Ice Beams” published in the proceedings of Offshore Technology Conference. I was the primary author of this manuscript and Dr. Rocky Taylor, Dr. Robert Sarracino, and Dr. Aleksey Marchenko co-authored the manuscript. The primary author of the manuscript was in charge of conducting all the simulations, drafting the manuscript, and revising the paper based on the feedback from the co-authors and reviewers. The co-authors helped the primary author with providing the experimental data, providing financial and logistic needs of performing the study, analysing the results, reviewing and revising the manuscript.

4.2. Abstract

Flexural failure of sea ice is of interest in many different applications, ranging from understanding rubble formation processes to modeling bending failure of ice sheets against sloped structures and ship hulls. In this chapter we present a brief summary of recent in-situ experiments carried out on side-loaded sea ice beam specimens on the ice fields near Storfjorden, Svalbard. Results from these tests have been used to parameterize a discrete element model of ice fracture under flexural loading. Simulations of these experiments in 3D have been carried out using a new material model within the open-source Discrete Element Method (DEM) code WooDEM which features cohesive bonds in tension, shear, flexure and torsion based on a contact model with normal, shear, torsional and flexural springs. A comparison of simulated and field test results, along with recommendations for future work is provided.

4.3. Introduction

In this chapter we present the results of Discrete Element (DEM) simulations of field tests conducted on sea ice beams near Svalbard in April, 2014 (Taylor et al. 2014). DEM is a direct modeling approach which has the potential to both describe and understand the behavior of brittle material, especially with regard to the evolution of damage towards failure (Potyondy and Cundall 2004). Our long-term goal is to understand and model large-scale ice breakage, ridge formation and ice-structure interaction under widely varied conditions, with particular emphasis on studying emergent behaviour which arises naturally out of evolving interactions between failure processes and broken ice geometry. As a step towards this goal we examine the effects of DEM model parameters on ice beam breakage on the small scale (length ~ 2.5 m), and compare the force-displacement curves from simulations with that obtained from the field test.

Ice is highly prone to brittle fracture, which plays a critical role in determining the morphology of sea ice in nature and also the ice failure mechanisms and associated loads which dominate during a given ice-structure interaction. Flexural failure of sea ice is of interest in many different applications, ranging from understanding rubble formation processes to modeling bending failure of ice sheets against sloped structures and ship hulls. Discrete fractures have been observed to play an important role in the flexural failure of sea ice beams.

Commonly employed approaches used to study ice failure processes include: in-situ (field) measurements, laboratory experiments, analytical computation and numerical simulation. Each method has its strengths and weaknesses. In-situ measurements provide excellent insight into full-scale behaviour but are expensive, may be prone to measurement uncertainties, lack reproducibility due to inherent natural variability, and can be logistically challenging to execute.

These contributing factors result in sparse field data sets. Ultimately, however, field trials are the only means to study real full scale processes, and are essential for calibration of analytical or numerical models. Laboratory experiments are more cost effective, but one can never truly replicate field conditions in the laboratory, and scalability issues pose significant challenges for scale model testing. As well, usually because of their costs, replication to establish variability has been lacking. Analytical methods serve as a valuable approach for modelling some ice loading scenarios, but are typically limited to idealized and relatively simple geometries. By comparison, numerical methods are cheap and reproducible and, moreover, allow capture of data in regions inaccessible to measurement devices. Detailed consideration of the underpinning assumptions and careful parameterization are all needed. It should be noted that whereas numerical simulations, related as they are to first principles, that could be more robust than purely phenomenonological models, ultimately their reliability does depend on verification with real physical data as close to full scale as possible.

In Section 4.4 we present a brief history of DEM modeling of ice. Section 4.5 summarizes the in-situ experiments carried out on side-loaded sea ice beam specimens near Storfjorden, Svalbard. The following section describes the ice material model which has been inserted into the open-source 3D DEM code WooDEM. In Section 4.7 we describe our simulations of the above-mentioned experiments and present the results of our simulations. Section 4.8 contains our discussion and conclusion, and offers suggestions for further work.

4.4. DEM Modeling of Ice

Use of the Finite Element Method (FEM) for simulating ice behavior has a long history. In recent years, however, the use of DEM for modeling ice has been growing for certain classes of problem,

largely because of its natural suitability for modelling brittle solids and material composed of unbonded particles or blocks.

Continuum mechanics methods have long been used to model ice keels by hiring techniques from the FEM treatment of soils, assuming the broken ice mass to behave like a Mohr-Coulomb granular material. In many cases, however, simulations do not take into account the individual blocks, whose size can be large enough that the 'continuum approximation' which justifies such an approach no longer applies. Hence, recent years have seen the growing use of DEM in modelling broken ice material. Tuhkuri and Polojärvi, (2005) used the 2D DEM to simulate punch tests on ice rubble. More recently Ranta, Polojärvi and Tuhkuri (2015) and Shushpannikov and Naumov (2013) used a 2D DEM to simulate ice pile up and rubble formation against a wall. Polojärvi, Tuhkuri and Pustogvar (2015) indicate that granular behavior of the ice rubble is important when simulating the experiments. Polojärvi et al. (2015), Lishman and Polojärvi (2015) and Berg and Lubbad (2015) simulated the ice rubble in the direct shear box experiments. 2D DEM has also been utilized by Polojärvi and Tuhkuri (2012); Polojärvi and Tuhkuri (2013) to simulate the punch through test.

Increasingly, DEM has also been used to model ice fracture and breakage. Paavilainen, Tuhkuri and Polojärvi (2009) and Paavilainen and Tuhkuri (2013) used a 2D combined finite-discrete element method to study multi-fracture of beam structures. Morgan et al. (2015) used DEM to simulate an ice sheet interacting with an upward-sloping cone. Liu et al. (2015) used DEM to model tank studies of the failure of a laboratory ridge keel in interaction with an artificial seabed. This latter study was notable in that it drew on the unique power of DEM to model both brittle solids and a very coarse-grained granular material, as the keel was composed of blocks initially bonded weakly by freeze-bonds which broke under stresses generated from a moving berm,

causing the blocks to separate. The simulation was able to reproduce the experimental results of detailed ice loading up to the initial load peak. The model used in the present work is the same as that used in this latter study.

4.5. In-situ Beam Flexure Strength Test

A number of field tests were conducted during the UNIS Field Expedition: 24 tests of uniaxial compression and seven indentation tests; the latter comprising three compressive indentation, two splitting indentation, and two beam bending to breakage (Taylor et. al, 2014). For this work we have chosen to model one of the beam bending indenter tests.

The particular experiment modeled in these simulations featured an ice beam of dimensions 2.5 m (length), 0.50 m (width) and 0.55 m (ice depth), loaded to failure by a cylindrical steel platen of diameter 15 cm at a velocity of 1 mm/s. A schematic is given in Figure 4-1, and photographs of the setup are given in Figure 4-2. A graph of load versus indentation distance is given in Figure 4-3. Details of these beam tests may be found in Oshaug et al. (2014) and Taylor et al. (2014).

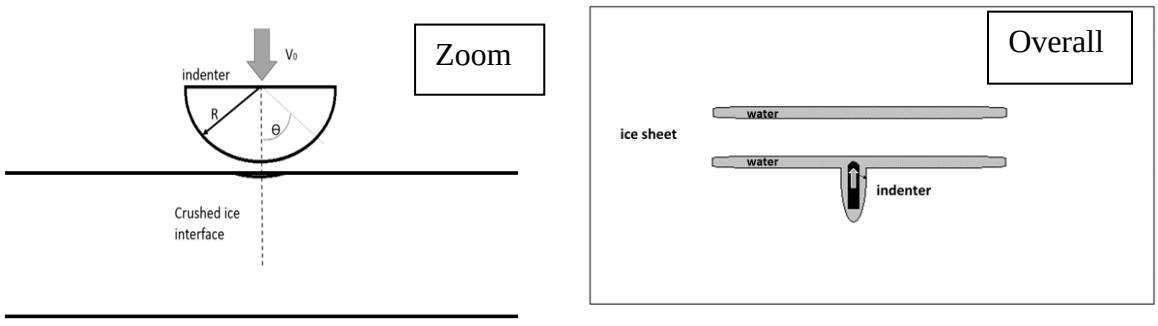

Figure 4-1. Schematic top view of the indented area of the beam

Figure 4-2. Photos of: (left) the beam test setup; (right) failed beam specimen

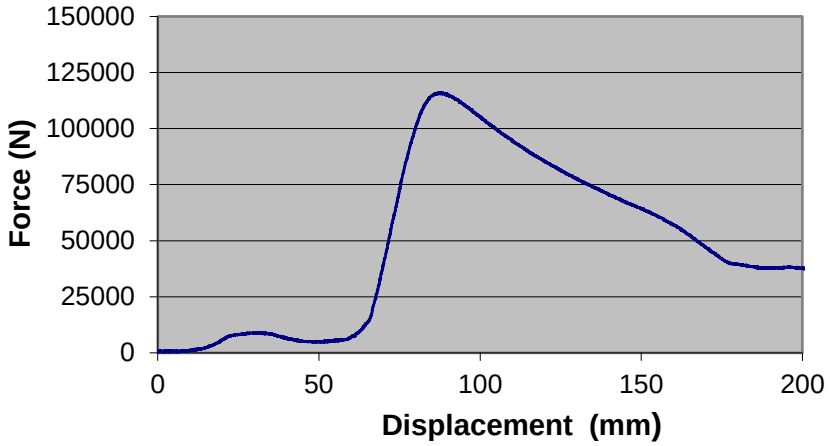

Figure 4-3. Measured force-displacement curve for beam indentation experiment

Several features of note from this test result are:

1- For displacement up to about 50 mm the platen experiences a 'settling in' period before the load begins to rise. This is due to a small amount of local crushing at the contact interface during initial contact between the platen and the ice beam. This is a feature that we were not able to model, since local ice crushing is a highly complex process and modelling these phenomena are beyond the scope of the present work.

2- Between displacements of around 60 mm and 90 mm the beam undergoes a linear elastic response, hence the effective Flexural modulus can be calculated from simple beam theory. For a center loaded rectangular beam fixed at the two ends,

$$E_{flex} = \frac{l^3}{48EI}\left(\frac{\Delta W}{\Delta y}\right), where\ I = \frac{hw^3}{12} \quad (4\text{-}1)$$

where E_{flex} is flexural modulus, referred a E in the remainder of the mansucript, l the beam length, h the beam height, w the beam width and $\frac{\Delta W}{\Delta y}$ the slope of the steepest part of the graph. Substituting $l = 2.5\ m, h = 0.55\ m, w = 0.5\ m, \Delta W = 75000\ N\ and\ \Delta y = 0.012\ m,$ we obtain an effective Young's modulus of around 0.35 GPa, significantly lower than that for laboratory ice.

3- The maximum load for this test is around 120,000 N. Simple beam theory can be used to calculate the yield strength of the specimen (this is not to say that this experiment can be fully explained by the main assumptions of the simple beam including linear elasticity, straight beam, small deflections, etc., but this value does provide a representative of the beam strength value that is consistent with the way flexural strength it often reported in the literature for ice) which is given by

$$\sigma = -\frac{Wl}{4Z} \tag{4-2}$$

where Z is the section modulus $Z = \frac{I}{z}$.

Here z is the distance from the neutral surface to the lower horizontal surface of the beam, ie, z=w/2. Substituting for the maximum load, $W = 120{,}000\ N$, we obtain a failure strength of around 3.6 MPa. A similar beam in pure tension and having the same effective Young's modulus (e.g., 0.35 GPa) would break at a strain of $\varepsilon = 0.01$.

4- Results indicate that upon reaching the peak load the beam experiences strain softening, with the load decreasing to half the maximum over a further displacement of around 70 mm from the point of peak load.

5- As may be seen in Figure 4-2 (right), a horizontal fracture splits the beam at its center at the moment of peak load. Shortly afterwards, as is clearly shown in Figure 4-2, a dramatic oblique crack from the platen to one of the far corners appears. In both of the beam bending tests which were conducted this dramatic oblique crack formed. In general this phenomenon would, of course, depend on the block aspect ratio.

4.6. The Ice Material Model in WooDEM

In this work we use a material model newly developed for the 3D DEM open-source code WooDEM, the ice model in the WooDEM documentation (Sarracino, Mohammadafzali, Šmilauer, in preparation). The ice model contains normal, shear, torsional and flexural springs that operate between neighboring particles that overlap due to compressive stresses or which are bonded. The spring stiffnesses can be set independently, but in these simulations we assume a linearly elastic,

isotropic material and set the relative spring stiffnesses so that two neighboring, bonded particles will behave as an 'equivalent beam' under tensile, compressive or shear stresses, or flexural or torsional moments.

Equations 1 to 4 show the cohesive forces and torques between bonded particles in response to relative linear or angular displacements (Sarracino, unpublished work):

$$F_n = K_n . u_n \tag{4-3}$$

$$F_t = K_t . u_t \tag{4-4}$$

$$T_w = K_w . u_\phi \tag{4-5}$$

$$T_r = K_r . u_\theta \tag{4-6}$$

where F_n, F_t, T_w and T_r represent the normal force, shear force, twist torque and bending torque respectively. K_n, K_t, K_w and K_r represent normal, shear, twist and bending spring stiffnesses, and u_n, u_t, u_ϕ and u_θ are normal displacement, shear displacement, angle of twist and angle of bending. The 'equivalent beam' condition requires:

$$k_n = E_{eff} \frac{A}{L} = E_{eff} \frac{\pi \min(r_1, r_2)^2}{r_1 + r_2} \tag{4-7}$$

$$k_t = (ktDivKn)_{eff} \cdot k_n \tag{4-8}$$

$$k_w = \frac{1}{2\pi} k_t \cdot \pi \min(r_1, r_2)^4 \tag{4-9}$$

$$k_r = \frac{3}{16\pi} k_n \cdot \pi \min(r_1, r_2)^4 \tag{4-10}$$

where E_{eff} is effective Young's modulus, $(ktDivKn)_{eff}$ is the ratio between the shear modulus and the Young modulus ($\frac{G}{E} = \frac{1}{1+2\nu}$, where ν is the Poisson ratio), A and L are area and length of the equivalent beam, and r_1 and r_2 are the radii of the two particles.

Two spheres can be bonded through any combination of normal, shear, torsional or flexural bonds with each bond corresponding to one of the stiffnesses above (Sarracino, unpublished work). The bond strengths are given by:

$$F_{nb} = c_n \cdot A \tag{4-11}$$

$$F_{tb} = c_t \cdot A = \beta_t c_n \cdot A \tag{4-12}$$

$$T_{wb} = c_w \cdot A^{3/2} = \beta_w c_t \cdot A^{3/2} \tag{4-13}$$

$$T_{rb} = c_r \cdot A^{3/2} = \beta_r c_n \cdot A^{3/2} \tag{4-14}$$

where c_n, c_t, c_w and c_r, the cohesion constants, have dimensions of stress. A bond will break under any of the strength conditions $F_n \geq F_{nb}$, $|F_t| \geq F_{tb}$, $|T_w| \geq T_{wb}$ or $|T_r| \geq T_{rb}$.

When bonds are broken or absent tensile forces vanish and the yield values in shear, torsion or flexure between overlapping particles become

$$F_{ty} = -\min(0, F_n tan\phi) \tag{4-15}$$

$$T_{wy} = -\sqrt{\frac{A}{\pi}}\ \min(0, F_n tan\phi) \tag{4-16}$$

$$T_{ry} = -\sqrt{\frac{A}{\pi}} \min(0, F_n \mu) \tag{4-17}$$

When forces or torques exceed the yield values perfectly plastic sliding occurs and the forces and torques are reset to the yield values (Sarracino, unpublished work). That is,

$$|F_t| > F_{ty} \quad \Rightarrow \quad F_t \rightarrow \frac{F_t}{|F_t|} F_{ty} \tag{4-18}$$

$$|T_w| > T_{wy} \quad \Rightarrow \quad T_w \rightarrow \frac{T_w}{|T_w|} T_{wy} \tag{4-19}$$

$$|T_r| > T_{ry} \quad \Rightarrow \quad T_t \rightarrow \frac{T_t}{|T_t|} T_{ry} \tag{4-20}$$

The model uses hysteretic damping rather than viscous damping (see, e.g., Potyondy and Cundall, 2004). That is, particles lose a proportion of their kinetic energy per cycle. The resulting damping force applied to the particles is:

$$F_d = -\alpha |F| sign(V) \tag{4-21}$$

where α is the damping coefficient, F is the total of unbalanced force on a particle and $sign(V)$ is the sign of the particle velocity.

WooDEM has a clumping model to enable simulation of material composed of angular grains or irregular blocks. In these simulations we did not use clumping.

4.7. Numerical Simulation and Results

Given that the present ice beam simulations are part of a longer-term program aimed at understanding and simulating large-scale processes associated with ice rubble formation, accumulation and interactions, some initial questions considered are:

1- Is the particular material model that has been inserted into the DEM code well suited for modeling ice?

2- If so, what effects do the parameters of interest have on the modelled ice behavior?
3- What is the range of parameter values which will adequately model the observed ice behavior from the field tests and do these parameter values make sense?

In this study there are three main features of the load-displacement curve of Figure 4-3 which we have aimed to reproduce: the slope of the initial load rise, the peak load, and the displacement between the load peak and half its value in the post-peak curve.

There are six parameters that influence these three features: E and ν, Young's modulus and Poisson's ratio, respectively; the two strength parameters, i.e., tensile strain to breakage (ϵ_b or $breakN$) and the ratio of shear strength to tensile strength β; the damping constant α; and the value of the maximum relative particle separation which will allow neighboring particles to bond during the formation phase of the DEM material (distFactor). The slope of the linearly elastic section of the load-displacement curve is determined primarily by the two elastic constants, although, since the aggregate slope up to the load peak is used to determine the effective Young modulus, parameter values affecting bond strength also play a minor role. The load peak and post-peak load decay are influenced by the other four parameters as well, with breakN playing a predominant role.

It should be noted that the effective elastic constants for a solid composed of randomly generated, bonded spheres will not be the same as the parameter values used for those constants – this is a feature which is intrinsic to a DEM system. What is important, however, is that simulations of solids under different loading conditions give the same effective stiffnesses for a given set of parameter values. Our simulations have shown that for small numbers of particles the

effective Young's modulus of a rectangular beam, E_{eff}, as determined by taking the ratio of axial stress to small strain in a uniaxial simulation, depends on particle number. However, as the number of DEM particles in the rectangular beam increases, E_{eff} tends towards a limit, which is substantially less than value assigned to the parameter value of E. As mentioned above this is a feature of DEM. There is no analytical formula which can be used to calculate this ratio; the only way to find it is to conduct simulations and to measure it. This ratio is scale-independent and depends only on the number of particles. Our work, to be published, has shown that for a beam with aspect ratio of 2:1:1 the effective Young's modulus reaches to within about 95% of the limiting value for a beam composed of around 1,000 particles (Sarracino et. al.). A greater number than that is needed in order for the beam *strength* to come within 5% of the limiting value; the above-mentioned work in preparation will address this particular issue.

It should be noted as well that the behavior of the ice beam may be affected by particle angularity. This study has used the basic spherical particles generated by WooDEM. Future simulations will investigate the effect of angularity by clumping the particles. Regarding distFactor, the higher the value of this parameter, the stronger the material will be since it increases the average number of bonds per particle in the material. In the present study a single value of distFactor was used for all particles in a given simulation. In future simulations other distFactor distributions may be considered.

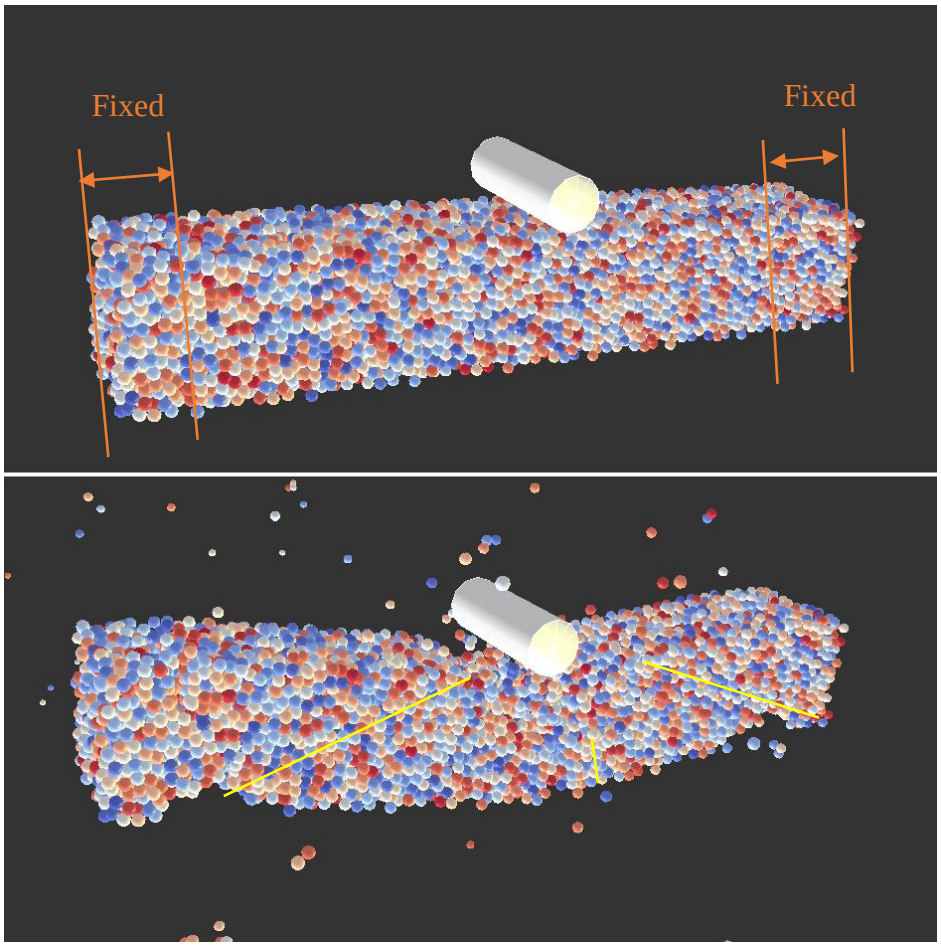

Figure 4-4. Screenshot of the simulation: (top) before; and (bottom) after indentation; yellow lines highlight failure planes

To simulate the loading conditions used in the field, a vertical cylindrical rod (the platen) is advanced at a constant speed through the mid-point of the ice beam of effective length 2.5 m, width 0.5 m and vertical height 0.55 m. The DEM beam consists of a bonded aggregate of spherical particles. The physics engine maintains the platen`s velocity at a constant value, causing a build-up of force that eventually causes failure and breakage of the beam. It should be noted that in our simulation each end of the beam was fixed in place by a small pad of placeholder ice particles extending 0.2 m from each end along the ice beam's lengthwise axis. The pad is fixed in place: its

particles may neither move nor rotate during the simulation, so that although the total construct has a length of 2.9 m, its effective length is 2.5 m.

For this study a total of seventy-five low-resolution (1,200 particle) and twelve high-resolution (13,000 particle) simulations have been conducted. The overall strategy was to use the low-resolution simulations for the initial phase of the parametric study, since this configuration allowed for decreased run-time. In the final phase of the study a higher resolution 13,000 particle configuration was used so as to give a more representative, 'smoother' failure process, which was used in the assessment of a more refined set of model parameters.

Figure 4-4 shows the setup of the 13,000-particle beam and the cylindrical platen before loading (top) and at the moment of maximum load (bottom). A noteworthy feature of the simulation results shown in Figure 4-4 (bottom) is that the general failure patterns (center crack, followed by oblique cracks) shown from the field results in Figure 4-2 (right) were well reflected in the simulation. A discussion of applicable results for selected runs from these simulations are provided below.

4.7.1. Parametric Study

To study the effects of individual parameters on beam failure, selected sets of simulation results are presented below (Table 4-1). Figure 4-5 to Figure 4-9 show the effects of the Young modulus *E*, *distFactor*, *breakN*, damping parameter α and the shear-to-normal cohesion ratio β, respectively on the force-displacement curve. From these plots one may note slightly different starting points of the different curves. This is a consequence of random seeding, which in each case results in a differently arranged initial assembly of particles, which in turn affects when initial

Table 4-1. Simulation setup and results for data shown in Figures 4-5 to 4-9.

Figure Number	***Test Number***	***Parameter Young's Modulus* [Pa]**	***distFactor* [-]**	***breakN* [-]**	***α* [-]**	***β* [-]**	***Effective Young's Modulus* [-]**	***1st Peak***	***2nd Peak***
5	1	8.00E+08	1.1	3.5E-03	1.0E-02	1.4	2.81E+08	8.05E+04	1.02E+05
	2	9.00E+08	1.1	3.5E-03	1.0E-02	1.4	3.14E+08	6.46E+04	9.25E+04
	3	1.00E+09	1.1	3.5E-03	1.0E-02	1.4	3.76E+08	6.78E+04	9.78E+04
	4	1.10E+09	1.1	3.5E-03	1.0E-02	1.4	4.10E+08	8.02E+04	1.09E+05
6	5	9.00E+08	1.01	3.5E-03	1.0E-02	1.4	3.07E+08	9.36E+04	1.12E+05
	6	9.00E+08	1.1	3.5E-03	1.0E-02	1.4	3.07E+08	9.18E+04	1.08E+05
	7	9.00E+08	1.4	3.5E-03	1.0E-02	1.4	3.04E+08	9.32E+04	1.04E+05
	8	9.00E+08	2	3.5E-03	1.0E-02	1.4	4.11E+08	6.90E+04	9.93E+04
7	9	9.00E+08	1.1	1.0E-04	1.0E-02	1.4	3.09E+08	2.50E+03	3.38E+03
	10	9.00E+08	1.1	1.0E-03	1.0E-02	1.4	3.55E+07	2.57E+04	2.68E+04
	11	9.00E+08	1.1	5.0E-03	1.0E-02	1.4	3.42E+08	1.04E+05	1.41E+05
	12	9.00E+08	1.1	1.0E-02	1.0E-02	1.4	5.20E+08	2.69E+05	NA
8	13	9.00E+08	1.1	3.5E-03	1.0E-01	1.4	3.01E+08	9.79E+04	1.17E+05
	14	9.00E+08	1.1	3.5E-03	1.0E-02	1.4	3.29E+08	5.40E+04	9.34E+04
	15	9.00E+08	1.1	3.5E-03	1.0E-03	1.4	3.05E+08	8.98E+04	1.03E+05
	16	9.00E+08	1.1	3.5E-03	1.0E-04	1.4	2.96E+08	8.63E+04	1.05E+05
9	17	9.00E+08	1.1	3.5E-03	1.0E-02	1.1	3.25E+08	8.93E+04	1.13E+05
	18	9.00E+08	1.1	3.5E-03	1.0E-02	1.5	3.02E+08	1.02E+05	1.09E+05
	19	9.00E+08	1.1	3.5E-03	1.0E-02	2	3.51E+08	8.88E+04	NA
	20	9.00E+08	1.1	3.5E-03	1.0E-02	3	3.04E+08	1.02E+05	1.18E+05

contact takes place. To minimize the effect of seed randomness, each simulation was run twice and the results averaged. This averaging coupled with the variable time of initial contact results in an apparent increase in the slope of the force-displacement line. This is purely an artifact of averaging; the actual slope is the later, upper, value. Details of each of the corresponding test cases used in Figures 4-5 to 4-9 are summarized in Table 4-1.

4.7.1.1. Effect of Young's Modulus (E)

Figure 4-5 and Table 4-1 illustrate that the effective Young's modulus rises with an increase in the parametric Young's modulus. As the Young's modulus of the particles increases, the bond stiffness and the slope of the displacement force curve also increase.

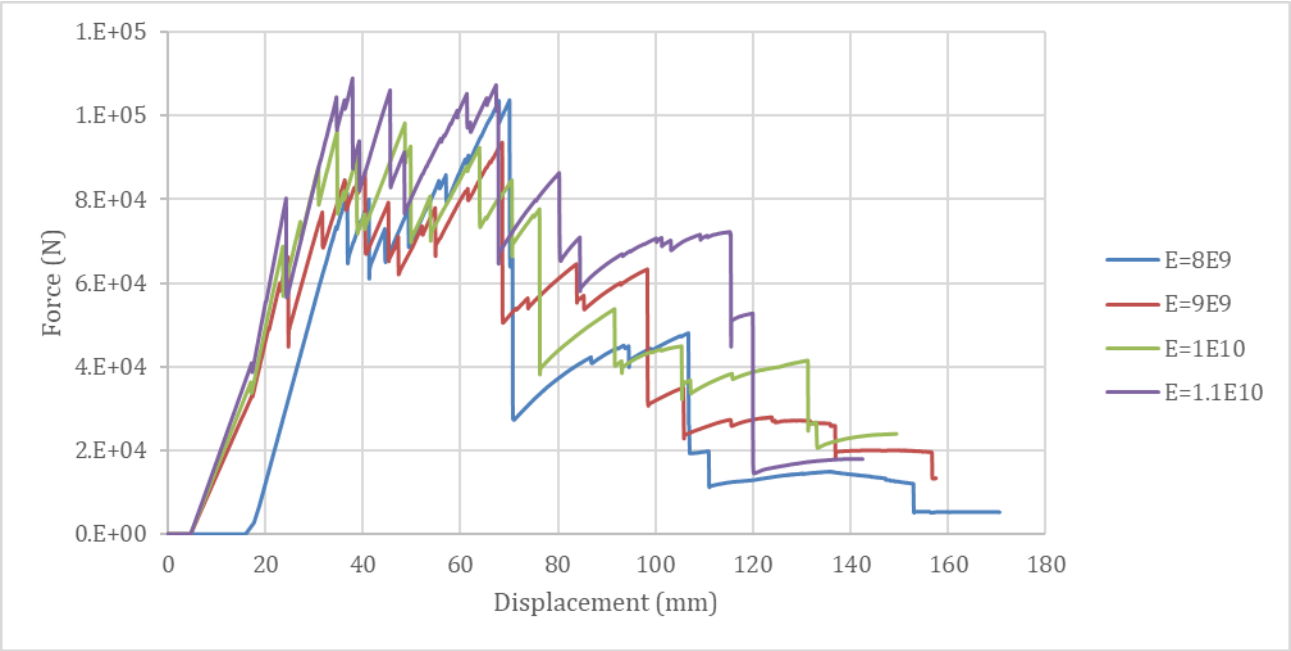

Figure 4-5. Effect of Young's modulus on the force-displacement curve; please see Table 1 for additional details

4.7.1.2. Effect of Distance Factor (*distFactor*)

Figure 4-6 shows that, in these simulations, *distFactor* increases the residual, or post-peak, strength of the beam. The distance factor is the minimum inter-sphere distance required for initial bond formation between particles. By increasing distance factor, we increase the average number of bonds per particle, which would increase the residual material strength after bonds break between

any two neighboring particles. This would have the effect of increasing residual beam strength after breakage begins.

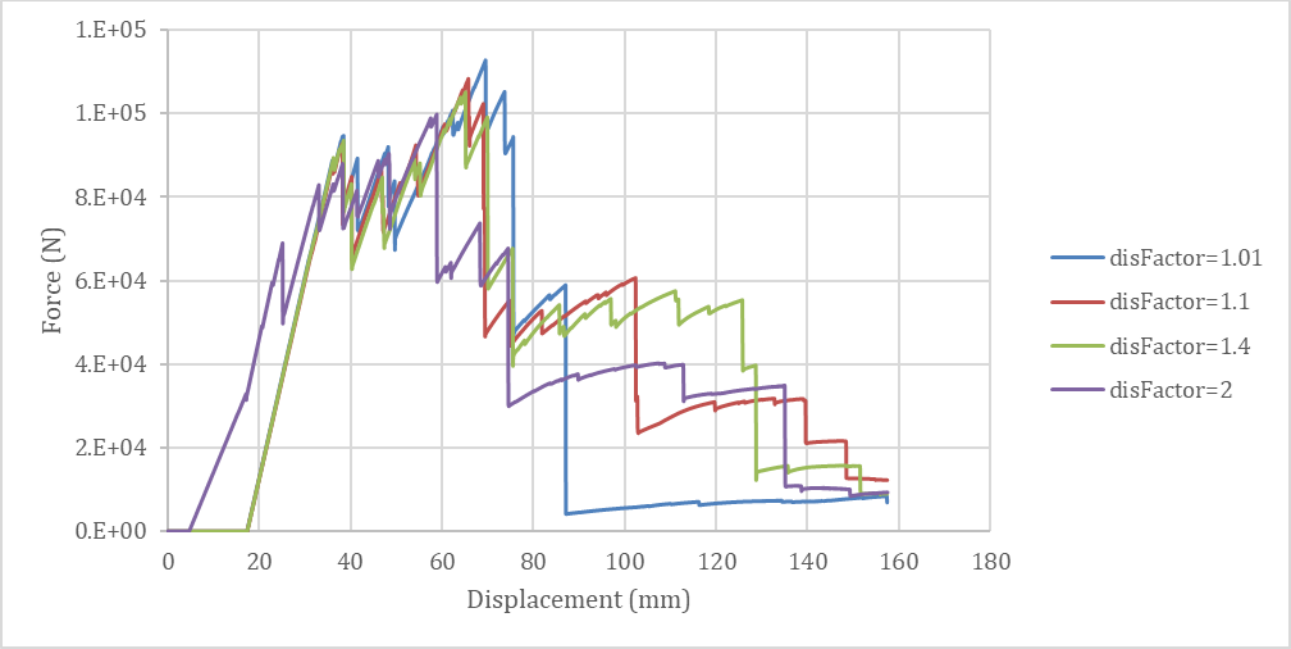

Figure 4-6. Effect of distance factor on the force-displacement curve; please see Table 1 for additional details

4.7.1.3. Effect of Normal Breakage Strain (*breakN*)

Figure 4-7 shows the effect of increasing *breakN*. As expected, the beam strength is directly proportional to *breakN*. This effect can be seen from Figure 4-7, where it is observed that increasing the normal breakage

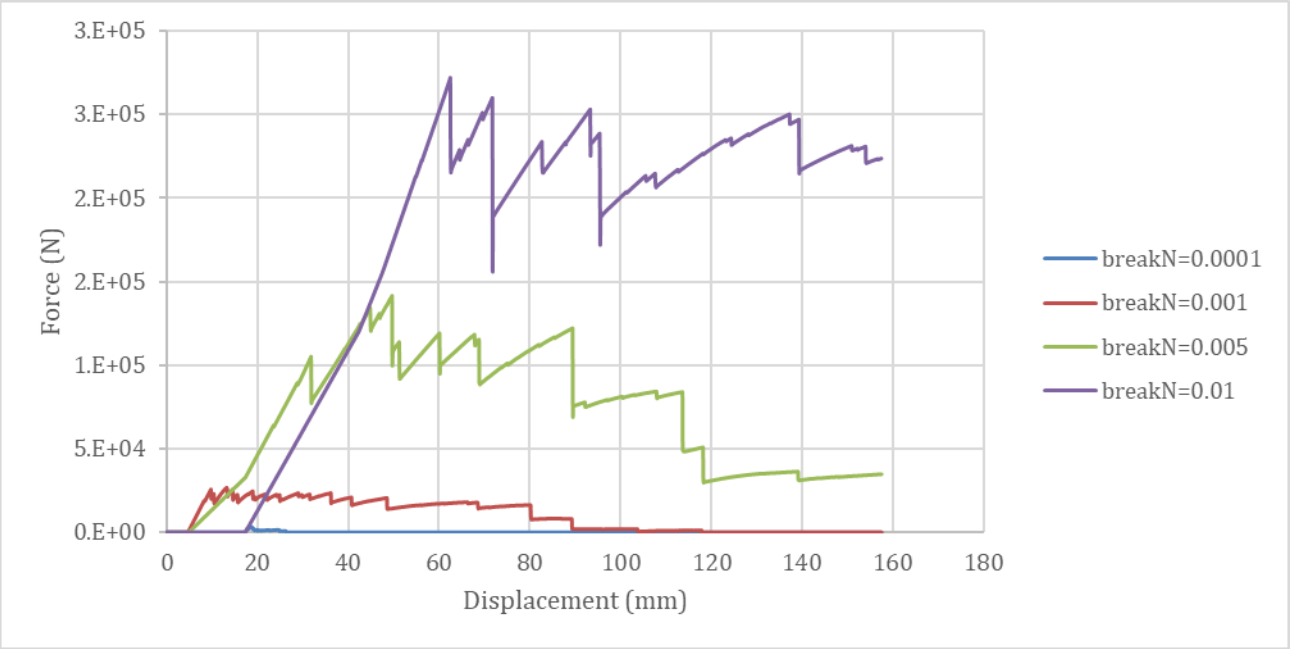

Figure 4-7. Effect of expected normal breakage strain on the force-displacement curve; please see Table 1 for additional details

strain results in a proportional increase to the peak force, as this parameter directly affects the maximum force a bond can resist before breakage. Since the normal breakage strain is only effective on the breakage of the bonds, the effective Young's Modulus as reflected in the first part of the curve which is the elastic part, is not affected by this parameter.

4.7.1.4. Effect of Damping Coefficient (α)

From Figure 4-8 it can be seen that the damping coefficient does not significantly affect either Young's Modulus or the peak strength, but it does have a significant affect on the residual strength of the beam – the higher the damping, the greater the residual strength. This would be expected, since bond breakage

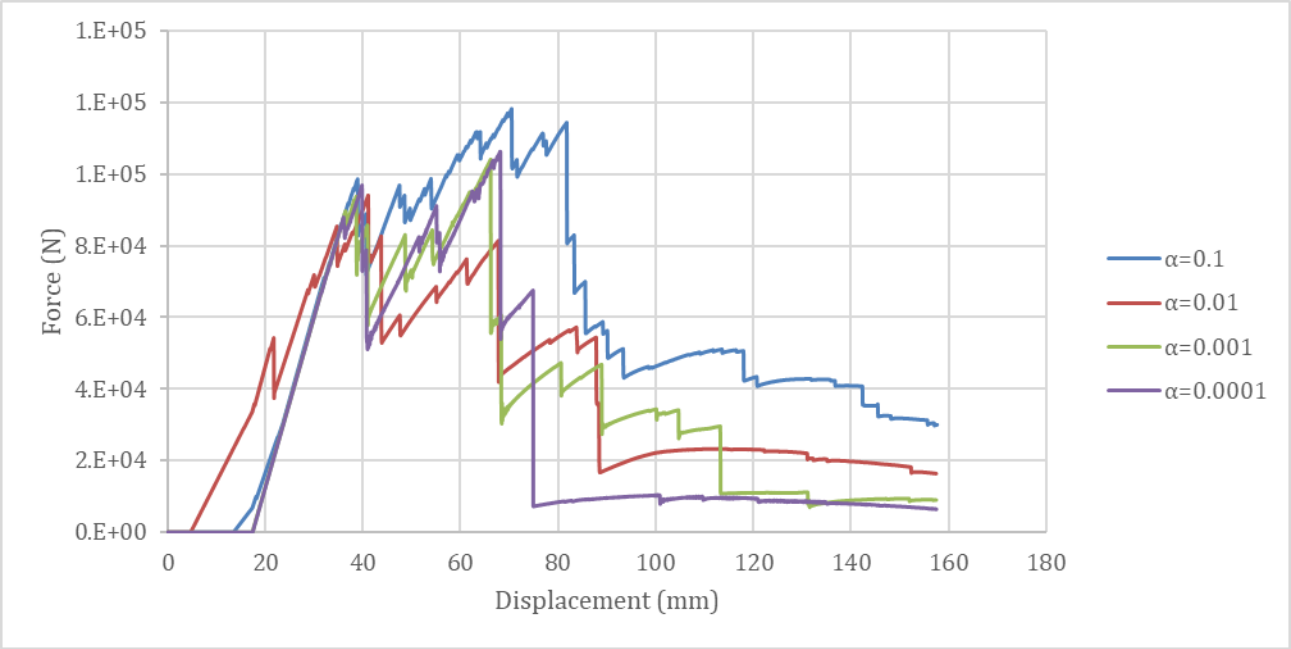

Figure 4-8. Effect of damping coefficient on the force-displacement curve; please see Table 1 for additional details

results in a release of potential energy which is then transmitted throughout the material. The higher the value of α, the greater this energy transmission would be damped.

4.7.1.5. Effect of Shear: Normal Cohesion Ratio (β)

Figure 4-9 shows the effect of varying the ratio of shear to normal cohesion, β. From the results in this figure it may be surmised that increasing β may tend to broaden the breakage peak – the distance from the point of initial breakage to the peak load. Further investigation of this parameter is recommended in future work to help clarify the extent of its effects, since a clear trend is not apparent from the results for

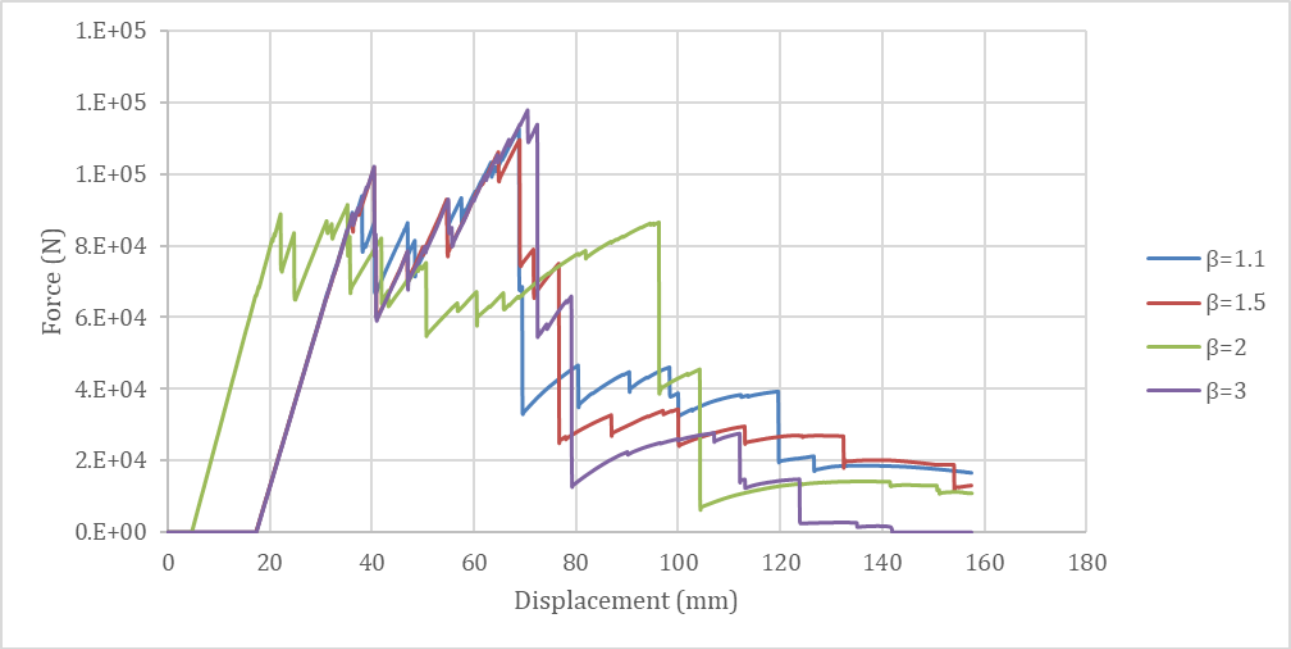

Figure 4-9. Effect of shear: normal cohesion ratio on the force-displacement curve; see Table 1 for additional details

the four simulations presented below. The ratio β is also expected to affect the location of the evolving fractures in the material, which will also be explored in further work.

4.7.2. High-Resolution Simulation Results

Using the results from the 1,200 particle simulations as a guide, a series of high resolution cases were simultated using 13,000 particles. The curve fit has been improved by a series of trial and error simulations. Figure 4-10 below shows the best match obtained between the parameter values considered and the experimental curve presented in Figure 3. The parameter values corresponding to the selected case shown in Figure 10 are:

$$E = 5.4 * 10^8 Pa$$

$$(E_{eff} = 3.5 * 10^8\ Pa)$$

$$distFactor = 1.1$$

$$breakN = 0.0037$$

$$\alpha = 0.1$$

$$\beta = 1.25$$

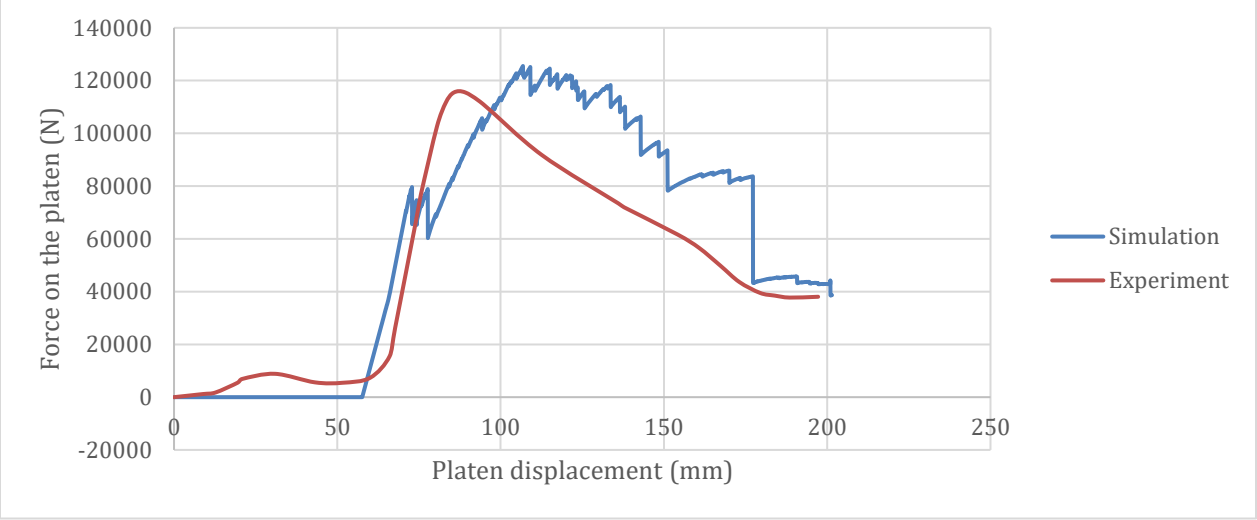

Figure 4-10. Force-displacement curve for field test and simulation results (using selected parameter values based on this study).

Comparing these two results it may be observed that the slope of the elastic part of the curve is within 1% of the experimental curve, and the peak force is within 5%, although it occurs at a greater displacement. In both simulation and experiment the force on the platen falls to half the

peak force after the platen has advanced a further 200 mm, yielding good general agreement between failure locations and load attributes.

4.8. Concluding Remarks

Based on the high-resolution simulation results, it may be concluded that these simulations provide a good overall agreement with the field test results, particularly in light of the relatively low number of DEM particles used (13,000) compared to the number of grains in an ice beam (around five hundred thousand). Several noteworthy features of this work and recommendations for further investigation are given below:

(1) The experimental curve shows an initial 'settling in' due to local ice crushing at the platen-ice interface. Simulating ice crushing behaviour is beyond the capabilities of current DEM models and is beyond the scope of the present work. Despite the complexities introduced by these local phenomena, the simulations captured main features of the beam failure reasonably well.

(2) In some simulations, particularly for large particle sizes (e.g. 1,200 particle model) an increase in the slope of the force-displacement curve before breakage was observed. As explained previously, this is an artifact of using different random number seeds to prepare the material, coupled with averaging the outputs.

(3) The experimental curve is linearly elastic up to the onset of failure and upon reaching peak load begins to decrease smoothly as a function of increased displacement. The curve from the simulations, on the other hand, is linearly elastic until it reaches a critical load level at which bond breakage begins, after which the force continues to rise at a lower average slope until the peak load is reached. Beyond this peak load, the material begins to

sufficiently ‘damage’ due to continued bond breakage, resulting in an apparent softening of the beam as a function of increased displacement. The coarseness of the discretization may be a potential cause for the lack of ‘smoothness’ in simulated force-displacement curves as compared to the field test results.

(4) Further work is recommended to better assess the sensitivity of simulation results to particle size. In addition, particles in this simulation were of the same size. An alternative approach would be to introduce a distribution of particle sizes, which would result in a smaller void volume since smaller particles would tend to fill gaps between the larger particles. Consideration of these aspects is recommended for future work.

(5) The value of the damping coefficient plays a significant role in post-peak behavior. This is expected, since this parameter influences the degree to which energy from the breakage of an individual bond will be transmitted throughout the material and thereby affect subsequent bond breakage.

(6) The authors recognize that in addition to brittle fracture, significant amounts of energy may be dissipated during ice-structure and ice-seabed interactions due to crushing, spalling, damage, and creep phenomena, depending on the temperature, loading rate and state of stress of the ice (e.g. for vertical-walled structures, such dissipative processes dominate the failure process). While these aspects are beyond the scope of the current model, inclusion of appropriate models of such dissipative processes is recognized as an essential long term goal for extending this work.

(7) As mentioned above the Field Expedition conducted a number of tests, and a wealth of data is available for further confirmatory simulations.

In summary, the 3D DEM ice model tested here has provided promising results and demonstrated value as a tool for exploratory research to better understand break-up of ice sheets during flexural failure, as would be expected during ice rubbling or during interactions with ship-shaped or sloped structures. Through continued development, this approach holds promise for providing new insights into emergent failure phenomena and associated loads, that arise as a result of the complex interplay between ice mechanical properties and continually evolving ice edge and ice block geometry. Such advances will help reduce modelling uncertainties and lay the foundation for the development of next generation ice load models needed to support offshore development in ice-prone regions.

4.9. References

Berg, M. van den and R. Lubbad, R. 2015. "The application of a non-smooth discrete element method in ice rubble modeling." In *Proceedings of the 23rd International Conference on Port and Ocean Engineering under Arctic Conditions*.

Goldstein, R. et al., 2013. Grounded ice pile-up. 2D dem simulation. In *Proceedings of the 22nd International Conference on Port and Ocean Engineering under Arctic Conditions*.

Lishman, B. and Polojärvi, A., 2015. 2D DEM of ice rubble: The effect of rate-dependent friction. In *Proceedings of the 23rd International Conference on Port and Ocean Engineering under Arctic Conditions*.

Liu, L. et al., 2015. Numerical Simulation of Ice Ridge Gouging. In *Proceedings of the ASME 2015 34th International Conference on Ocean, Offshore and Arctic Engineering*. pp. 1–8.

Morgan, D. et al., 2015. Simulations of Ice Rubbling Against Conical Structures Using 3D DEM. In *Proceedings of the 23rd International Conference on Port and Ocean Engineering under Arctic Conditions*.

Oshaug, M. et al., 2014. *Ice mechanics, loads on structures and instrumentation*,

Paavilainen, J., Tuhkuri, J. and Polojärvi, A., 2009. 2D combined finite-discrete element method to model multi-fracture of beam structures. *Engineering Computations*, 26(2004), pp.578–598.

Paavilainen, J., Tuhkuri, J. (2013) 'Pressure distributions and force chains during simulated ice rubbling against sloped structures', *Cold Regions Science and Technology*, Volume 85, 2013, Pages 157-174, ISSN 0165-232X, https://doi.org/10.1016/j.coldregions.2012.09.005.

Polojärvi, A. and Tuhkuri, J., 2013a. 2D FEM-DEM simulations of punch through tests: Effects of partly consolidated rubble deformation. In *Proceedings of the 22nd International Conference on Port and Ocean Engineering under Arctic Conditions*.

Polojärvi, A. and Tuhkuri, J., 2013b. On modeling cohesive ridge keel punch through tests with a combined finite-discrete element method. *Cold Regions Science and Technology journal*, 85, pp.191–205.

Polojärvi, A., Tuhkuri, J. and Pustogvar, A., 2015. DEM simulations of direct shear box experiments of ice rubble: Force chains and peak loads. *Cold Regions Science and Technology*, 116, pp.12–23.

Potyondy, D.O. and Cundall, P.A., 2004. A bonded-particle model for rock. *International Journal of Rock Mechanics and Mining Sciences*, 41(8 SPEC.ISS.), pp.1329–1364.

Ranta, J., Polojärvi, A. and Tuhkuri, J., 2015. Ice load estimation through combined finite-discrete element simulations. In *Proceedings of the 23rd International Conference on Port and Ocean Engineering under Arctic Conditions*.

Sarracino, R., S. Mohammadafzali, and V. Šmilauer. 2017. *A new "Ice Material Model" inserted to WooDEM*. Manuscript in Preparation.

Taylor, R. et al. 2014. *UNIS Field Expedition Project: (ArcticTECH Program under the HPQ Element)*

Tuhkuri, J. and a. Polojärvi. 2005. "Effect of particle shape in 2D ridge keel deformation simulations." In *Proceedings of the 18th International Conference on Port and Ocean Engineering Under Arctic Conditions*. 939–948.

5. INVESTIGATION OF THE EFFECT OF BLOCK SIZE, SHAPE AND FREEZE-BOND STRENGTH ON FLEXURAL FAILURE OF FRESHWATER ICE RUBBLE USING THE DISCRETE ELEMENT METHOD

5.1. Preface

This chapter of this thesis is based on a manuscript titled "Investigation of the Effect of Block Size, Shape and Freeze Bond Strength on Flexural Failure of Freshwater Ice Rubble Using the Discrete Element Method" published in the Journal of Offshore Mechanics and Arctic Engineering. I was the primary author of this manuscript and Dr. Rocky Taylor, Dr. Eleanor Bailey, Dr. Robert Sarracino, Dr. Marjan T. Boroojerdi co-authored the manuscript. The primary author of the manuscript was in charge of conducting all the simulations, drafting the manuscript, and revising the paper based on the feedback from the co-authors and reviewers. The co-authors helped the primary author with providing the experimental data, providing financial and logistic needs of performing the study, analysing the results, reviewing and revising the manuscript.

5.2. Abstract

As part of the Mechanics of Ice Rubble project, recent experiments have been carried out to study the strength and failure behavior of ice rubble beams and the freeze-bonds that form between individual ice blocks. In this study we present results obtained from a newly developed model for the 3D DEM open-source code LIGGGHTS. The ice model contains normal and shear springs that operate between neighboring particles which are bonded or that overlap due to compressive stresses. Energy dissipation is accounted for using a viscous damping model. Using this DEM model, medium-scale freshwater ice rubble punch tests have been simulated. Rubble specimens

were generated by “raining” individual DEM ice pieces into a rectangular form and compacting the rubble mass to achieve the target porosity. Before the compacting pressure was removed, bonds between contacting blocks were introduced with parameter values based on representative freeze-bond experiments. The rubble beam was then deformed by pushing a platen vertically downward through the center of the beam until failure occurred. Two types of block size and shapes have been simulated: cuboid blocks generated based on the size distribution of the actual rubble, and rubble blocks generated by image processing of actual blocks of broken ice used in the comparison experiments. The mechanism of flexural rubble failure for both cuboid block [Section 5.6.2] simulations and empirical block [Section 5.6.3] simulations is in line with experimental results; however, the empirical block simulations provide a significantly better estimation of the failure force.

5.3. Introduction

Better understanding of the ice environment and ice characteristics in ice-prone regions is essential for safe and economical marine, coastal and offshore activities. Observing ice conditions in the Arctic, one can see that pressure ridges, which comprise 10-40% of total drift ice volume, are a common form of ice (Leppäranta, 2011). Many structures are therefore designed to withstand the loads of deformed ice features such as ice ridges. It has been found that the sail of a ridge has only a minor effect during interaction, and consequently in calculation of forces the sail is often neglected in favor of the consolidated layer and the keel (G. W. Timco, 2011). Since the strength of consolidated layers is typically modelled using techniques developed for level ice, estimating the flexural strength and failure mechanism of partially consolidated ice rubble in ridge keels is important for the design and operation of engineered structures for ice environments.

Considerable effort has gone into understanding the behavior of ice rubble under shear. The size of full-scale features and the high degree of variability in ice block geometry and conditions throughout a ridge keel pose challenges for conducting representative experiments. The problem is further compounded by the fact that several methods – most notably direct shear box, simple shear box and biaxial shear – mainly focused on measuring the shear strength of ice rubble. Based on these experiments it has been suggested that the failure behavior of ice rubble can be described as a Mohr-Coulomb material (Prodanovic, 1979) , (Fransson & Sandkvist, 1985) , (Ettema & Urroz, 1989) , (G. W. Timco et al., 1992) , (Løset & Sayed, 1993)-(Yasunaga et al., 2002). McKenna et al. (1996) and Azarnejad and Brown (2001) also conducted a series of punch test experiments on freshwater ice rubble to approximate the in-situ failure behavior of ice rubble.

Conducting field tests on ice ridges is difficult and expensive, resulting in a very limited number of in-situ ridge tests and the resulting ice strength values from these tests are highly variable and have high levels of uncertainty. Moreover, since total force is measured in such tests, it can be difficult to distinguish between load contributions from the keel and those associated with the consolidated layer (Palmer & Croasdale, 2013). Other types of in-situ tests that evaluate the strength of the ice rubble include punch test (Leppäranta & Hakala, 1992; G. Timco et al., 2000), as well as direct shear test and pull-up test. Several full-scale in-situ experiment have been conducted in Helsinki University of Technology within Validation on Low Level Ice Forces on Coastal Structures (LOLEIF) project (1997-2000) and Measurements on Structures in Ice (STRICE) project (2001-2003). These programs aimed to measure the mechanical properties of ridge keel in Northern Gulf of Bothnia with total of 33 experiments including punch tests, bending tests, horizontal compression and shear tests, and an uplift test (Heinonen, 2004). Bruneau (1996) introduced a regression model for failure of ice rubble based on previous and new rubble failure

experiments. An extensive review of the ice rubble failure experiments can be found in Ettema and Urroz (1991), Timco and Cornett (1999), Liferov and Bonnemaire (2005) and Bailey et al. (2015)

For interactions with sloping structures or ice class vessels, interactions with the higher and more consolidated layers of ridge keels are of particular interest. As has been discussed by Shayanfar et al. (2018), as the strength of the bonds between individual rubble block increases, such regions of a keel tend to behave more like a brittle porous solid and are more prone to fail in flexure rather than shear. The flexural failure of rubble is complex, and the shear strength, tensile strength, and compressive strength of the ice blocks and the bonds between them are highly important (Mohammadafzali et al., 2016). The availability of direct flexural tests on ice rubble is very limited and the flexural strength of rubble is often estimated by analytical approaches.

Recent studies carried out by the Development of Ice Ridge Keel Strength (DIRKS) and the Mechanics of Ice Rubble (MIR) projects in the Centre for Arctic Resource Development (CARD) provide a unique opportunity to gain a deeper and more accurate insight to the failure of the rubble. Bailey et al. (2015) investigated the change of the rubble blocks properties over time and the process of formation of the freeze-bond and sintering between the ice blocks. Shayanfar (2017) carried out a series of punch box rubble failure experiments under various submersion times, confinement pressures and initial ice temperatures. These factors were found to highly influence the strength of the freeze-bonds formed between the ice blocks and as a result change the strength and failure mechanism of the rubble beam. To gain a better understanding of the failure of ice rubble, one needs to account for the effects of the freeze-bonding between the ice blocks (Ettema & Urroz, 1989), (Shayanfar et al., 2018), (Boroojerdi et al., 2016), (Serré et al., 2011) . Bailey et al. (2012) studied the bond strength formed between pieces of rafted ice and reported two

mechanisms of bonding: thermodynamic bonding (weaker) and mechanical bonding (stronger). Ettema and Schaefer (1986) carried out a series of laboratory experiments to determine the effect of confinement, submersion time, bonding area, and salinity on the shear strength of freeze-bond. In these experiments, the confinement of the ice blocks was provided by adding dead weights on top of the blocks so the maximum achieved normal pressure in this study was 3 kPa. Boroojerdi et al. (2016, 2019) studied the effects of confinement pressure, submersion time and indentation rate on the shear strength of freeze-bonds. The applied confinement pressure during formation of the freeze-bond and shear failure of the freeze-bond was up to 100 kPa, which as will be shown in the following, is a better representative of the internal confinement pressures on the rubble blocks in the nature.

While experimental studies provide a valuable qualitative understanding on the effect of freeze-bonding on the behavior of the ice rubble, their ability to quantify this effect and evaluate the internal failure mechanism of ice rubble is limited. For instance, with current tools and methods, it is not possible to locate the exact location and the mode of failure of the broken bonds and evaluate the detailed failure mechanism. Numerical tools has a unique capability to provide a new insight to the mechanical behavior of ice rubble and examine the effect of freeze-bonding on their failure mechanism.

One tool that has proved to be an efficient method for simulating ice rubble is the Discrete Element Modeling (DEM). Some of the first uses of DEM for simulating the failure of ice is by Løset (1994a, 1994b). Løset used a 2D model to simulate broken pieces of ice as circular objects. With advances in computational resources, more researchers have started using DEM for simulating the failure of ice rubble. A 2D combined Finite Element Method (FEM) DEM model was developed by Paavilainen et al. (2009) and later was used to simulate the multi-fracture of sea ice against

sloped structures and punch-through experiments of partially consolidated ice rubble (Paavilainen et al., 2009; Paavilainen & Tuhkuri (2013); Polojärvi & Tuhkuri, 2013; Ranta et al., 2015) The elements of the beam in this model are elastic FEM components, each working as a DEM particle. Polojärvi and Tuhkuri (2013) concluded that the buoyancy-gravity force that moves the broken pieces of rubble vertically plays an important role in failure behavior of ice rubble.

The dominant failure mechanism for relatively thin first-year sea ice under confinement is flexure. Hopkins (1994) introduced a two-dimentional particle based model that simulates the formation of ice rubble based of flexural failure of an intact thin sheet of lead ice against a multiyear floe. This model was later used to improve the energy disipation estimation during pressure ridging procedure (Hopkins, 1997).

Other work has examined a variety of interaction scenarios for ice rubble. For example, Goldstein et al. (2013) employed a 2D DEM model to study the pile-up of grounded sea ice against a sloping structure and suggested an equation to estimate the height of grounded ice rubble pile-up. Polojärvi et al. (2015) developed a 2D DEM model to simulate direct shear box experiments of ice rubble. Lishman and Polojärvi (2015) used a 2D DEM model to understand and estimate the rate dependency of the ice-ice friction, which demonstrated how a dynamic friction coefficient that decreases with sliding speed affects the behavior of ice rubble in shear.

Liu et al. (2015) simulated the failure of ice rubble keel during the gouging of a sea bed using a Cohesive Frictional Mode (CFM). The cohesion model consisted of normal, shear, and torsion springs, and the sea bed was modeled as a rigid body. Berg and Lubbad (2015) implemented a non-smooth DEM (NDEM) model to simulate the failure of unconsolidated ice rubble both in the lab and in full scale. NDEM models are faster than smooth models but can induce artificial vibration to the system that amplifies with the increase of the particle size.

Bonded 3D DEM models are also used to simulate the interaction of sea ice and conical structures. Yulmetov et al. (2017) and Morgan et al. (2015) used a bonded 3D DEM model to simulate the interaction of sea ice with the Confederation Bridge. These studies suggest that simulating ice in multiple layers results in more accurate simulations but increases the simulation cost significantly. Further detail of model developments, including a comprehensive review of the DEM models used to simulate the interaction of ice and offshore structures can be found in Ghobadi et al. (2015).

In this study, a new methodology for calibrating and implementing freeze-bond strength for a DEM model of ice failure has been developed and applied to enhance our understanding of freeze-bonds and their links to flexural failure of ice rubble for freshwater ice. In this method, size and geometry of the rubble blocks is reproduced from the measurement of the size and geometry of the experimental blocks. The strength of the freeze-bonds between the ice blocks are estimated based on the physical properties of the rubble, using empirical formulations. The estimated freeze-bond strength is used to set the bond parameters in the simulation. Each rubble blocks is made of several spherical particles, so the contacting neighbor blocks can form one or several bonds and thus the total strength of the bonds varies by the orientation and shape of the neighboring blocks.

To achieve this end we first calibrate the parameters of our DEM model (see Section 5.5) by simulating freeze-bond strength tests conducted by Boroojerdi et al (2016). These experiments determined the freeze-bond strengths between cylindrical fresh-water blocks as a function of immersion time, confining pressure and initial block temperature. We then simulated ice rubble failure, comparing our results to those of Shayanfar (2017). In Section 5.4 we outline the DEM model. Sections 5.5 and 5.6 detail, respectively, the freeze-bond formation experiments and simulations, and the ice rubble experiments and simulations. Our conclusions are presented in Section 5.7.

The simulation of flexural failure of large scale ice rubble and ice ride is undergoing and is aimed to use the developed model to study the effect of freeze-bond strength and consolidated layer to keel height ratio on the flexural failure of ice rubble. However, it is beyond the scope of the current publication to examine the scalability of the model and use the model for large scale rubble simulations.

5.4. Mathematical Model

The numerical model used in this work was a bonded-particle model based on Potyondy and Cundall (2004). The ice model contains normal and shear springs that operate between neighboring particles that overlap due to compressive stresses or which are bonded (Mohammadafzali et al., 2016; Sarracino et al., 2017). Forces between neighboring spherical particles arise from a cohesive visco-elastic contact model (spring-dashpot model). The force is given by:

$$\vec{F}_{ij} = F_{n(ij)}\ \hat{n}_{ij} + \ F_{t(ij)}\ \hat{t}_{ij} \tag{5-1}$$

where $\hat{n}_{ij}$ is the unit vector from the center of particle *i* to the center of particle *j*, and $\hat{t}_{ij}$ is a unit normal to $\hat{n}_{ij}$ in the direction of incremental tangential strain, due to sliding, between the two particles from one time step to the next. The first term in this equation is the normal force and the second term is the tangential force, each force having two components, the spring force and the damping force. The force components $F_{n(ij)}\ and\ F_{t(ij)}$, both applied to the center of the particles, are given by:

$$F_{n(ij)} = k_n \Delta r_{(ij)} + \gamma_n v_{n(ij)} \quad \text{and} \quad F_{t(ij)} = k_t \Delta t_{(ij)} - \gamma_t v_{t(ij)} \tag{5-2}$$

where normal overlap $\Delta r_{(ij)}$ is:

$$\Delta r_{(ij)} = r_{(ij)} - r_i - r_j \,, \tag{5-3}$$

and $\Delta t_{(ij)}$ is the incremental tangential displacement for the duration of contact due to sliding (tangential overlap) as shown in Figure 5-1 (Kloss et al., 2012). Here r_i *and* r_j are the radii of particles i and j, respectively, and $r_{(ij)}$ is the distance between the centers of the two particles.

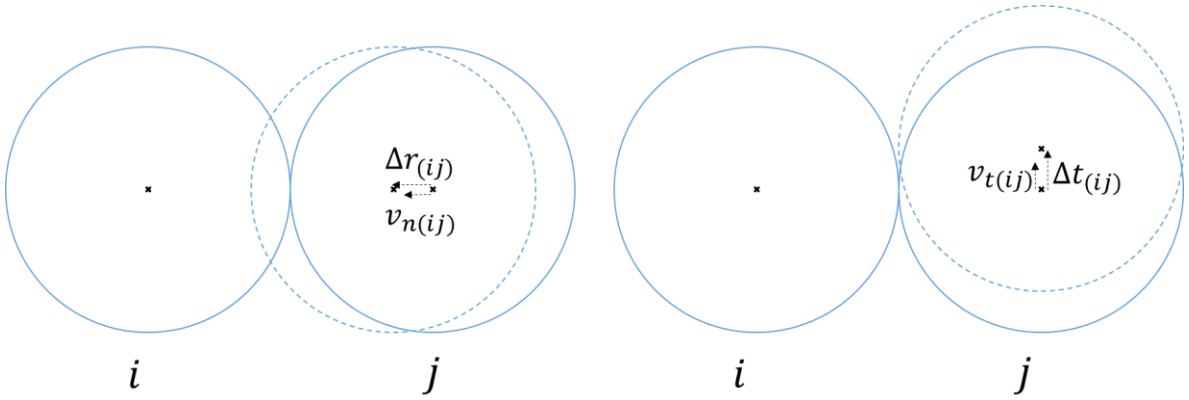

Figure 5-1- Schematic of the normal and tangential overlaps and relative velocities

The relative velocities are given by:

$$v_{n(ij)} = \frac{dr_{(ij)}}{dt}; \;\; v_{t(ij)} = \frac{d\Delta t_{(ij)}}{dt} \tag{5-4}$$

In the formulas above $\vec{F}_{ij}$, $\hat{n}_{ij}$ and $\hat{t}_{ij}$, are anti-symmetric in the indices *i* and *j*, and $r_{(ij)}$, $\Delta n_{(ij)}$, $\Delta t_{(ij)}$, $F_{n(ij)}$, $F_{t(ij)}$, $v_{n(ij)}$ and $v_{t(ij)}$ are symmetric in the indices *i* and *j*.

Figure 5-1 shows a schematic of the normal and tangential overlap and relative velocities. A "rolling friction" model was also used in the simulations to account for non-sphericity. Normal and tangential torques on bonds, T_n and T_t are calculated incrementally:

$$T_n \mathrel{+}= k_t J \omega_n dt \quad \text{and} \quad T_t \mathrel{+}= k_n I \omega_t dt \tag{5-5}$$

where ω_n and ω_t are normal and tangential angular velocities, and *I* and *J* are polar moments of inertia defined as:

$$J = 0.5\pi \min\left((r_1, r_2\right)^4 \quad \text{and} \quad I = 0.25\pi \min\left((r_1, r_2\right)^4 \tag{5-6}$$

The spring stiffness can be set independently, but in these simulations we assumed a linearly elastic, isotropic material and set the relative spring stiffness as:

$$k_n = 2(1+\nu)k_t = \frac{1}{4}\pi E D \tag{5-7}$$

where ν is the Poisson ratio, E is the elastic modulus and D is the particle diameter. The stiffness of the bonds were calculated based on the "equivalent beam" theory (Mohammadafzali et al., 2016; Sarracino et al., 2017). That is, two neighboring particles with elastic modulus of E_1 and E_2 and radii of $r_1$and r_2 becomes a cylindrical beam of radius *r*, cross-section area *A*, and length *L*, where $r = \min(r_1, r_2),\ L = r_1 + r_2,\ A = \pi \min(r_1, r_2)^2$, and the elastic modulus of the equivalent beam E_{eq} is:

$$E_{eq} = (r_1 + r_2)\left(\frac{r_1}{E_1} + \frac{r_2}{E_2}\right)^{-1} \tag{5-8}$$

The time-step was set proportional to the characteristic period of oscillation (Yulmetov et al., 2017), small enough to maintain the stability of the simulation:

$$\Delta t = cD\sqrt{\frac{\rho_i}{E_p}} \tag{5-9}$$

where ρ_i is the density of ice and the constant c is set to 0.1.

The model was implemented on the open source DEM code LIGGGHTS which itself is based on classical Molecular Dynamics (MD) code LAMMPS, designed to run efficiently on multiple processors (Kloss et al., 2012). The model is a modified version of the Hooke contact model, available in LIGGGHTS. A cohesion model, described above, is added to the model to represent the bonding between the ice particles and freeze-bonding between ice blocks.

5.5. Freeze-Bond Experiments and Simulations

Freeze-bond simulations are based on experiments conducted as a part of the MIR project during 2015-2018 (Boroojerdi et al., 2016; Ghobadi et al., 2015; Shayanfar, 2017). A series of freeze-bond tests were conducted on non-grain-seeded freshwater polycrystalline ice cylinders to gain a better understanding of the influence of submersion time, initial temperature and confinement during bond formation on freeze-bond formation and strength. Freeze-bonds were formed between two ice cylinders by putting two cylindrical ice blocks of 9 cm diameter and 10 cm length in contact in a confinement frame and applying a normal load. The frame was then submerged in freezing water for a specific period of time before removal from the water and testing. The specimen was sheared using Asymmetric Four Point Bending (AFPB), which produces a nearly pure shear stress state at the center of the specimen (Figure 5-2).

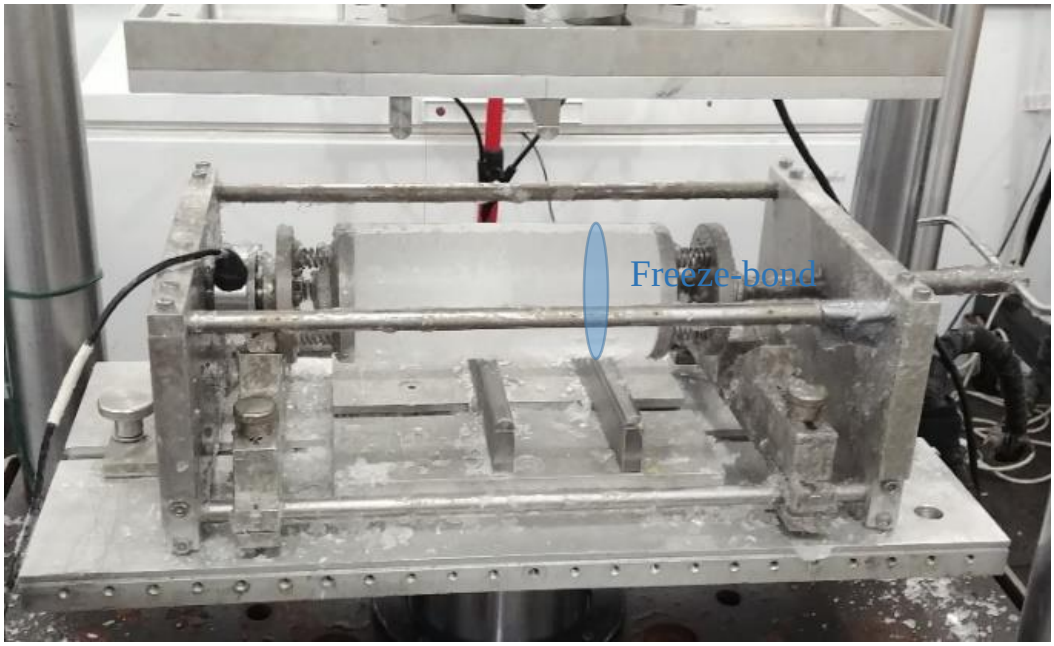

Figure 5-2- The freeze-bond shear apparatus

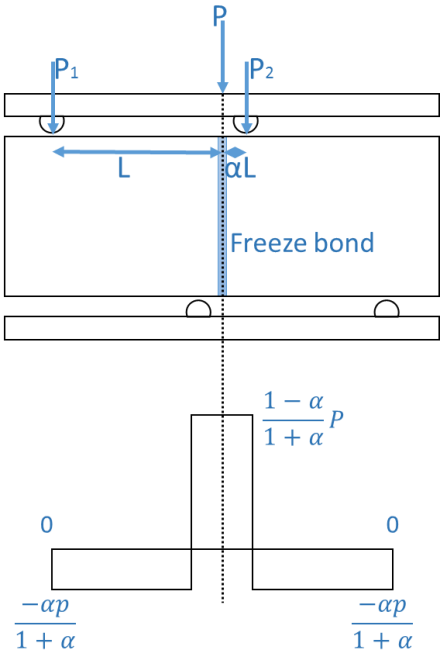

Figure 5-3- Schematic of the shear stress in the AFPB (Boroojerdi et al., 2019)]

According to simple beam theory, if no normal force is applied to the plane of failure, the shear stress τ would be at its maximum at the center of the beam. The shear stress is given by

$$\tau_{max} = \frac{4}{3}\frac{(1-\alpha)}{(1+\alpha)}\frac{P_{max}}{\pi r^2} \tag{5-10}$$

where P_{max} is the peak load ($P_1 + P_2$ of Figure 5-3), r is the radius of the beam, and α is a geometrical coefficient. Figure 5-3 shows a schematic of the AFPB experiments.

These experiments showed that for low initial temperatures (−18°C in this example), the strength of the bond initially increased with submersion time, reaching an initial maximum at about 5 minutes. From then it slowly decreased with increased submersion time, reaching a minimum value after about 3 hours. From that point it began increasing again, due, we surmise, to a combination of sintering and creep processes, with strength approaching that of the parent ice after more than a week (Boroojerdi et al., 2016). Since the ultimate goal of this work is to simulate the rubble tests by Shayanfar (2017), the set of conditions which were selected from the freeze-bond experiments by Boroojerdi et al. (2016) for calibration of the DEM model were set to cover the whole range of freeze-bond parameters in the rubble experiments by Shayanfar (2017).

The numerical model introduced in Section 4.6 was employed in simulating these freeze-bond shear strength experiments. Bonded spherical particles with diameter $d = 15$ mm were used to create a cylindrical DEM specimen identical to the geometry of the freeze-bond experiments (Figure 5-4). The maximum element separation allowing bond formation at the beginning of the simulations was $1.1d$. Two support plates, applying constant confinement pressure of 25 kPa (the confinement applied during the bond breakage tests), were placed at the two ends of the beams. Two fixed indenters at the bottom and two moving indenters at the top applied shear stress to the two freeze-bonded ice blocks until the bond connecting them failed in shear. The strength of the internal block bonds (particles that form each block) is set based on the tensile and shear strength of the freshwater ice and is significantly higher than the freeze-bond strength, so the shear failure mostly happen at the freeze-bonds.

The forces on the indenters, forces on each particle, internal bond forces and freeze-bond forces were recorded. In each simulation, shear stress versus strain was plotted to study the effect of the strength of the freeze-bonds, the elastic modulus of the bonds and contacts (which affects the stiffness of the springs), as well as the packing of the particles and particle size.

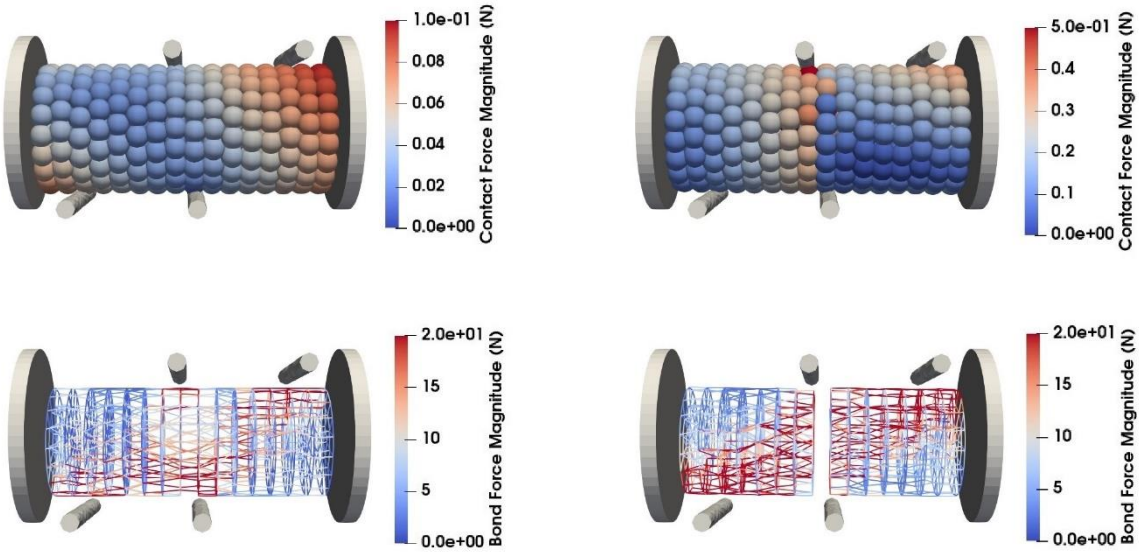

Figure 5-4- Example of contact forces (top) and bond forces (bottom) before (left) and after (right) the failure of the freeze-bond

A total of 30 simulations has been conducted to investigate the effect of studied parameters of the shear failure of the freeze-bond. The results of the freeze-bond calibration simulations yielded several important findings:

i) The effective shear strength of the freeze-bond S_{eff} has a linear relationship with the parametric (particle) shear strength S_p:

$$S_{eff}[\text{pa}] = 0.3555 \times S_p[\text{Pa}] - 13761 \qquad (5\text{-}11)$$

ii) The elastic modulus of the freeze-bond E_{eff} has an exponential relationship with the parametric elastic modulus E_p:

$$E_{eff}[\text{pa}] = 10^7 \ln\left(E_p[\text{Pa}]\right) - 2 \times 10^8 \quad (5\text{-}12)$$

It is noted that by definition, the elastic modulus of a solid elastic material is the slope of the stress-strain curve in the elastic regime. However, since the freeze-bond is a highly brittle material, the slope of the stress-strain curve changes during the progressive failure of the bond. As a practical approach, in this study the stress-strain curve was linearized by taking the elastic modulus E_{eff} to be the ratio of the peak stress to the magnitude of the strain at maximum stress.

iii) By changing the packing of the DEM particles from regular packing to random packing, the resulting freeze-bond strength increases by 20%.

iv) The DEM particle size r_p does not affect the elastic modulus. However, when using smaller particles, the likelihood of initiating the first DEM bond failure increases resulting in a weaker freeze-bond, Figure 5-5. In these experiments, by reducing the size of the DEM particles to 4 mm (*1/r = 250*), this effect becomes negligible (asymptote line in Figure 5-5):

$$\frac{1}{S_{eff}} = 2 \times 10^{-8} \times \frac{1}{r_p} - 2 \times 10^{-6} \quad (5\text{-}13)$$

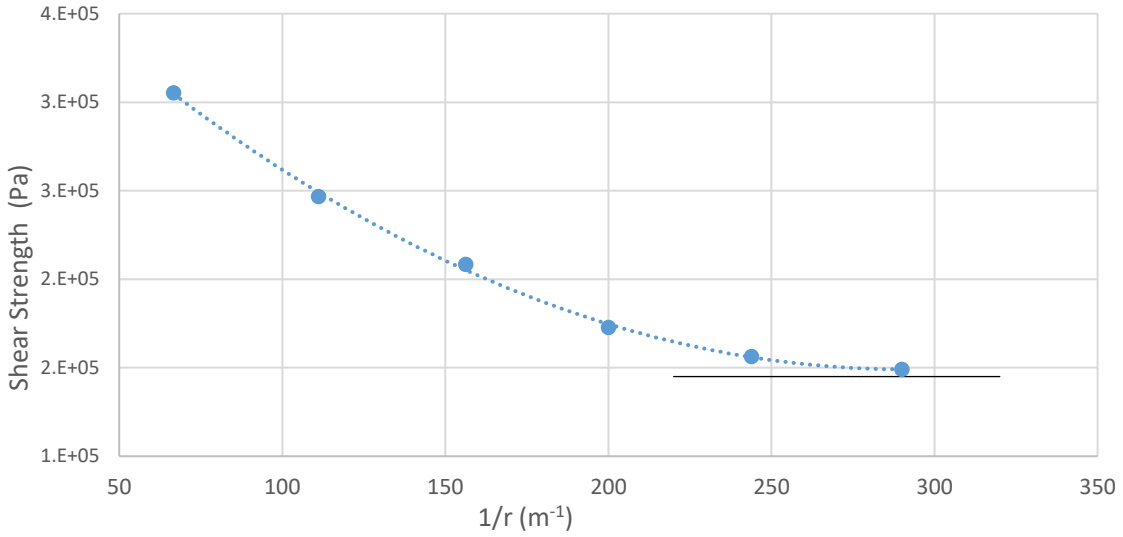

Figure 5-5- Effect of the particle size on the freeze-bond shear strength

5.6. Rubble Beam Experiments and Simulations

To assess the effects of block size and shape distribution, a set of ice rubble beam simulations based on a randomly selected experiment from (2017) were prepared. In the first case, cuboid ice blocks were generated based on the size distribution of the rubble beam experiments reported by Shayanfar (2017) and the contact pressure between the ice blocks were calculated analytically. In the second case, simulations were conducted based on a block size and shape distribution matched to measured size and area of individual ice blocks extracted from pictures of the blocks which were taken prior to assembling the ice rubble beams in the experiments. A custom code was written to generate DEM rubble blocks using shape and size details from the image data, and the contact pressure between the blocks was estimated numerically.

5.6.1. Simulation Set-up

This series of simulations were carried out based on the punch box ice rubble beam test set-up described in Shayanfar (2017), conducted at the C-CORE cold room facilities. As depicted in Figure 5-6, the test apparatus consisted of a Plexiglas punch box measuring 3.05 m in length and 0.94 m in width and height. Pieces of random sized ice blocks created from ice sheets with nominal thickness of 10 cm were put into the punch box and filled with water at about 0 ^{o}C, to form a 50 mm thick ice rubble beam. The ice rubble rested in the box for a specified period of time and was confined under an external confinement prior to being deformed by a centered platen that vertically loaded the ice rubble beam at a rate of 5 mm/s.

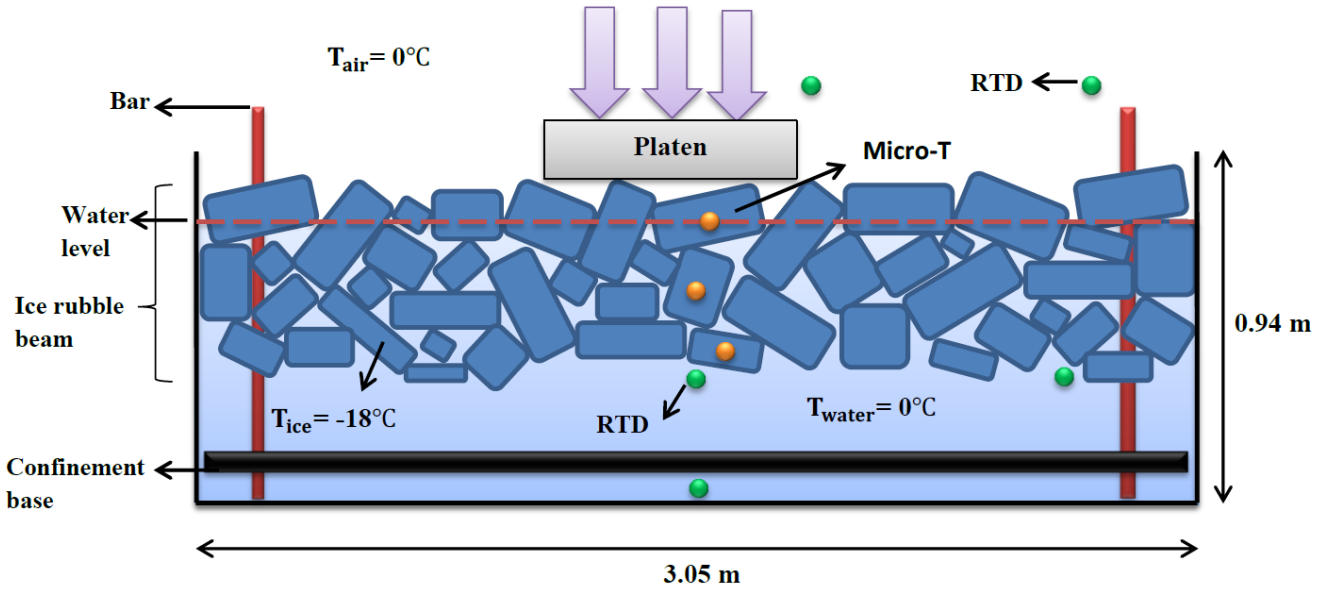

Figure 5-6- Schematic from rubble punch test, reprinted from Shayanfar el al.(2018)

To model this test set-up, a random selection of DEM blocks based on the size distribution of the punch box experimental blocks were first generated using the open-source Bullet physics engine, which is designed to simulate collision detection, and soft and rigid body dynamics. The rubble blocks particles were 55 mm in diameter and arranged in hexagonal close packing (HCP) with two layers. Next the rubble beam was formed by raining the generated blocks into the water. Four infinite frictionless walls were placed around the rubble. Buoyancy, gravity and water drag force were applied to the blocks at this stage and the blocks were defined as non-breakable (for this initial stage), Figure 5-7. It is noted that the freeze-bonding force was absent in this stage, since this is simply part of the rubble macro geometry generation process. After the blocks dropped into the water, the simulation continued for the duration of one minute to allow the rubble to find buoyancy and gravitational equilibrium.

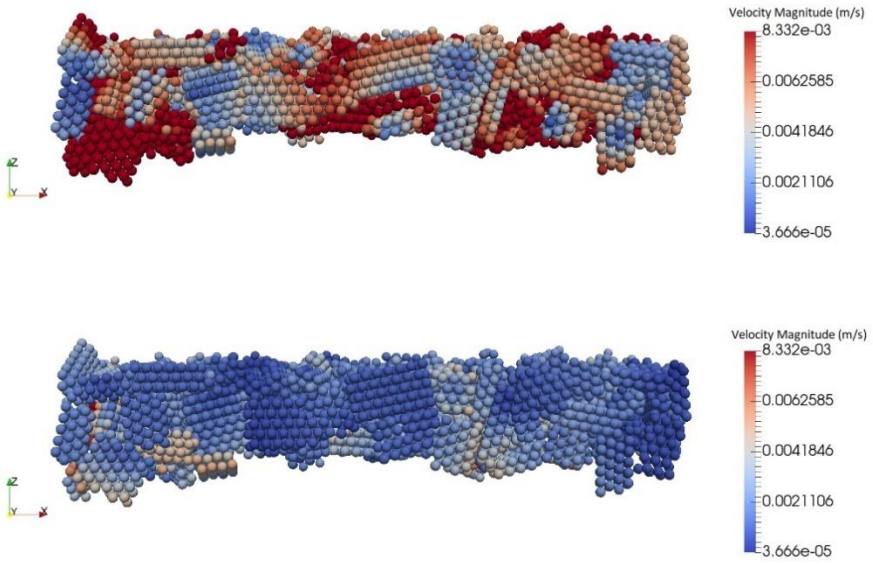

Figure 5-7- Formation of the rubble under gravity and buoyancy. Particle velocity before (up) and after (bottom) settlement

When the rubble achieved equilibrium, the freeze-bonds were then applied to the contacts between individual blocks. Due to the nature of DEM, in most blocks the particle at the corner of a given block was often in contact with four particles on another block, as shown in Figure 5-8, making four freeze-bonds at each contact point. The exception was for blocks that rested in parallel, which resulted in more than four freeze-bonds per block. As shown in Figure 5-8, due to the nature of DEM model, the block to block contact configuration might result in some geometrical interlocking friction (geometrical interlock prevents the DEM blocks to freely move relatively) that adds up to the freeze-bonding force. However, since the engineering friction that happens between two surfaces in the nature is non-existence in this type of DEM model, this geometrical interlocking friction along with the rolling friction between the particles can be a considered as a representative of engineering friction. The rolling friction coefficient used in this study is based on Yulmetov et al. (2017), further investigation on the block to block friction in bonded-particle DEM is recommended for future work.

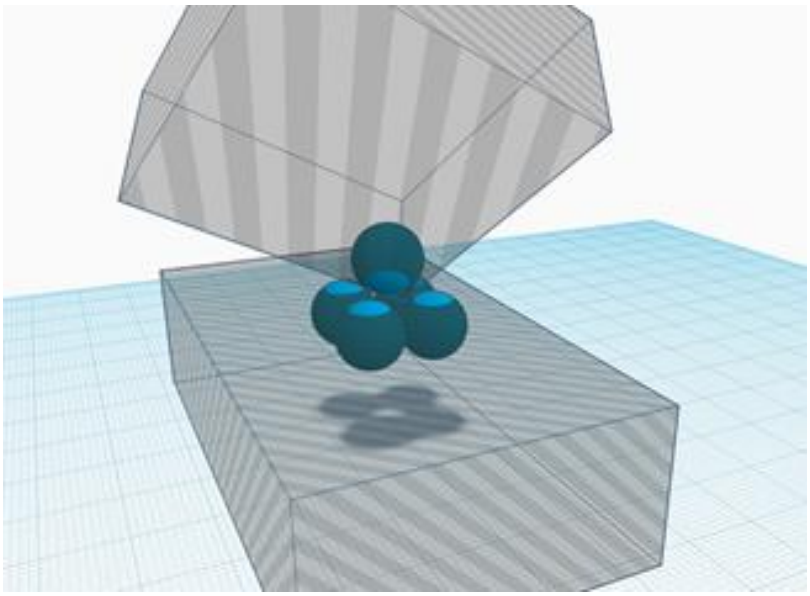

Figure 5-8- Schematic of a typical DEM freeze-bond

5.6.2. Cuboid Block Shape Distribution Simulations

To model the freeze-bonds in the DEM simulation for the cuboid blocks, estimates of freeze-bond areas needed to be compared with those from experiments. In the experiments, the ice blocks were initially at $-18℃$ when they were submerged in $0℃$ water. For this scenario, the thermodynamic ice growth of the blocks can be estimated as (refer to Figure 5-9):

$$m_i c_i \Delta\theta = \Delta m_i L_m \tag{5-14}$$

$$c_i = 2.108 \left[\frac{\text{kJ}}{\text{kgK}}\right] \qquad L_m = 334 \left[\frac{\text{J}}{\text{g}}\right] \qquad \Delta\theta = 18\ [℃]$$

$$m_i \times 2.108 \times 18 = \Delta m_i \times 334 \qquad \Delta m_i = 0.114 m_i$$

Mass and volume growth can be related by:

$$m_i = \rho_i v_i \qquad \Delta m_i = \Delta\rho_i v_i$$

$$\Delta v_i = v_i' - v_i = 0.114 v_i \qquad v_i = whl$$

$$v_i' = (w + \Delta l)(h + \Delta l)(l + \Delta l)$$

For the ice blocks used in this study:

$$h = 10\ [\text{cm}] \qquad \frac{l}{w_{ave}} = 1.4 \qquad w = 0.714l$$

$$v' = (0.714l + \Delta l)(10 + \Delta l)(l + \Delta l)$$

$$\frac{v_i' - v_i}{v_i} = 0.114$$

$$\frac{17.14l\Delta l + 0.714l^2\Delta l + 1.714l\Delta l^2 + 10\Delta l^2 + \Delta l^3}{7.14l^2} = 0.114$$

And so the length growth can be defined as a function of initial mass:

$$\Delta l = \frac{-17.14 - 0.714 + \sqrt{(17.14 + 0.714l)^2 - 4(1.714 + \frac{10}{l})(-0.814l)}}{2(1.714 + \frac{10}{l})} \qquad (5\text{-}15)$$

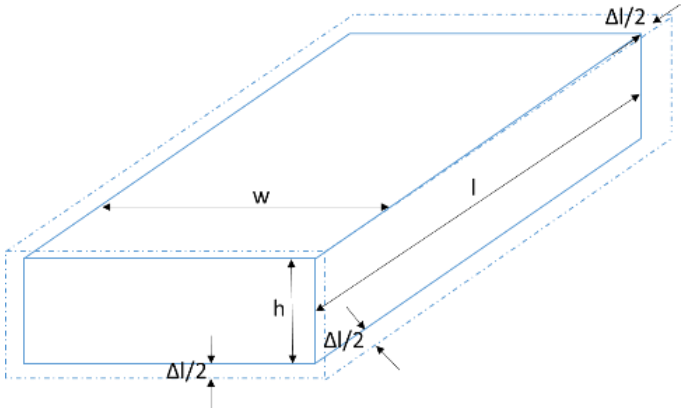

Figure 5-9- Schematic of the growth of an ice block

where m is the mass, c_i is the specific heat capacity, θ is the temperature, L_m is freezing fusion capacity, l, w and h are the length, width and height on the block, respectively. Having Δl as a function of the block length, the average linear ice growth for each block in the rubble has been

calculated. The average isotopic linear ice growth for the first five experiments was $\Delta l_{ave} = 0.32$ cm. This calculation is consistent with observed experimental ice growth and the numerical modeling of ice growth by Ghobadi et al. (2015).

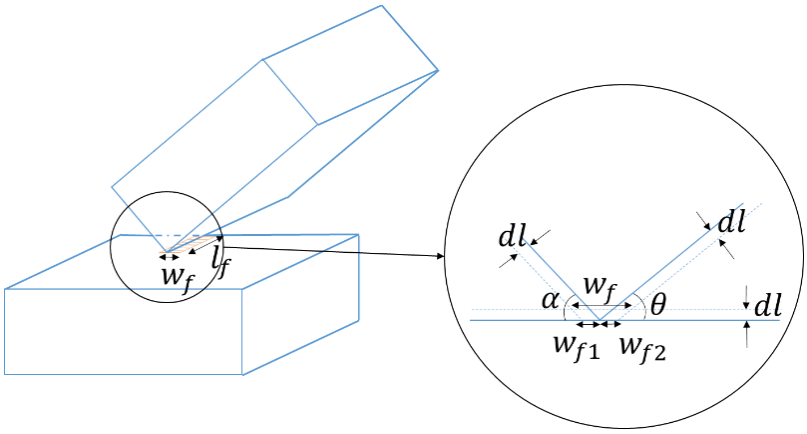

Figure 5-10- Schematic of the typical freeze band area

Based on the assumed freeze-bond geometry shown in Figure 5-10, ice growth between neighboring blocks which is associated with the formation of freeze-bond between the blocks can be estimated as:

$$w_{f1} \sin\theta = dl \qquad w_{f1} = \frac{dl}{\sin\theta}$$

$$w_{f2} \cos\theta = dl \qquad w_{f2} = \frac{dl}{\cos\theta}$$

$$w_f = w_{f1} + w_{f2} + \frac{dl}{\sin\theta \cos\theta}$$

$$w_f = \frac{dl}{\sin\theta} + \frac{dl}{\cos\theta} + \frac{dl}{\sin\theta \cos\theta} \tag{5-16}$$

where w_f and l_f are width and length of the freeze-bond.

For an average value of $dl_{ave} = 0.32$ cm, this yields a value of :

$$w_{f_{ave}}(for\ \theta = 5\ \rightarrow \theta = 85) = 0.0394\ [\text{m}] = 3.94\ [\text{cm}]$$

Assuming the blocks have edge to surface contact at average length of 5 cm, the average freeze-bonding area A_f would be:

$$A_{f_{experimental}} = 5 \times 3.94 = 19.7\ [\text{cm}^2]$$

Whereas the freeze-bonding area between two block for the DEM simulations, consists of four bonded particles is:

$$A_{f_{DEM}} = 4\pi r^2 = 4\pi \times 2.75^2 = 95.04\ [\text{cm}^2]$$

As the force needed to break a freeze-bond is proportional to the freeze-bond area, the freeze-bond strength and elastic modulus in the DEM simulations are related by contact area factor c_f which must be applied to the strength parameters and is calculated as:

$$c_f = \frac{A_{f_{experimental}}}{A_{f_{DEM}}} = \frac{19.7}{95.04} = 0.207 \tag{5-17}$$

Since the rubble blocks are underwater, the effects of hydrostatic pressure must also be considered. According to Ettema & Schaefer (1986) the internal stress within layers of floating ice σ_z due to hydrostatic pressure, as illustrated in Figure 5-11, can be written as:

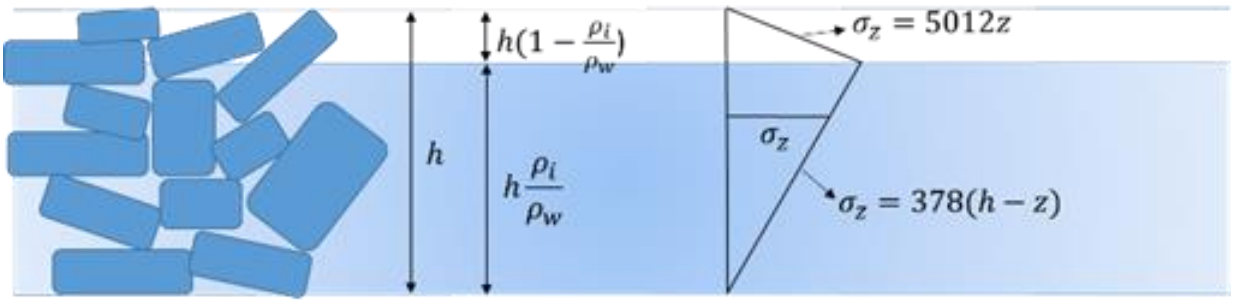

Figure 5-11- Schematic of the gravity-buoyancy pressure

$$\begin{cases} \sigma_z = (1-p)\rho_i g z, & for\ 0 \le z \le \rho_i h \\ \sigma_z = (1-p)(\rho_w - \rho_i) g (h-z), & for\ z \ge \dfrac{\rho_i}{\rho_w} h \end{cases} \quad (5\text{-}18)$$

The average internal stress σ_{ave} acting over the nominal projected area (length *L* x width *W*) of the ice rubble mass may be calculated for $h = 0.5$ m, $\rho_i = 934\,\frac{\text{kg}}{\text{m}^3}$, $\rho_w = 1000\,\frac{\text{kg}}{\text{m}^3}$ using Eq. (10) to yield a value of $\sigma_{ave} = 82.7$ Pa.

To estimate the contact pressure at the block-block interface due to this hydrostatic pressure, we must next estimate the ratio of the nominal projected area to the corresponding contact area between blocks. In the above section, the average freeze-bond area between two blocks during experiments was estimated to be 19.7 cm^2. Similarly the estimated nominal projected area for each pair of blocks was estimated from numerical simulations to be approximately 432 cm^2. It is therefore estimated that the contact pressure between blocks is $\frac{432}{19.7} = 21.9$ times greater than the average internal stress due to the hydrostatic pressure. Correspondingly the average contact pressure between blocks due to hydrostatic effects may be estimated as $\sigma_{ave-b} = 82.7 \times 21.9 =$ 1.81 kPa.

Based on Boroojerdi et al. (2016) and accounting for the submergence time of 4 hours and the estimate contact pressure of σ_{ave-b}= 1.81 kPa, the freeze-bond strength has been estimated as:

$$S_{FB\_exp} = 88.8 \text{ kPa}$$

Accounting for the area correction factor c_f the DEM freeze-bond strength value has been estimated as:

$$S_{DEM_{eff}} = c_f \times S_{FB\_exp} = 0.207 \times 88.8 = 18.38 \text{ kPa}$$

Once the above confinement levels were applied to the ice rubble blocks, freeze-bonds were inserted between the simulated ice blocks. The freeze-bond strength value $S_{DEM_{eff}}$ was set using the value noted above and elastic modulus were set based on the freeze-bond calibration simulations. To represent the end conditions in the experiments, the two ends of the rubble were fixed to the ends of the box. The indenter plate was then added to the simulation at the mid-point of the rubble beam to allow for simulate loading of the beam until flexural failure of the rubble beam occurred. Shear force vs. deformation curve results obtained for this simulation are shown compared the corresponding experimental results in Figure 5-12.

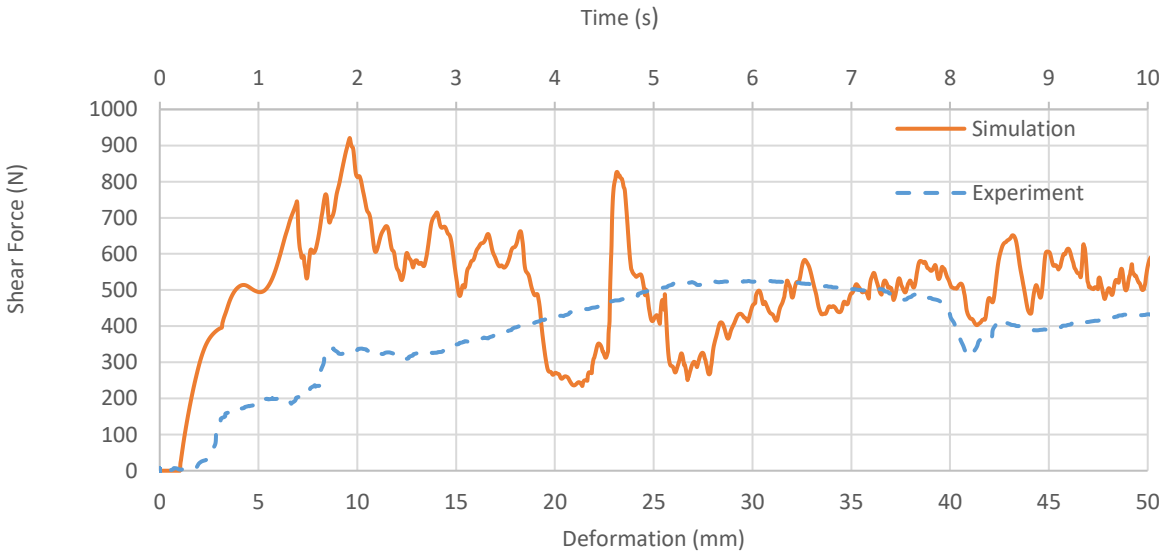

Figure 5-12- Comparison of shear force vs. deformation curves from simulations for cuboid blocks with experimental results

As may be seen in Figure 5-12, in both the simulation and the experiment, the initial force on the platen continues to increase before freeze-bonds begin to break in the center of the rubble, which is followed by a drop in the force. Following this initial failure, the residual strength results from a combination of unbroken bonds and friction between the blocks.

Although this DEM simulation with cuboid blocks over predicts the flexural strength of the rubble beam, it is capable of showing the mechanism of the failure and provides agreement with the residual rubble strength. Repeats of the same simulation with random initialization of the blocks did not significantly affect the peak load and behavior of the rubble. These differences are largely attributed to the effect of shape, since cuboid blocks provide larger flat areas that can potentially form bigger freeze-bonds and the strength of the rubble beam is highly dependent of the strength and amount of freeze-bond area. Other factors such the impact of block geometry on friction may also play a role. To help address these issues and increase the accuracy of the geometric representation of the ice blocks and their corresponding interaction areas, a new method for generating ice block geometry based on observed ice rubble block shapes is introduced below.

5.6.3. Empirical Block Shape Distribution Simulations

To generate the ice rubble for this setup, the first step was to generate the set of individual block geometries. To do this, the size and area of each block was based on captured pictures of the rubble blocks from the experiments. A cuboid DEM block was then generated based on the dimensions of each block and a custom code was written to randomly and iteratively cut the cuboid blocks until the area of the DEM block matches the area of the actual block, Figure 5-13.

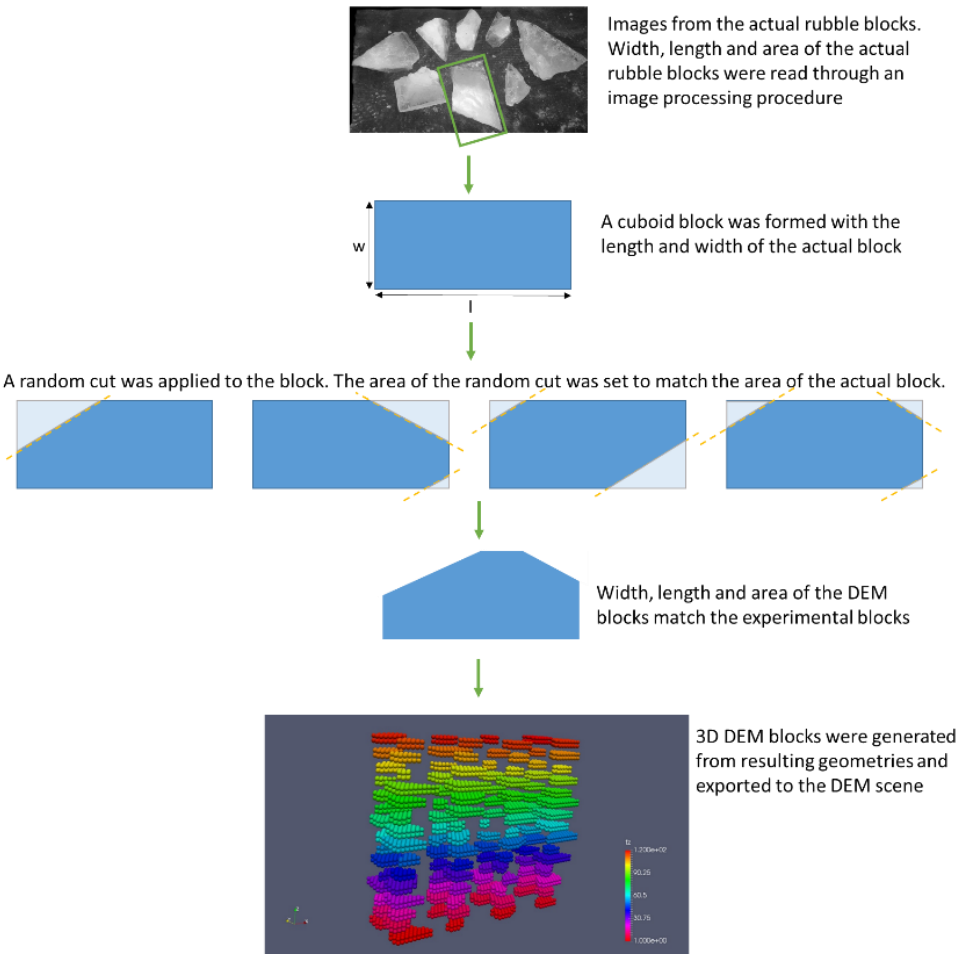

Figure 5-13- Formation of the Empirical DEM ice blocks

These blocks were then rained into a former using a similar manner described in Section 5.6.1 so as to generate a rubble beam with randomly oriented blocks having the appropriate dimensions. For the rubble beams produced using these block shapes, the ice rubble was exported to an open-source DEM code WOODEM, to allow for extraction of details of the block-block contact pressures to model the relationship between average applied pressure and average contact pressure between blocks when subjected to hydrostatic pressure, which was found to be about 2.74 kPa per bond pair. It is noted that this is higher than for the case of the cuboid blocks because the contact takes place through a larger number of smaller contact pairs, each of which have a smaller area over which the force is transmitted.

Based on this estimated contact pressure of σ_{ave-b}= 2.74 kPa, the freeze-bond strength was estimated using the results form Boroojerdi et al. (2016) to be 89.45 kPa. Similarly, accounting for the correction factor c_f, the DEM freeze-bond strength value was estimated as 18.52 kPa. Using these values, along with other model parameter values given in Table 1, the the shear force vs. deformation results in Figure 5-14 were obtained and compared with corresponding experimental results.

Table 5-1- Simulation parameter values

Freeze Bond Parameter	Material specific/experimental	Estimation method	Cuboid block simulations	Estimation/generation method	Empirical block simulations	Estimation/generation method
Poisson ratio, ν	0.32	Timco et al. (2009)	0.32	Timco et al. (2009)	0.32	Timco et al. (2009)
Shear strength, S [kPa]	88.8-89.45	Boroojerdi et al. (2019)	48.1	Equation (5,7,11)	48.3	Equation (5,7,11)
Tensile strength, S_y [kPa]	195	Gold (1977), Timco (1982), Frederking (1988), Assumption (i)	105.82	Assumption (i), S_p	103.62	Assumption (i), S_p
Freeze Bond elastic modulus, E [MPa]	50	Boroojerdi et al. (2019)	1300	Equation (6,11)	1300	Equation (6,11)
Shear spring stiffness, k_t [MPa]	N/A	N/A	31.13	Equation (2)	31.13	Equation (2)
Normal spring stiffness, k_n [MPa]	N/A	N/A	51.05	Equation (2)	51.05	Equation (2)
Block size	Random length and width, 10cm height	Image processing	Experimental size distribution	Shayanfar et al. [21]	Experimental block sizes	Custom code
Block shape	Random, semi-cuboid	Image processing	Cuboid	N/A	Semi cuboid	Custom code

Assumption (i): The shear to tensile strength ratio of fresh water ice is equal to shear to tensile strength ratio of fresh water freeze-bond

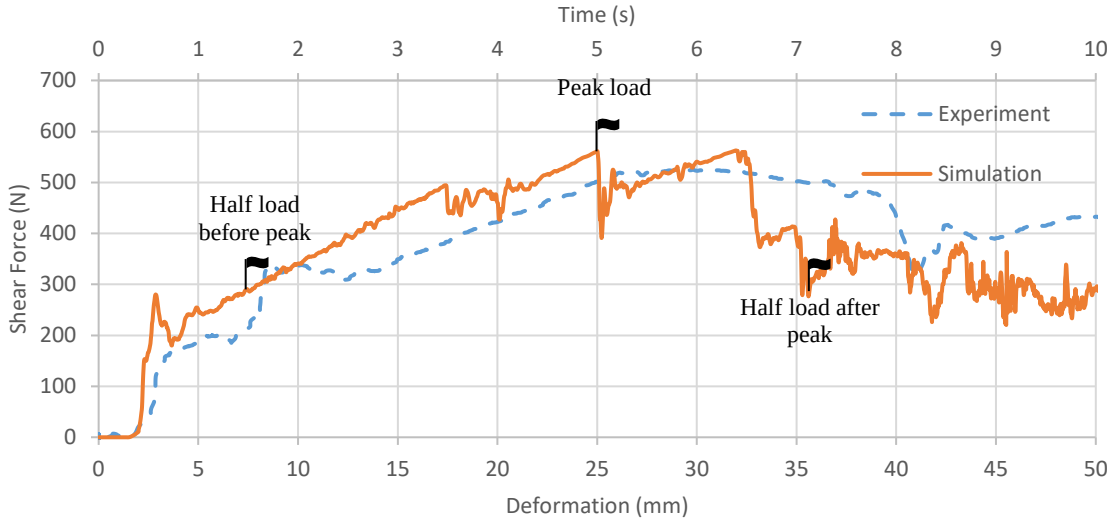

Figure 5-14- Comparison of shear force vs. deformation curves from simulations for empirical block shapes with experimental results

As can be seen from Figure 5-14, for simulations based on empirical rubble block shapes, not only does the failure mechanism of the rubble failure match much better between simulation and experiment, but the peak flexural strength of the rubble beam also matches more closely with the experiment than did the results for the cuboid rubble blocks. It is expected that the cuboid rubble blocks over-estimate the maximum force through two effects. First, the total contact area between the cuboid rubble blocks was higher than the empirically-based block shape, hence although they estimated to have a slightly weaker freeze-bond strength, they increased the overall strength of the rubble. Second, as the cuboid rubble blocks have a higher volume, they artificially increase the buoyancy force exerted by the platen.

The force on the platen reaches a local maximum of about 290 N in about 3 mm of deformation, where the force drops by 30 N due to a local bond failure. The force then continues to increase consistently to about 500 N at a deformation of 17 mm, at which point several local failures occur. The load continues to rise again, ultimately failing at about 33 mm deformation when the crack penetrates through the full thickness of the beam. This flexural failure of the rubble beam is followed by a sharp decline in the force, with some continued local maximums occurring as broken clusters of blocks interact, which results in frictional forces and failure of unbroken freeze-bonds. The residual strength of the beam therefore depends on the friction between these blocks, the location of bond breakages in the rubble matrix, the strength of the surviving freeze-bonds, as well as the orientation of the blocks. Overall the simulation for this model set-up provides good general agreement with observations and measurements from the corresponding ice rubble experiment. Repeats of the same simulation with random initialization resulted in comparable force-displacement curve and did not significantly affect the peak load.

5.6.4. Effect of Buoyancy

The forces measured at the platen are attributed by both the flexural failure of ice rubble and the increase of the buoyancy due to submersion of the ice rubble and platen. To measure the pure flexural strength of the ice rubble, one has to subtract the forces exerted by this buoyance force.

Shayanfar (2018) estimated the buoyancy force during the experiment by measuring the rise in the water level. It was estimated that from the maximum load of 522 N, 439 N, is attributed by buoyancy and 83 N is attributed by the failure of ice rubble. In the cuboid and empirically-based block shape rubble simulation, the buoyancy contributes 543 N and 391 N to the total load respectively at maximum load. As the volume of the cuboid rubble blocks are naturally larger than the empirically-based rubble blocks, they exert a higher buoyancy force to the indenter.

5.6.5. Mechanism of Failure

As the indenter pushes the rubble vertically downward, movement of the rubble blocks places the freeze-bonds under stress resulting in breakage in some bond. This in turn, changes the geometric configuration of the rubble. The forces acting on the bonds, including the bonds within the ice blocks and the freeze-bonds between the blocks, during failure, as well as the location and number of broken bonds were extracted by a custom code that uses Visualization Toolkit (VTK) bond outputs of the LIGGGHTS as its input.

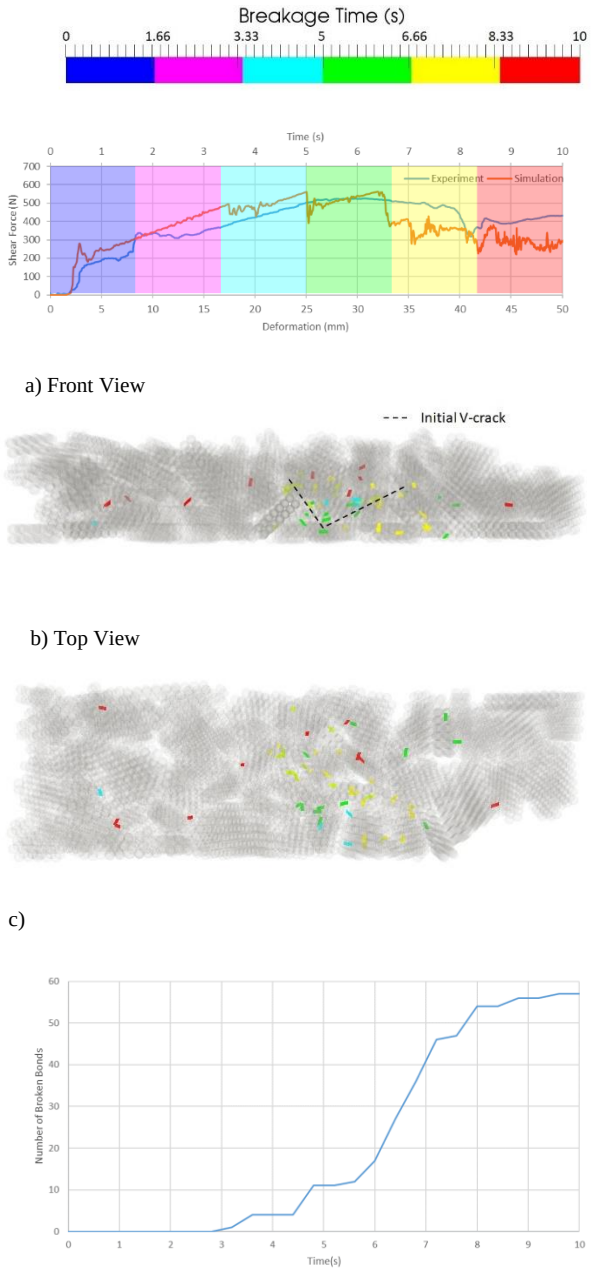

Figure 5-15- Location (a and b) and time (c) of the failure of bonds

To better understand internal forces within the rubble force data were extracted for three times of interest: half load before peak, peak load, and half load after peak. As shown in Figure 5-15, early in the loading process, no bonds are broken yet, so the whole rubble behaves as a solid mass connected through the freeze-bond network. Forces on the blocks can be transferred to the neighboring blocks through this network of bonds. Figure 5-16 shows the average stress on the

bonds at each spatial location at these times of interest. As can be seen from Figure 5-16, prior to the peak load, the stress on the bonds is significantly lower than the stress at the peak load or even at half load after peak. At this point, the porosity of the rubble has not yet reached its minimum, and the rubble blocks have some room to move before undergoing a significant stress.

As shown in the plot in Figure 5-15(c). during the first 3.6 seconds of the simulation, no breakage of the freeze-bonds has been observed, so the rubble beam behaves as a solid beam under flexure; the bottom of the rubble is under tension, and the top of the rubble is under compression. As the tensile strength of the ice and freeze-bonds are significantly lower than their compressive strength, between 3.6 and 6 seconds into the simulation, some of the freeze-bonds close to the bottom of the rubble start to fail in tension, as shown in Figure 5-15. Meanwhile, some of the freeze-bonds in the right side of the rubble, where the rubble is thinner, and the fixed support is smaller (compared to the left side), start to fail in shear making the already weakened central part of the rubble even weaker.

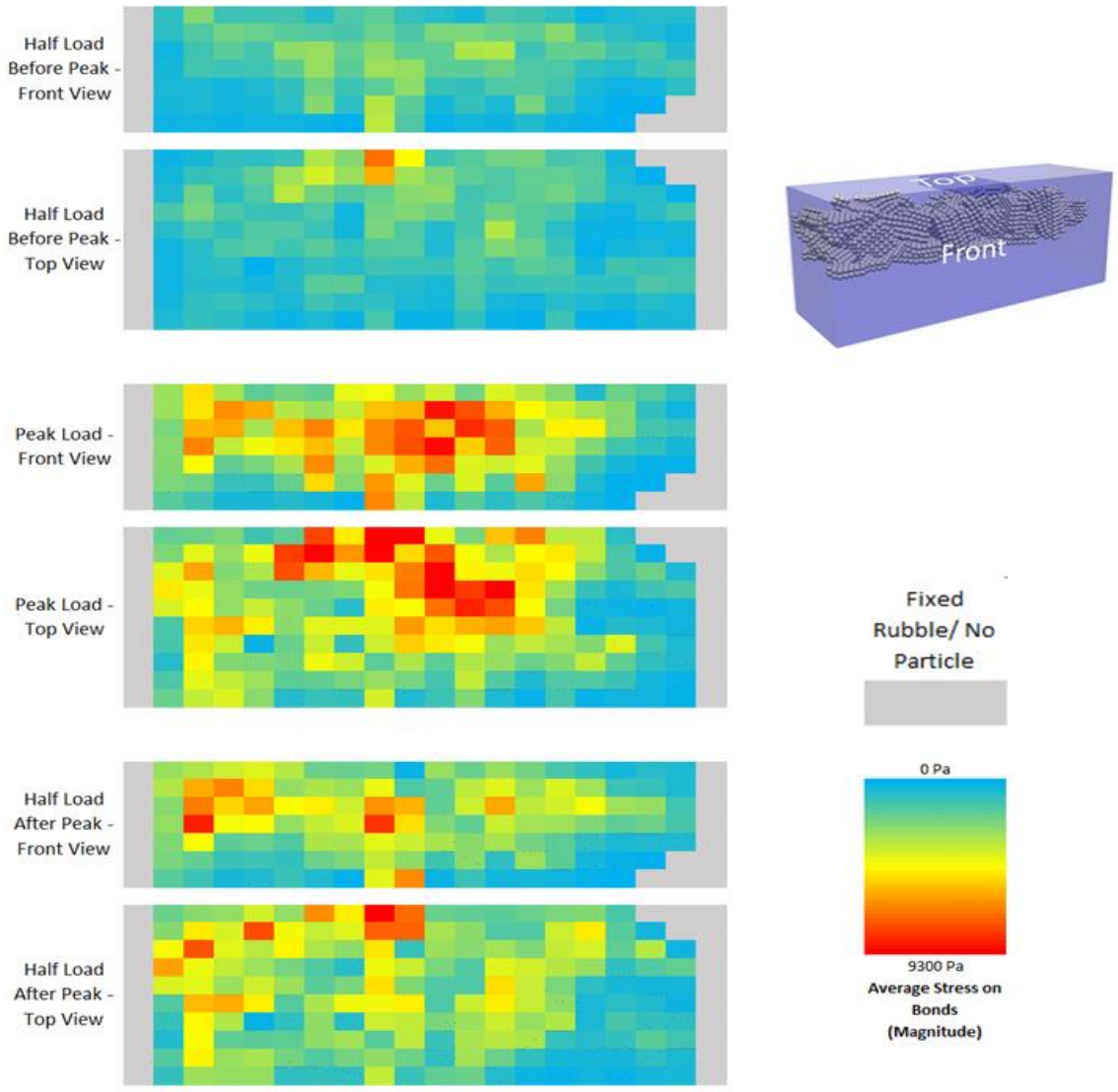

Figure 5-16- Average stress on the bonds at three points of interest

Around 6 seconds into the simulation, most of the freeze-bonds between the blocks located in the bottom center and the bottom right of the rubble have broken under tension and shear. During the next 2 seconds, two types of freeze-bond failure were observed: in the center of the beam, under the indenter, the remainder of the freeze-bonds make the rubble beam behave as a solid beam, the cracks initiated in the previous steps diagonally penetrate to the top of the beam in a V-shape. In the meantime, a global shear failure can be seen throughout the length of the rubble.

During the last 2 seconds of the simulation (8s-10s), the V-shaped crack caused by flexure of the beam has fully penetrated to the top of the beam and the localized flexural failure does not play an important role in the failure of the rubble. However, the ice beam continues to fail globally under shear, so the residual strength of the rubble beam at this stage is dominated by friction, the interlocking of the ice blocks, and the shear strength of the freeze-bonds.

Interestingly, Bailey et al. (2015), Shayanfar (2017), and Shayanfar et al. (2018) reported the same failure mechanisms in their rubble beam experiments. Shayanfar (2017) describes these two types of failure as "localized tensile failure" and "localized shear failure." As stated above, the failure of the rubble in the simulation starts at the central bottom of the rubble, where the freeze-bonds in this area start to fail in tension as a result of flexural load. The shear failure continues to deform the rubble through the total length of the beam and to define its residual strength. Shayanfar (2017) states, "It was observed in the majority of punch tests that the ice blocks are separated at the central bottom part of the beam… a partial failure caused the ice blocks to separate in tension in the central part of the beam… the rubble failure on the macroscopic scale was shearing through the whole beam thickness."

The results of the DEM simulations are consistent with the experimental results, not only on predicting the force vs deformation curve but also on the details of the mechanism of failure. This consistency highlights the capabilities of the DEM model developed in this study for modelling loads and simulating details of failure mechanisms observed in ice rubble. This in turn provide new insights into the failure processes and associated mechanics of ice rubble strength development.

5.7. Conclusion

In this chapter, results have been presented from calibration simulations based on recent freeze-bond experiments by Boroojerdi et al. (2016), as well as simulations of ice rubble beam tests which utilize parameters from these calibrations. These ice rubble beam simulations have been compared with corresponding experimental results from Shayanfar (2017). The use of AFPB shear tests to calibrate freeze-bond parameters for strength and elastic modulus in the DEM model was found to be an effective approach for establishing a physical basis for parameter values used in the numerical model. Methodology to account for the differences in freeze-bond area and account for the effects of hydrostatic pressure and initial temperature on DEM model parameters have been proposed.

To study the effect of block shape and size distribution, cuboid rubble block simulations and empirically-based block shape simulations have been conducted. From these results it was observed that the cuboid rubble simulations tend to overestimate the maximum load prior to flexural failure of the rubble beam, whereas the simulations with empirically-based block shapes yield significantly better agreement with the experiments. However, one needs to consider the actual geometry of rubble blocks of the experiment of interest before utilizing this block type, as utilization of this block type might not be appropriate for all scenarios. The good general agreement between simulation results and experimental results suggest that the simplifications and assumptions made in the approach presented herein provide a reasonable approximation of the physical rubble matrix from the laboratory tests.

Two mechanisms of failure of the freeze-bonds have been observed during the flexure of the rubble beam. During initial stages of the loading, the failure of the beam is dominated by the development of a crack that initiates in the central bottom region of the beam and penetrates to the top of the

beam, breaking the freeze-bonds primarily in tension. During this type of failure, the entire rubble behaves as a solid beam under flexure. Following this stage, shear failures are also observed through the whole length of the beam. These simulation results are in good agreement with observed failure behavior reported from experimental studies of ice rubble beam failure (Mohammadafzali et al., 2016).

Results from this study highlight the capabilities of DEM for simulating the macroscopic behavior of ice rubble masses based on block-block interaction mechanics and freeze-bond properties calibrated from fundamental bond property experiments. For such scenarios, DEM models have the advantage of being able to simulate freeze-bonds and post-failure friction between blocks with sufficient accuracy to represent macroscale properties and strength, while maintaining sufficiently low computational cost to enable simulation of larger domains needed for large ice features, such as ice ridges and rubble fields. Moreover, such an approach also allows for use of breakable bonds for solid ice masses, which is important for simulations of interactions that include ridges with consolidated layers and level ice, which will be explored in future work.

An important outcome of this work is the establishment of linkages between experiments in which details of the physical mechanisms of freeze-bond strength have been characterized by Boroojerdi et al. (2016) and DEM simulations which can utilize these test results as a basis for larger scale simulations. Continued work to expand and validate this approach is planned. Areas for further investigation include an evaluation of how the macroscopic behavior of simulated ice rubble masses varies as freeze-bond strength changes as a function of applied confinement, submersion time and loading rate. Through such work, it hoped that stronger linkages between the physics of freeze-bond formation and macroscale ice rubble behavior can be established, to ultimately help increased confidence in simulations tools used for engineering design.

5.8. References

Azarnejad, A., & Brown, T. G. (2001). Ice Rubble Behavior in Punch Tests. *J. Cold Reg. Eng.*, *15*(3), 135–153.

Bailey, E., Sammonds, P. R., & Feltham, D. L. (2012). The consolidation and bond strength of rafted sea ice. *Cold Regions Science and Technology*, *83–84*, 37–48. https://doi.org/10.1016/j.coldregions.2012.06.002

Bailey, E., Taylor, R., & Croasdale, K. (2015, June). Mechanics of Ice Rubble Over Multiple Scales. *Proceedings of the ASME 34th International Conference on Ocean, Offshore and Arctic Engineering*. https://doi.org/10.1115/OMAE2015-42004

Berg, M. van den, & Lubbad, R. (2015). The application of a non-smooth discrete element method in ice rubble modeling. *Proceedings of the 23rd International Conference on Port and Ocean Engineering under Arctic Conditions*.

Boroojerdi, M. T., Bailey, E., & Taylor, R. (2019). Experimental study of the effect of submersion time on the strength development of freeze bonds. *Cold Reg. Sci. Technol.*, *Under Revi*.

Boroojerdi, M. T., Ghobadi, M., Taylor, R., Bailey, E., & Arctic, C. (2016). Experimental Study on Shear Strength of Freeze Bonds in Freshwater Ice. *Proceeding of Arctic Technology Conference 2016*, 1–9.

Bruneau, S. E. (1996). Development of a first year ridge keel model [Memorial University of Newfoundland]. In *Doctor of Philosophy*. https://doi.org/10.1017/CBO9781107415324.004

Ettema, R., & Schaefer, J. A. (1986). EXPERIMENTS ON FREEZE-BONDING BETWEEN ICE BLOCKS IN FLOATING ICE RUBBLE. *Journal of Glaciology*, *32*(112), 397–403.

Ettema, R., & Urroz, G. E. (1989). *Cold Regions Science and Technology*, *16 (1989) 237-247*. *16*, 237–247.

Ettema, R., & Urroz-Aguirre, G. E. (1991). Friction and cohesion in ice rubble reviewed. *Proceedings of the 6th International Speciality Conference Cold Regions Engineering*, 316–325.

F. McKenna, R., Bruneau, S., & M. Williams, F. (1996). In situ shear strength measurements of model ice rubble using a punch technique. *49th Canadian Geotechnical Conference of the Canadian Geotechnical Society*, 279–286.

Fransson, L., & Sandkvist, J. (1985). Brash ice properties—laboratory tests. *Proc. of the 8th Int. Conf. on Port and Ocean Engineering under Arctic Conditions Narssarssuaq*, 75–87.

Frederking, R. M. W., Timco, O. J., & G.W., S. and. (1988). On Measuring the Shear Strength of Ice. *IAHR Ice Symposium*, 76–88.

Ghobadi, M., Bailey, E., & Taylor, R. (2015). *Thermal Behavior and Growth of Submerged Ice Blocks: Experimental and Numerical Results*. *May*, 1–9. https://doi.org/10.1115/OMAE201541894

Gold, L. W. (1977). Engineering Properties of Fresh-Water Ice. *Journal of G/AcioloD*, *19*(81).

Goldstein, R., Onishchenko, D., Osipenko, N., Shushpannikov, P., & Naumov, M. (2013). Grounded ice pile-up. 2D dem simulation. *Proceedings of the 22nd International Conference on Port and Ocean Engineering under Arctic Conditions*.

Heinonen, J. (2004). *Constitutive Modeling of Ice Rubble in First-Year Ridge Keel*. Helsinki University of Technology, Espoo, Finland.

Hopkins, M. A. (1994). On the ridging of intact lead ice. *Journal of Geophysical Research*, *99*(C8). https://doi.org/10.1029/94jc00996

Hopkins, M. A. (1997). Onshore ice pile-up : a comparison between experiments and simulations. *Cold Region Sience and Technology*.

Kloss, C., Goniva, C., Hager, A., Amberger, S., & Pirker, S. (2012). Models , algorithms and validation for opensource DEM and CFD-DEM Models , algorithms and validation for opensource DEM and CFD-DEM. *Progress in Computational Fluid Dynamics*, *12*(2/3), 140–152. https://doi.org/10.1504/PCFD.2012.047457

Leppäranta, M. (2011). *The Drift of Sea Ice* (Second Edi). Springer Science & Business Media.

Leppäranta, M., & Hakala, R. (1992). The structure and strength of first-year ice ridges in the Baltic Sea. *Cold Regions Science and Technology*, *20*(3), 295–311. https://doi.org/10.1016/0165-232X(92)90036-T

Liferov, P., & Bonnemaire, B. (2005). Ice rubble behaviour and strength: Part I. Review of testing and interpretation of results. *Cold Regions Science and Technology*, *41*(2), 135–151. https://doi.org/10.1016/j.coldregions.2004.10.001

Lishman, B., & Polojärvi, A. (2015). 2D DEM of ice rubble: The effect of rate-dependent friction. *Proceedings of the 23rd International Conference on Port and Ocean Engineering under Arctic Conditions*.

Liu, L., Bailey, E., Sarracino, R., & Taylor, R. (2015, June). Numerical Simulation of Ice Ridge Gouging. *ASME 34th Int. Conf. on Ocean, Offshore and Arct. Eng.At: St. John's, Canada*. https://doi.org/10.1115/OMAE2015-41886

Løset, S. (1994a). Discrete element modelling of a broken ice field - Part I: model development. *Cold Regions Science and Technology*, *22*(4), 339–347. https://doi.org/10.1016/0165-232X(94)90019-1

Løset, S. (1994b). Discrete element modelling of a broken ice field - Part II: simulation of ice loads on a boom. *Cold Regions Science and Technology*, *22*(4), 349–360. https://doi.org/10.1016/0165-232X(94)90020-5

Løset, S., & Sayed, M. (1993). Proportional strain tests of fresh-water ice rubble. *J. Cold Reg. Eng.*, *7*, 44–61.

Mohammadafzali, S., Sarracino, R., Taylor, R., Stanbridge, C. W., & Marchenko, A. (2016). Investigation and 3D Discrete Element Modeling of Fracture of Sea Ice Beams. *Proceedings of 5th Arctic Technology Conference (ATC2016).*, 1–9.

Morgan, D., Sarracino, R., McKenna, R., & Thijssen, J. W. (2015). Simulations of Ice Rubbling Against Conical Structures Using 3D DEM. *Proceedings of the 23rd International Conference on Port and Ocean Engineering under Arctic Conditions*.

Paavilainen, J., Tuhkuri, J., & Polojärvi, A. (2009). 2D combined finite-discrete element method to model multi-fracture of beam structures. *Engineering Computations*, *26*(2004), 578–598. https://doi.org/10.1108/02644400910975397

Paavilainen, J., Tuhkuri, J. (2013) 'Pressure distributions and force chains during simulated ice rubbling against sloped structures', *Cold Regions Science and Technology*, Volume 85, 2013, Pages 157-174, ISSN 0165-232X, https://doi.org/10.1016/j.coldregions.2012.09.005.

Palmer, A., & Croasdale, K. (2013). *Arctic offshore engineering*. 42–47. https://doi.org/10.1142/8283

Polojärvi, A., & Tuhkuri, J. (2013). 2D FEM-DEM simulations of punch through tests: Effects of partly consolidated rubble deformation. *Proceedings of the 22nd International Conference on Port and Ocean Engineering under Arctic Conditions*.

Polojärvi, A., Tuhkuri, J., & Pustogvar, A. (2015). DEM simulations of direct shear box experiments of ice rubble: Force chains and peak loads. *Cold Regions Science and Technology*, *116*, 12–23. https://doi.org/10.1016/j.coldregions.2015.03.011

Potyondy, D. O., & Cundall, P. A. (2004). A bonded-particle model for rock. *International Journal of Rock Mechanics and Mining Sciences*, *41*(8 SPEC.ISS.), 1329–1364. https://doi.org/10.1016/j.ijrmms.2004.09.011

Prodanovic, A. (1979). Model Tests of Ice Rubble Strength. *Proceedings of the 5th International Conference on Port and Ocean Engineering under Arctic Conditions, POAC*, 89–105.

Ranta, J., Polojärvi, A., & Tuhkuri, J. (2015). Ice load estimation through combined finite-discrete element simulations. *Proceedings of the 23rd International Conference on Port and Ocean Engineering under Arctic Conditions*.

Sarracino, R., Mohammadafzali, S., & Šmilauer, V. (2017). A new "Ice Material Model" inserted to WooDEM. *Manuscript in Preparation*.

Serré, N., Repetto-Llamazares, A. H. V., & Høyland, K. V. (2011). Experiements on the relation between freeze-bond and ice rubble strength, Part I: Shear box experiments. *Proceedings of the 21st International Conference on Port and Ocean Engineering under Arctic Conditions*.

Shayanfar, H. (2017). *An Experimental Investigation on the Strength and Failure Behavior of Freshwater Ice Rubble* (Issue December). Memorial University of Newfoundland.

Shayanfar, H., Bailey, E., Pritchett, R., & Taylor, R. (2018). The effects of consolidation time on the strength and failure behavior of freshwater ice rubble. In *International Journal of Naval Architecture and Ocean Engineering* (Vol. 10). https://doi.org/10.1016/j.ijnaoe.2018.02.007

Timco, G., Croasdale, K. R., & Wright, B. (2000). *An overview of first-year sea ice ridges*. National Research Council of Canada, Technical Report HYD-TR-047.

Timco, G. W. (2011). Isolated ice floe impacts. *Cold Regions Science and Technology*, *68*(1–2), 35–48. https://doi.org/10.1016/j.coldregions.2011.04.008

Timco, G. W., & Cornett, A. M. (1999). Is φ a constant for broken ice rubble? *Proc. of the 10th Workshop on River Ice Management with a Changing Climate.*, 318–331.

Timco, G. W., & Frederking, R. M. W. (1982). Comparative strengths of fresh water ice. *Cold Regions Science and Technology*, *6*(1), 21–27. https://doi.org/10.1016/0165-232X(82)90041-6

Timco, G. W., Funke, E. R., Sayed, M., & Laurich, P. H. (1992). A laboratory apparatus to measure the behaviour of ice rubble. *Proc. of Offshore Mechanics and Arctic Engineering Conf*, 369–375.

Timco, G. W., & Weeks, W. F. (2010). A review of the engineering properties of sea ice. *Cold Regions Science and Technology*, *60*(2), 107–129. https://doi.org/10.1016/j.coldregions.2009.10.003

Yasunaga, Y., Kioka, S., Matsuo, Y., Furuya, A., & Saeki, H. (2002). The strength of the unconsolidated layer model of ice ridge. *Proc. of the 16th Int. Symp on Ice*, 62–68.

Yulmetov, R., Bailey, E., & Ralph, F. (2017). A Discrete Element Model of Ice Ridge Interaction with a Conical Structure. *Proceedings of the 24th Inernational Confrence on Port and Ocean Engineering under Arctic Conditions\, June*.

6. DISCRETE ELEMENT MODELING OF FLEXURAL FAILURE OF MEDIUM SCALE ICE RIDGES

6.1. Preface

This chapter of this thesis is based on a manuscript titled “Discrete Element Modeling of Flexural Failure of Medium Scale Ice Ridges” submitted to the Journal of Offshore Mechanics and Arctic Engineering and is under revision. I was the primary author of this manuscript and Dr. Rocky Taylor and Dr. Robert Sarracino co-authored the manuscript. The primary author of the manuscript was in charge of conducting all the simulations, drafting the manuscript, and revising the paper based on the feedback from the co-authors and reviewers. The co-authors helped the primary author with providing the experimental data, providing financial and logistic needs of performing the study, analysing the results, reviewing and revising the manuscript.

6.2. Abstract

Ice ridges pose significant concerns for shipping, offshore structures, and subsea structures when they scour the seabed. The primary objective of the current study is to investigate how the bond strength, consolidated layer thickness, and ridge keel thickness impact the flexural behavior of ice ridges. To achieve this, a mathematical model using Discrete Element Modeling is introduced here, which represents the ice as bonded spherical particles. This mathematical model is implemented in an Open Source DEM Particle Simulation Software, LIGGHTS, to simulate ice ridges consisting of a solid layer on top (representing the consolidated layer) and interconnected ice blocks (representing the keel). A total of sixteen trials were conducted: twelve to examine the effects of consolidated layer thickness and freeze-bond strengths on the flexural strength of the ice ridge,

and four to investigate the impact of doubling the keel depth. The results indicate that within the typical range of keel to consolidated layer thickness ratio, the strength of the freeze-bond between the ice blocks does not significantly contribute to the flexural failure of ice ridges. Instead, the consolidated layer thickness primarily determines the flexural strength. However, when the keel depth exceeds the consolidated layer thickness by a significant margin, increasing the freeze-bond strength can considerably affect the flexural strength of the ridge beam and, in certain cases, surpass the strength of the consolidated layer. Altering the thickness and consolidation of the rubble keel can impact both its strength and mechanical behavior. For weaker and thinner ice keels, the failure mechanism is primarily governed by the flexural failure of the consolidated layer. Based on the simulation results, when the keel depth rises, the keel's strength becomes increasingly important in determining failures. In extreme situations, the initiation of ice ridge failure can be primarily driven by the V-shaped failure of the thick rubble keel.

6.3. Introduction

Ice ridges are the most prevalent type of deformed ice feature in nature, making them a crucial consideration in the design of structures in ice-prone areas (Leppäranta and Hakala, 1992). Ice ridges can form via two main mechanisms: shear and pressure. Pressure ridges are the most prevalent type of deformed ice feature and account for 30-40% sea ice area and one half of the total sea ice volume (Hansen, 2014). They are a major concern for shipping, offshore structures and, when scouring the seabed, for subsea structures. However, our understanding of their structure and mechanical behavior remains limited (Palmer and Croasdale, 2013).

When interacting with sloping structures, the upper and more consolidated layers of the ridge define the limiting load on the structure. If the bond strengths between the rubble pieces are high,

the ice ridge can exhibit brittle porous solid behavior and fail in flexure, rather than shear (Shayanfar et al., 2018). Flexural failure is a complex mode of failure; shear, tensile, and compressive strength of both the rubble pieces and the bonds between them can affect the failure mechanism and forces (Afzali et al., 2021). Freeze-bonding between submerged ice pieces can occur even at low confining pressures and can affect the friction angle and shear strength of ice rubble (Ettema and Urroz, 1989). Astrup et al. (2013) and Liferov and Bonnemaire (2005) suggest that failure of ice rubble occurs in two main stages: the primary stage, which is controlled by the strength of the freeze-bonds, and the secondary stage, which is controlled by the overall strength of the rubble accumulation.

Numerous studies have been conducted to measure the flexural strength of sea ice, including research by Weeks and Assur (1967), Vaudrey (1977), Timco and Frederking (1982), Timco and O'Brien (1994), Blanchet et al. (1997), Jordaan (2001), Lu et al. (2016), Aly et al. (2019), and Karulina et al. (2019); however, limited data is available on the flexural strength of refrozen ice rubble. Data obtained from full-scale interactions between ice and offshore structures can be utilized to develop and validate ice ridge failure models. Notably, data collected from the Molikpaq in the Beaufort Sea during the mid-1980s, as well as interactions of ice ridges with the Norströmsgrund lighthouse, are among the most valuable sources of information on full-scale ridge loads on offshore structures (Timco et al., 2000; Bjerkas et al., 2010; Zvyagin and Ziemer, 2017; Ervik et al., 2019; Lemee and Brown, 2005). Other observations of ridge interactions with offshore structures include artificial islands, shallow and deep caissons, Cook Inlet platforms, and lighthouses.

With limited available detailed full-scale data on the flexural failure of ice ridges and ice rubble, laboratory experiments and numerical simulations can be used to enhance our understanding of

their failure mechanism. To investigate the mechanical behavior of freshwater ice rubble, Azarnejad and Brown (2002) and Lemee and Brown (2002) conducted laboratory experiments using punch-through tests. Their findings revealed that the freeze-bonding between the blocks of ice rubble can significantly affect the frictional behavior of the rubble. Serré et al. (2011) also carried out experimental investigations on the shear strength of ice rubble and observed that the failure of the ice rubble often initiates with the failure of the freeze-bond. Other studies by Sayed and Sayed (1986), Bruneau (1996), Bailey et al. (2014), Liu et al. (2015), Yulmetov et al. (2017), and Shayanfar et al. (2018) have also reported on the influence of block-to-block freeze-bond strength on the overall behavior of ice rubble. Further insights on ice rubble failure experiments can be found in the comprehensive reviews by Ettema and Urroz-Aguirre (1991), Timco and Cornett (1999), Liferov and Bonnemaire (2005), and Bailey et al. (2015).

While these experiments provide valuable insights into the failure mechanism of ice rubble and ice ridges, the mode of failure in these experiments is shear. To address this limitation, Shayanfar (2017) and Shayanfar et al. (2018) conducted a series of laboratory experiments to investigate the effect of confinement pressure and submersion time on the flexural failure of ice rubble. Despite freeze-bond shear strength being commonly considered and studied as the main contributor to the strength of ice rubble, Shayanfar (2017) and Shayanfar et al. (2018) observed that a significant portion of freeze-bonds would fail in tension when the rubble is subjected to flexure.

The shear strength of the freeze-bond has been investigated by Ettema and Schaefer (1986), Repetto et al. (2011a, 2011b), Shafrova and Høyland (2008), Høyland and Møllegaard (2014), Bueide and Høyland (2015), Boroojerdi et al. (2016, 2019a, 2019b), Frederking and Timco (1984), Bailey et al. (2012) (Møllegaard, 2012), and Marchenko and Chenot (2009). It was found that the strength of the freeze-bond increases with reducing temperature, increasing confinement pressure,

and reducing salinity and porosity. The strength of the freeze-bond initially increases with submersion time until it reaches a peak at 2-4 minutes. After that, with the increase of the freeze-bond temperature the strength gradually decreases to a minimum at 3-5 hours. The slow process of sintering becomes dominant at this point and the strength starts to slowly increase again, reaching its maximum at around three weeks. The peak and minimum strength times can be affected by the initial temperature and size of the ice blocks.

Afzali et al. (2023) studied the effect of confinement pressure and initial ice temperature on the tensile strength of fresh-water freeze-bonds in uniaxial tensile testing. It was found that, similar to the shear strength, the tensile strength of the freeze-bond increases with the confinement pressure. It was also found that the strength of the freeze-bond initially increases with submersion time, then drops to its minimum at around 3 hours of submersion. Murdza et al. (2021) used four-point bending tests to determine the flexural strength of freeze-bonds formed between rectangular ice blocks in air. It was found that the increase in the salinity of the bond material and temperature decreased the strength of the freeze-bond. As discussed by Leguillon et al. (2015), the ratio between tensile and flexural strength can vary, with the flexural strength of brittle material typically being between 1-2 times its tensile strength. Szabo and Schneebeli (2007) studied the tensile strength of the bond formed between micro conical ice samples. The main sintering mechanism in this time scale is the freezing of the liquid layer between the two samples.

The main purpose of the current study is to investigate the effect of bond strength and consolidated layer and ridge keel thickness on the flexural behavior of ice ridges. A mathematical model for Discrete Element Modeling of the ice ridge is introduced that models the ice as bonded spherical particles. This mathematical model is implemented in an Open Source DEM Particle Simulation

Software, LIGGHTS, to simulate ice ridges composed of a solid layer on the top, representing the consolidated layer, and pieces of bonded ice blocks, representing the keel.

6.4. Mathematical Model

The Discrete Element Method (DEM) has had wide success in modelling granular materials and brittle solids, the former through the application of frictional interaction between adjacent particles, and the latter by adding bonds between adjacent particles. By giving the bonds resistance to normal, shear and torsional stresses, and by allowing bonds to fail under tensile, shear and torsional overloading, DEM becomes well-suited to modelling the initiation and propagation of fractures, as well as post-fracture material response. DEM has had wide use in modelling ice and ice-structure interactions.

Løset (1994a, 1994b) introduced a 2D DEM model with circular elements in order to simulate a broken ice field Particles in this model contacted neighboring particles by a visco-elastic-plastic rheology. Paavilainen et al. (2009), Paavilainen and Tuhkuri (2013) and Ranta et al. (2015) used elastic FEM components as DEM particles to simulate the multi-fracture of sea ice against sloped structures. This model, compared to conventional DEM, provided better understanding of beam micro behavior during failure at a higher computational cost. FEM/DEM ice models were also used by Polojärvi and Tuhkuri (2013a, 2013b) for simulating punch through experiments of partially consolidated ice rubble.

Goldstein et al. (2013) utilized a 2D DEM model to investigate the accumulation of grounded sea ice against a sloping structure. Polojärvi et al. (2015) introduced another 2D DEM model to simulate direct shear box experiments involving ice rubble. Traditionally, the dynamic friction coefficient of ice has been considered constant; however, Lishman and Polojärvi (2015) employed a 2D DEM model to better understand and estimate the rate-dependent nature of ice-ice friction

based on experimental observations. The findings of the study revealed that the dynamic friction coefficient of ice decreases with increasing sliding speed, which impacts the behavior of ice rubble during shear.

Liu et al. (2015) employed a 3D DEM model to simulate the failure of an ice rubble keel during gouging with the sea bed. In their model, a Cohesive Frictional Mode (CFM) was utilized to represent the spherical particles. The cohesion model included normal, shear, and torsion springs, while the sea bed was modeled as a rigid body.

Berg and Lubbad (2015) utilized a non-smooth discrete element method (NDEM) to simulate the failure of unconsolidated ice rubble in laboratory and full-scale settings. NDEM models are known for their speed compared to smooth models, but they can introduce artificial vibrations into the system, particularly when larger particles are involved. Additionally, NDEM models do not account for the viscoelastic behavior of contacts, which can be significant in terms of energy dissipation within the system.

Bonded 3D DEM models have also been employed to simulate the interaction between sea ice and conical structures. Yulmetov et al. (2017) and Morgan et al. (2015) both utilized a bonded 3D DEM model to simulate the interaction between sea ice and the Confederation Bridge. Morgan et al. (2015) investigated the impact of various factors, such as ice sheet width and length, DEM parameters, and cone angle, on the height, shape, volume, and formation mechanisms of the rubble pile. The study suggests that simulating ice in multiple layers can lead to more accurate simulations, but it also significantly increases the cost of the simulation.

Lilja (2021) proposed a finite-discrete element model for fracture analysis of large, cellular, plate-like structures. This was used for studying sea ice sheet fracture with three applications: uniaxial tensile fracture, vertical penetration fracture, and circular hole breakage by a truncated cone.

Prasanna and Polojärvi (2023) introduces an innovative particle breakage model for quasi-static DEM simulations, addressing shear failure of non-spherical particles. Based on experimental observations and high-resolution modeling, the model's integration into a DEM code improved simulation accuracy, particularly in direct shear box experiments with ice rubble.

Sarracino, working at CARD, developed a material model in DEM which included normal, tensile, flexural and torsional springs and bonds, and a hysteretic damping model (Sarracino, unpublished work). Some aspects of this numerical model were based on a bonded-particle model developed by Potyondy and Cundall (2004). Sarracino and Morgan commissioned Kloss and Goniwe to incorporate a subset of this model into LIGGGHTS with minor modifications (Sarracino, unpublished work), subsequently utilized by Morgan et al. (2015) and Afzali et al. (2023) and the current study.

The ice model contains normal and shear springs that operate between neighboring particles that overlap due to compressive stresses or which are bonded (Mohammadazali et al., 2016). Forces between neighboring spherical particles arise from a cohesive visco-elastic contact model (spring-dashpot model). The force is given by:

$$\vec{F}_{ij} = F_{n(ij)}\ \hat{n}_{ij} + F_{t(ij)}\ \hat{t}_{ij} \tag{6-1}$$

where $\hat{n}_{ij}$ is the unit vector from the center of particle *i* to the center of particle *j*, and $\hat{t}_{ij}$ is a unit normal to $\hat{n}_{ij}$ in the direction of incremental tangential strain, due to sliding, between the two particles from one time step to the next. The first term in this equation is the normal force and the

second term is the tangential force, each force having two components, the spring force and the damping force. The force components $F_{n(ij)}$ and $F_{t(ij)}$, both applied to the center of the particles, are given by:

$$F_{n(ij)} = k_n \Delta r_{(ij)} + \gamma_n v_{n(ij)} \quad \text{and} \quad F_{t(ij)} = k_t \Delta t_{(ij)} - \gamma_t v_{t(ij)} \qquad (6\text{-}2)$$

where normal overlap $\Delta r_{(ij)}$ is:

$$\Delta r_{(ij)} = r_{(ij)} - r_i - r_j \,, \qquad (6\text{-}3)$$

and $\Delta t_{(ij)}$ is the incremental tangential displacement for the duration of contact due to sliding (tangential overlap) as shown in Figure 6-1 (Kloss et al., 2012). Here r_i and r_j are the radii of particles i and j, respectively, and $r_{(ij)}$ is the distance between the centers of the two particles.

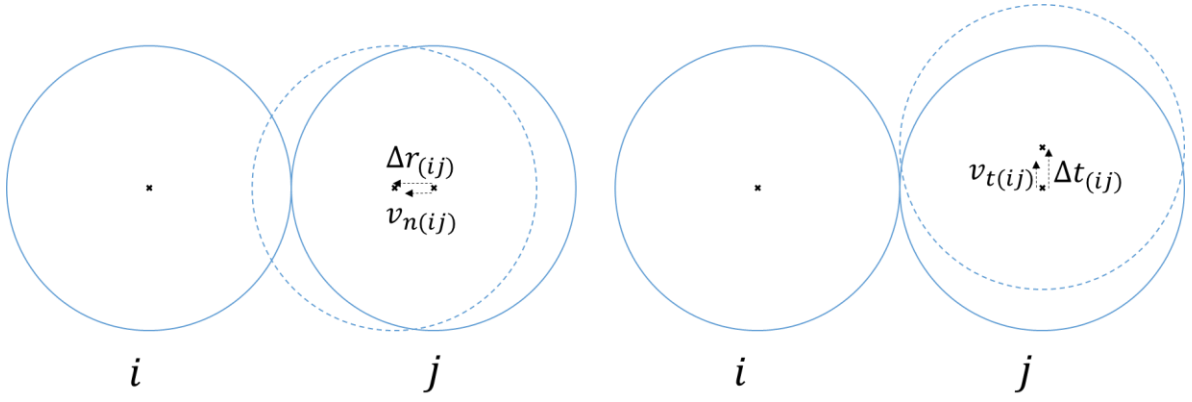

Figure 6-1- Schematic of the normal and tangential overlaps and relative velocities

The relative velocities are given by:

$$v_{n(ij)} = \frac{dr_{(ij)}}{dt}; \;\; v_{t(ij)} = \frac{d\Delta t_{(ij)}}{dt} \qquad (6\text{-}4)$$

In the formulas above $\vec{F}_{ij}$, $\hat{n}_{ij}$ and $\hat{t}_{ij}$, are anti-symmetric in the indices *i* and *j*, and $r_{(ij)}$, $\Delta n_{(ij)}$, $\Delta t_{(ij)}$, $F_{n(ij)}$, $F_{t(ij)}$, $v_{n(ij)}$ and $v_{t(ij)}$ are symmetric in the indices *i* and *j*.

A “rolling friction” model was also used in the simulations to account for non-sphericity. Normal and tangential torques on bonds, T_n and T_t are calculated incrementally:

$$T_n \mathrel{+}= k_t J \omega_n dt \quad \text{and} \quad T_t \mathrel{+}= k_n I \omega_t dt \tag{6-5}$$

where ω_n and ω_t are normal and tangential angular velocities, and *I* and *J* are polar moments of inertia defined as:

$$J = 0.5\pi \min\left((r_1, r_2)^4\right) \quad \text{and} \quad I = 0.25\pi \min\left((r_1, r_2)^4\right) \tag{6-6}$$

The spring stiffness can be set independently, but in these simulations a linearly elastic, isotropic material was assumed and the relative spring stiffness were set as:

$$k_n = 2(1+\nu)k_t = \frac{1}{4}\pi E D \tag{6-7}$$

where ν is the Poisson ratio, E is the elastic modulus and D is the particle diameter. The stiffness of the bonds were calculated based on the “equivalent beam” theory (Mohammadafzali et al., 2016). That is, two neighboring particles with elastic modulus of E_1 and E_2 and radii of $r_1$and r_2 becomes a cylindrical beam of radius *r*, cross-section area *A*, and length *L*, where $r = \min(r_1, r_2)$, $L = r_1 + r_2$, $A = \pi \min(r_1, r_2)^2$, and the elastic modulus of the equivalent beam E_{eq} is:

$$E_{eq} = (r_1 + r_2)\left(\frac{r_1}{E_1} + \frac{r_2}{E_2}\right)^{-1} \tag{6-8}$$

The time-step was set proportional to the characteristic period of oscillation (Yulmetov and Bailey, 2017), small enough to maintain the stability of the simulation:

$$\Delta t = cD\sqrt{\frac{\rho_i}{E_p}} \tag{6-9}$$

where ρ_i is the density of ice and the constant c is set to 0.1.

The model was implemented on the open source DEM code LIGGGHTS which itself is based on the classical Molecular Dynamics (MD) code LAMMPS, designed to run efficiently on multiple processors (Kloss et al., 2012). The model is a modified version of the Hooke contact model, available in LIGGGHTS. A cohesion model, described above, is added to the model to represent the bonding between the ice particles and freeze-bonding between ice blocks.

6.5. Methodology

The ice rubble samples used in this study are composed of two layers: a consolidated layer of ice on top and pieces of ice blocks that form an ice rubble keel on the bottom. The ice blocks forming both the consolidated layer and the keel are made of bonded spherical DEM particles. The strength of the freeze-bond between the consolidated layer and the ice rubble is assumed to be similar to the strength of the freeze-bond between the blocks of ice rubble. Two types of bonds were used in the simulations: internal bonds between the DEM particles forming the consolidated layer and the ice blocks, with strengths matching the strength of solid ice, and external bonds between neighboring ice blocks, with strengths conforming to freeze-bond strengths.

When detailed information on the consolidated layer of a first-year ridge is not available, the thickness of the consolidated layer may be assumed to be 1.5 to 2 times the surrounding level ice thickness (ISO 19906, 2010). This estimate is only a guideline, and the thickness of the consolidated layer may vary based on environmental conditions (Sudom & Timco, 2013). The consolidated layer of the ice ridge is often composed of solid ice, slush, snow, and voids (Salganik,

2020; Leppäranta & Hakala, 1992; Croasdale and Associates, 1998) and may not be directly comparable to the level ice. So, the ISO 19906 (2010) recommendation of using 1.5 to 2 times the surrounding level ice thickness for strength may also take into account this consideration.

The consolidated layer (CL) to level ice thickness ratio may also be dependent on the climate and the time of measurement; in the sub-Arctic environment or after the end of the freezing season, the level ice around the ridge may melt at a faster rate than the consolidated layer, and this can result in a higher consolidated layer thickness ratio. Measurements that are taken during the freezing season or in the lab at sub-zero temperatures mostly result in ratios between 1 and 2 (Høyland & Løset, 1999; Tuhkuri et al., 1999; Lepparanta, Hakala, 1989), but measurements during the spring in the sub-Arctic areas can result in ratios up to 8 when the surrounding level ice is mostly melted (Croasdale and Associates, 1998).

Sudom et al. (2011) reviewed the keel and CL thickness of ridges in various geographical locations and reported that on average, the CL has a thickness around 20% of the keel. Guzenko et al. (2021) reviewed drilling data from 129 first-year ridges in the Kara and Laptev Seas, and CL thicknesses of 1.32-2.7 m were observed for keel thicknesses of 7.18-12.27 m, with the keels on average being 4.5 times thicker than the CL.

In this study, the keel to consolidated layer thickness ratio ranges between 2.5 and 10 which covers most of the ridges find in the nature during both warm and cold seasons. The thickness of the consolidated layer ranges between zero and 20 cm, double the thickness of the rubble keel blocks.

To generate the ice rubble for this setup, the first step was to generate a set of individual block geometries. The size and area of each block was based on pictures captured of the rubble blocks by Shayafrar (2019). A cuboid DEM block was then generated based on the dimensions of each

block and a custom code was used to randomly and iteratively cut the cuboid blocks until the area of the DEM block matches the area of the actual block, Figure 6-2.

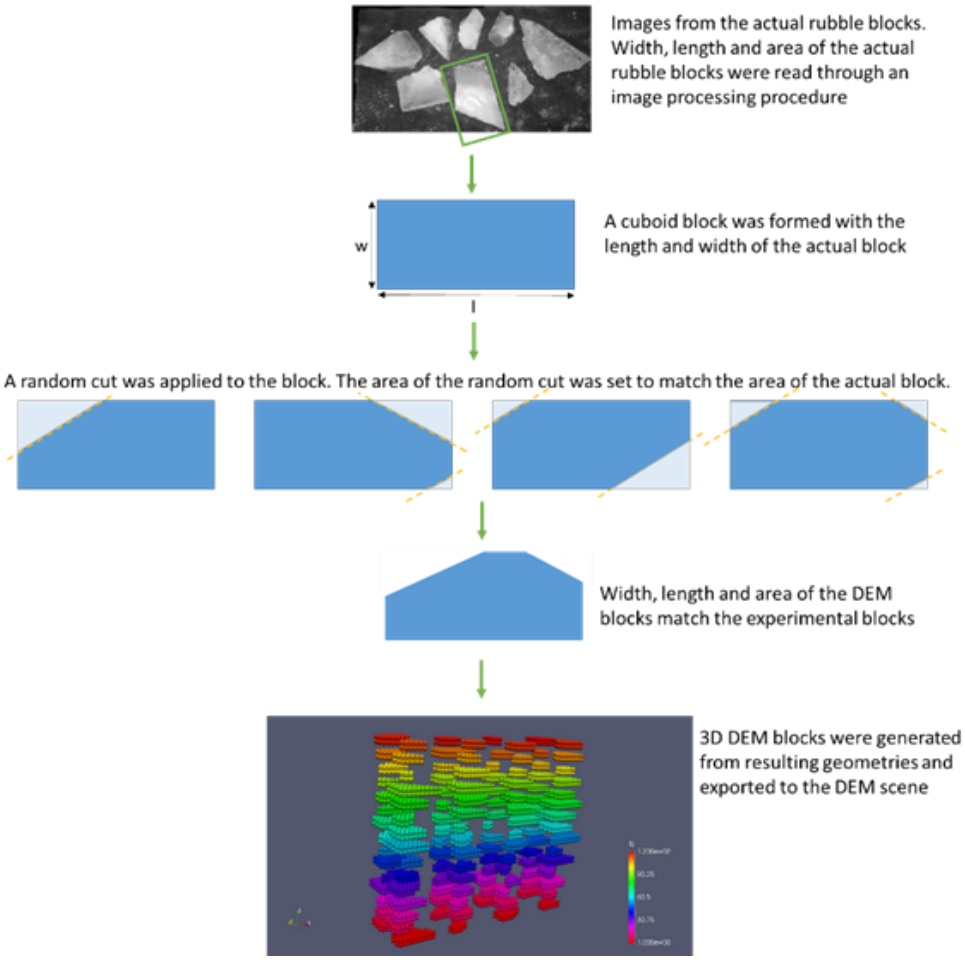

Figure 6-2- Generation of ice rubble based on Shayanfar (2018) experiments (after Afzali et al. (2021))

Two different methods were considered and tested for placing and bonding the level ice onto the rubble keel. In the first method, a rigid ice sheet was placed on top of the rubble mass, the rubble mass was fixed on the bottom and the ice sheet moved vertically down to increase its contact area with the rubble mass. After 10 cm of vertical displacement, the physical shape of the rubble was formed and internal and external bonds for rubble blocks and ice sheet were introduced. Using this

method resulted in high internal rubble pressures and the contact area between the level ice and rubble mass was small.

In the second method, the particles at the top 5 cm of the rubble mass were removed at the beginning. The rigid level ice was then added on the top and moved 1 cm vertically down to increase contact with the rubble mass. Next, internal and external bonds for the rubble blocks and ice sheet were introduced A sample result of ice ridge made by this method is shown in Figure 6-3. This method had two advantages over the first method: (1) It did not introduce artificially high pressures within the rubble mass, and (2) the contact area between the level ice and rubble mass was greater. On this basis this method was chosen to be implemented in the simulation.

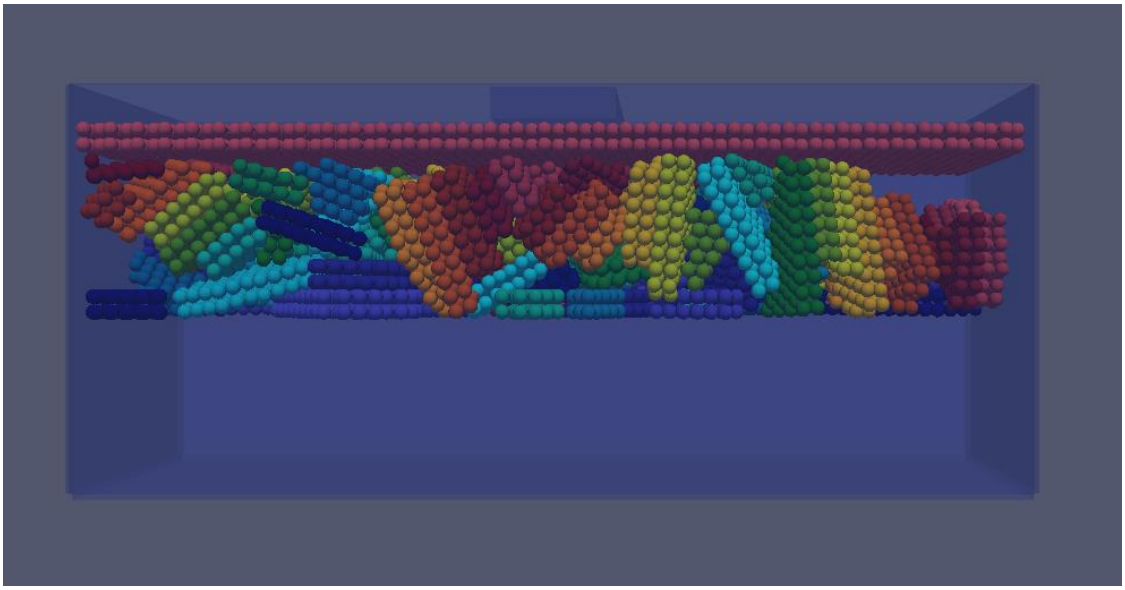

Figure 6-3- Final geometry of ice ridges in DEM

The initial parameters used as the rubble properties was based on Afzali et al. (2020) for 4 hours of submersion; please refer to this article for more detailed information. At the estimated contact pressure of σ_{ave-b}= 1.81 kPa the average shear and tensile freeze-bond strength was estimated, based on Boroojerdi et al. (2019) and Afzali (2023), to be 88.8 kPa and 26.9 kPa respectively.

Accounting for the correction factor c_f, the DEM freeze-bond strength value was set to 18.38 kPa see Afzali et al (2023). The freeze-bond shear strength and tensile strength were then adjusted by submersion time based on Boroojerdi et al. (2019) to 364.1 and 121.4 kPa for 2 minutes submersion and 683.8 and 207.1 kPa for ultimate strength (long submersion) respectively. In these calculations, it was assumed that the development of the freeze-bond shear and tensile strength depends on time followed the same behavior.

The parameters of the level ice sheet were calibrated to match the flexural strength of freshwater ice in three point bending tests based on Aly et al. (2019). In this study Aly et al. (2019) compiled a comprehensive data base giving the flexural strengths of nearly 5000 freshwater and saline ice beams.. A scale dependant empirical model was developed to estimate the flexural strength of the freshwater ice as a function of its volume using regression analysis:

$$\sigma_f = 839(\frac{V}{V_1})^{-0.13}$$

where σ_f denotes the flexural strength of the ice beam in kPa, V is the volume of the ice beam in m^3, and V_1 is the reference volume of $1m^3$. The linear dimensions of the consolidated layer for all the beams used in this study were $0.94m \times 3.05m$ with the thickness of $0.1m, 0.15m,$ and $0.2m$ resulting volumes of $0.287\ m^3, 0.430\ m^3$, and $0.573\ m^3$. The estimated flexural strength of the consolidated layer freshwater ice beams foe the above noted volumes was $987\ kPa, 936\ kPa,$ and $902\ kPa$ respectively and the DEM parameters were calibrated to reproduce these strength values using three-point bending simulations.

The strength of the bond between the consolidated layer and the ridge keel also can affect the flexural behavior of the ridge. It is important to measure the strength of this bond in the simulations and compare it to the limited field data available on the keel- consolidated layer bond strength. To

achieve this, two additional validation simulations were conducted to measure the shear and tensile strength of the keel- consolidated layer bond strength. Figure 6-4 shows a schematic of the test setup for these simulations. In these simulations the consolidated layer moved vertically upward and horizontally to the right, for the pull up and direct shear tests respectively, while the keel was fixed.

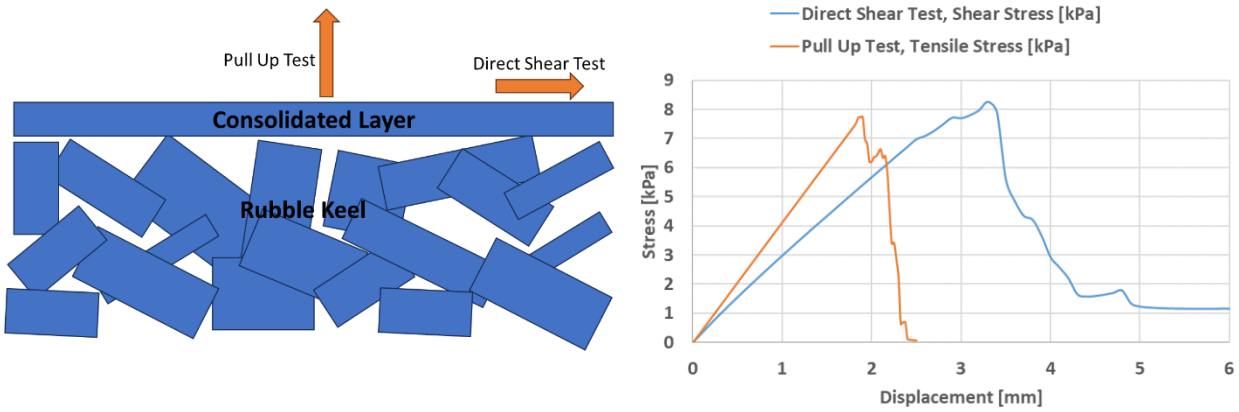

Figure 6-4- Left: schematic of the direct shear and pull up test setup in the simulations, right: shear and tensile stress during the direct shear and pull up tests

The strength of the freeze-bond for these experiments was set to its ultimate value as a representative of the ice ridges in the nature that survive for the long enough time (three weeks or more) to form an ultimate bond. The shear and tensile strength of the keel-consolidated layer bonds in these simulations were recorded 8.3 and 7.7 kPa respectively.

Limited field data is available on the shear and tensile strength of the keel-consolidated layer bond. The direct shear and pull up setups were successfully used in field campaigns in Canada and Russia, but the Russian tests results remain confidential. Those studies aimed to measure shear and tensile strength between the consolidated layer and ice keel using a hydraulic ram and potentiometers. Styrofoam rods were used to evaluate deformation along the shear plane.

Croasdale (1997) reported a maximum shear strength of 22.6kPa and an average of 14.1kPa at air temperature of $-4.5^{\circ}C$. The maximum and average tensile strength of the bond for these experiments were 26 kPa and 17 kPa respectively. In 1998 (Croasdale, 1998) the air temperature was higher at $-1.6^{\circ}C$ and the measured shear and tensile strength were significantly lower. The maximum and average shear strength were 13.2 kPa and 9.2 kPa and maximum and average tensile strength were 9 kPa and 6.2 kPa.

While it is challenging to compare the field data at different temperature and salinity to the simulation results, it can be seen that the strength of the bond between the consolidated layer and keel falls within a reasonable range. The simulations were set based on the properties of freshwater ice ridge at air temperature of $0^{\circ}C$, while 1998 experiments were carried out at $-1.6^{\circ}C$ air temperature on saline ice ridges, one factor increasing the bond strength and the other factor reducing the strength. The simulations and experiments resulted in shear strengths of 8.3 kPa (simulated) and 9.2 kPa (field), and tensile strength of 7.7 kPa (simulated) 6.2 kPa (field) respectively. On this basis, the strength values of 8.8 kPa and 7.7 kPa were judged as reseanable values to use.

6.6. Results and Discussion

Sixteen trials in total have been conducted; 12 to study the effects of consolidated layer thickness and freeze-bond strengths on the flexural strength of the ice ridge, and 4 to investigate the effect of doubling the keel depth. Table 6-1 summarizes the test conditions and final flexural strength values for all the simulations.

Table 6-1- Simulations conditions matrix

Keel Depth [m]	Submersion Time	Freeze-bond Shear Strength [kPa]	Freeze-bond Tensile Strength [kPa]	Consolidated Layer Thickness [cm]	Failure Force [N]	Flexural Strength [kPa]	Equivalent Beam Thickness [m]
0.5	2 mins	364.1	121.4	0	689	4.5	0.061
				10	3927	17.7	0.146
				15	6428	24.7	0.186
				20	10416	34.5	0.237
	4 hrs	88.8	26.9	0	563	3.7	0.055
				10	3756	16.9	0.142
				15	6599	25.3	0.189
				20	10133	33.5	0.234
	ultimate	683.86	207.1	0	843	5.5	0.067
				10	3891	17.5	0.145
				15	6424	24.7	0.186
				20	11066	36.6	0.244
1	4 hrs	88.8	26.9	0	794	1.3	0.065
				10	3851	5.2	0.144
	ultimate	683.8	207.1	0	5741	9.3	0.176
				10	7429	10	0.200

The flexural strengths of the beams are calculated based on the three-point bending test with rectangular cross-section $\sigma_f = \frac{3FL}{2BD^2}$ where σ_f is the flexural strength, F is the failure force, and L, B, and D are length, width and depth. The equivalent beam thicknesses are calculated using the same formula $D = \sqrt{\frac{3FL}{2\sigma_{f_1}B}}$ where σ_{f_1} is a reference flexural strength, here taken $902\ kPa$, the flexural strength of a $3.05m\ (L) \times 0.94m(B) \times 0.2m(D)$ freshwater ice beam.

It was seen that regardless of the keel freeze-bond strength, the flexural strength significantly increases with the increase of consolidated layer thickness as expected, see Figure 6-5; it is true even for the rubble at its ultimate strength (long submersion). The strength of the beam at 2 mins, 4 hours, and ultimate submergence time increased by 95%, 98%, and 109% respectively by increasing the consolidated layer thickness from 10 cm to 20 cm. Increasing the strength of the

freeze-bonds did not significantly increase the flexural strength of the $0.5m$ keel ridges, but did significantly increase the strength of the $1m$ keel ridges.

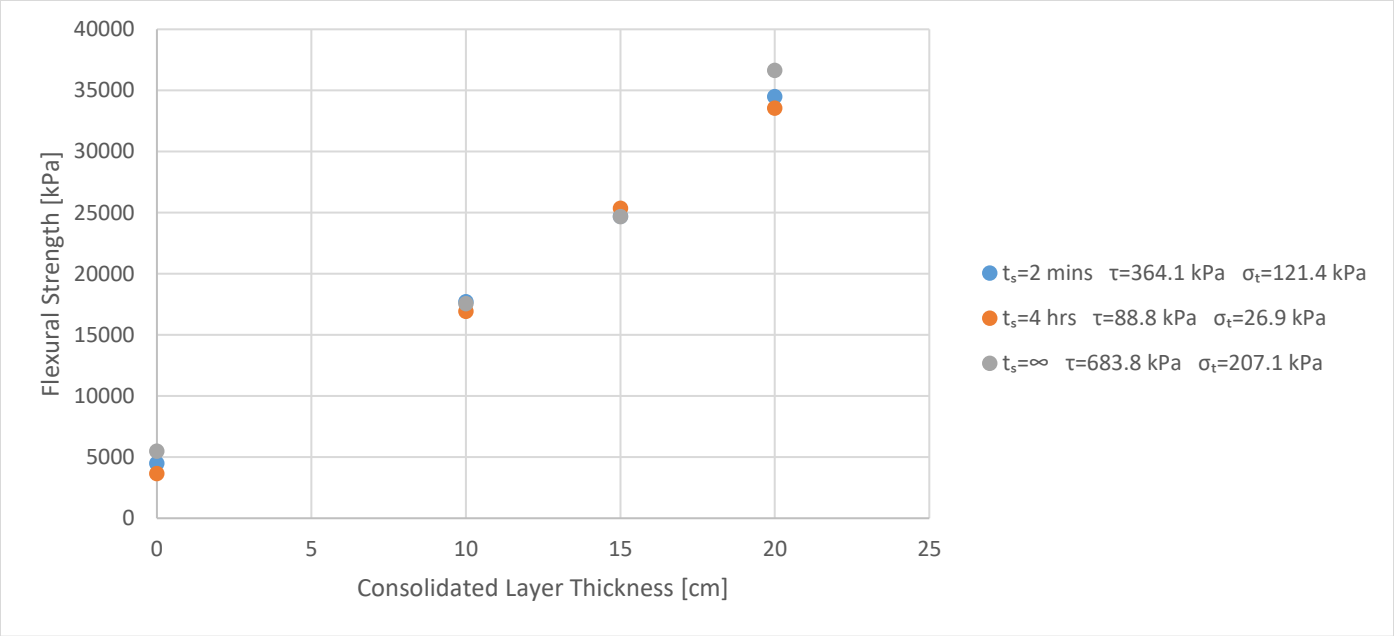

Figure 6-5- Effect of consolidated layer thickness on the flexural strength of 0.5 m keel ridges

It was also seen that, for the partially consolidated ridges (4 hours of submersion), the equivalent beam thickness did not significantly increase by increasing the keel depth from 0.5m to 1m and the thickness of the consolidated layer is the main contributor the equivalent beam thickness. However, when the freeze-bonds in the keel are at their ultimate strength, doubling the depth of the keel can significantly increase the equivalent beam thickness and contribute to the total strength, at a comparable level as the consolidated layer.

As it is shown in Figure 6-6, the thickness of the consolidated layer overwhelmingly dominated the flexural strength of the ice ridges in most cases and variations in thickness and freeze-bond strength of the rubble keel does not significantly affect the total flexural strength of the rubble

beams. The strength of the rubble keel can be a major contributor to the flexural strength of ridges only when the rubble keel is significantly deeper than the consolidated layer and is at its ultimate freeze-bond strength.

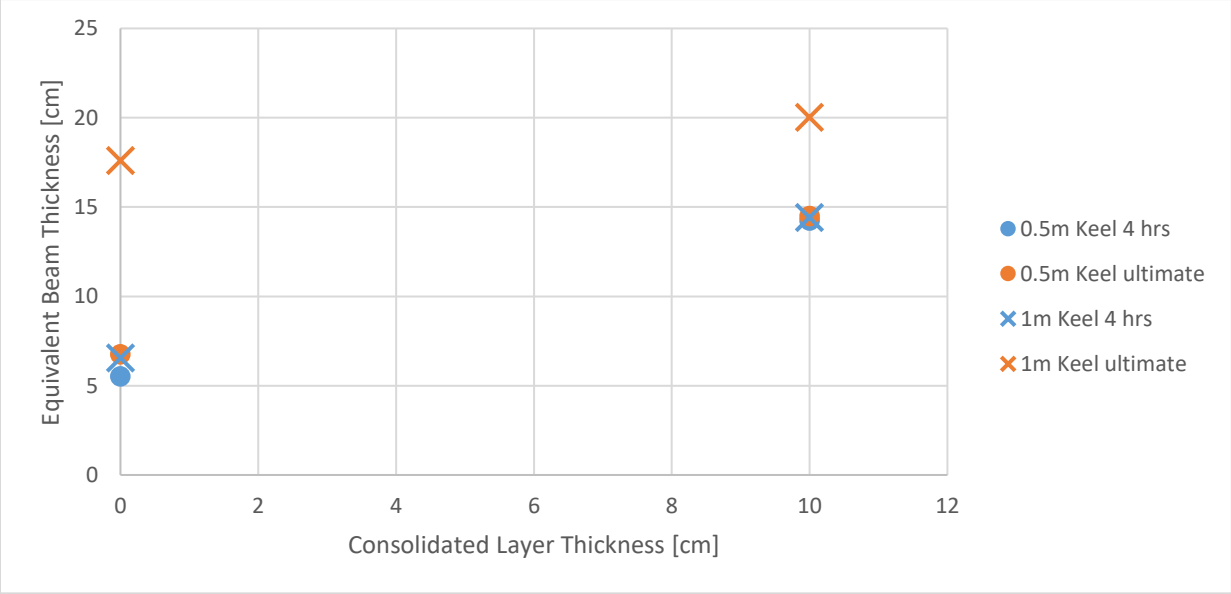

Figure 6-6- Effect of consolidated layer thickness, keel depth, and freeze-bond strength on total strength of the ice ridge

As can be seen from Figure 6-7, the mechanism and location of the ridge failure are significantly affected by the thickness of the keel and consolidated layer. The following modes of failure were observed for the ice rubble at its ultimate freeze-bond strength:

- In the absence of consolidated layer, the 0.5 m keel behaves comparable to a solid ice beam, the failure of the rubble keel initiates at the bottom center of the keel and is dominated by the tensile failure of the freeze-bonds.
- Consolidation of the upper 10 cm of the rubble, both significantly increases its strength and changes its behavior. As can be seen in Figure 6-7, the failure of ridge keel in this case

is dominated by flexural failure of the consolidated layer at the center and rubble keel, although at its ultimate strength, does not play an important role in the failure process.

- The mechanism of failure of the 1 m rubble keel at its ultimate freeze-bond strength is comparable to 0.5 keel. The keel behaves similar to a solid beam and V-shaped flexural failure initiates at the bottom of the keel and diverges to the two sides as it grows to the top.
- An ice ridge with 10 cm of consolidated layer and 1 m rubble keel, shows significantly higher flexural strength compared to 1 m ice rubble with no consolidated layer. In this case a mixed mode of failure, was observed; the ice keel failed at a near ideal V-shaped crack growing from its bottom sides to top center and the consolidated layer underwent major tensile stress in the middle. However, the peak force was recorded at the failure of the rubble keel, prior the failure of the consolidated layer. The behavior of the ridge in this case was comparable to a composite two-layer composite solid beam.

When the ice rubble is not at its ultimate strength, the failure of the ice ridges is dominated by the flexural failure of the consolidated layer, regardless of the thickness of the rubble keel and consolidated layer. In the absence of a consolidated layer, reducing the strength of the keel freeze-bonds affects their failure mode. Although in all the cases rubble beams fail in flexure, in weaker keel beams, plung shear failure of the rubble in the middle is more apparent, whereas in the stronger keel beams, rubble keel fails in a clear bottom-up V-shaped crack and the proportion of the bonds failing in tension is higher.

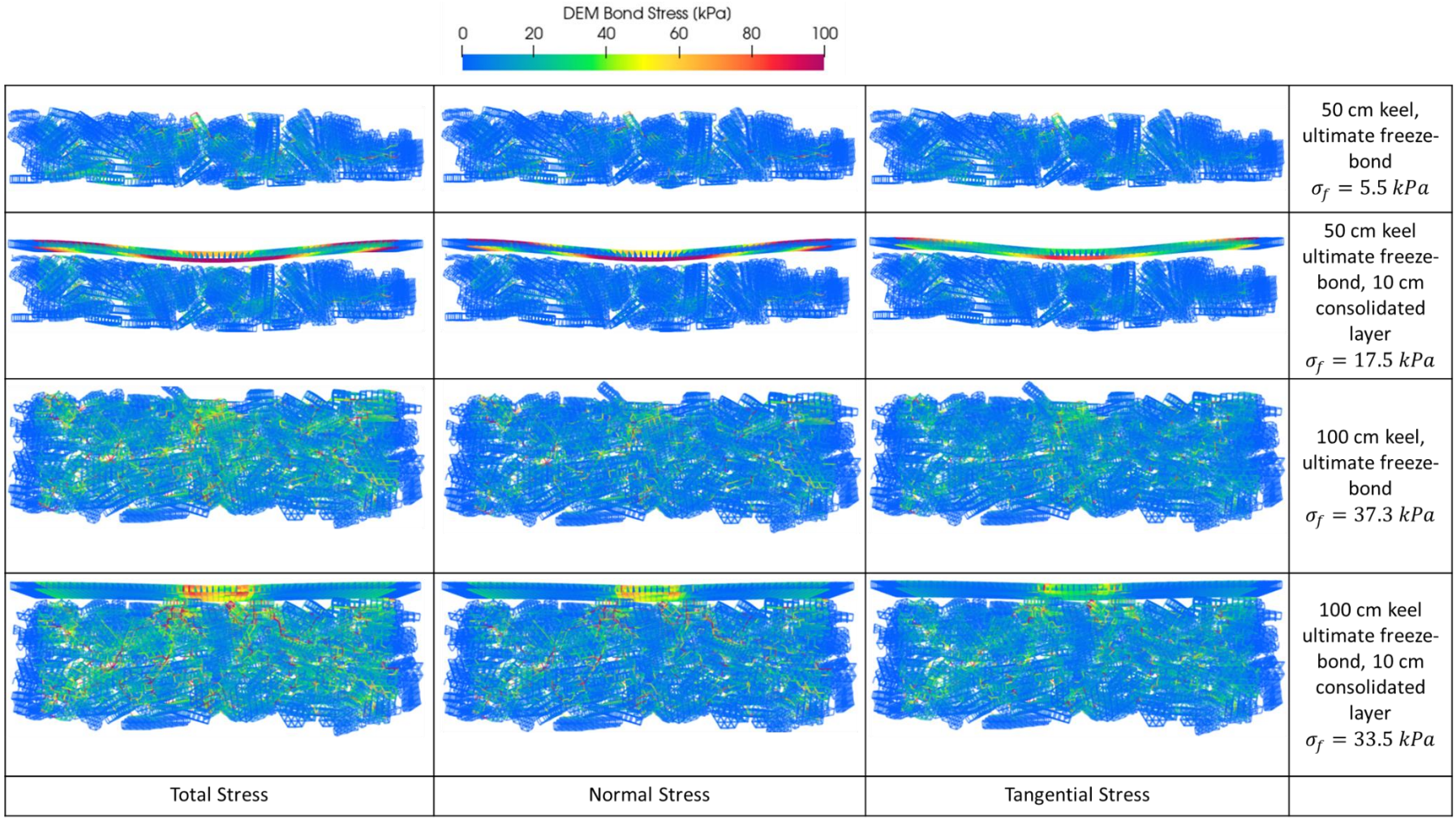

Figure 6-7- Bond stress at the onset of failure for ridges and rubble at ultimate freeze-bond strength

Based on the results of the presented simulations, in most natural conditions, when the thickness of the rubble keel is up to 7-8 times the consolidated layer, consolidated layer dominates the failure force and mechanism and thickness and consolidation of the keel does not play an important role in the flexural failure of ice ridges. However, in some extreme cases, where the keel depth is more than 7-8 time the consolidated layer thickness, and the keel is consolidated for a long period of time, it can majorly contribute to the flexural failure mechanism and load.

6.7. Conclusion

The flexural failure of ice ridges is one of the main limiting concerns for the design load in ice prone areas, yet limited data on the flexural strength of ridges is available and design loads are typically calculated based on the thickness of the consolidated layer only. In this work the effect of the ice-rubble keel on the overall strength of ice ridges was studied, using 3D DEM simulations to simulate both the consolidated layer and the keel, with the consolidated layer modelled as a single ice sheet, and the keel modelled as a collection of ice blocks bound to each other by freeze bonds.

It was found that in the normal range of keel to consolidated layer thicknesses, that is, for keel / consolidated layer thickness ratios between 2.5 and 7-8, the keel does not play an important role in the flexural failure of ice ridges, even when the freeze-bonds are at their ultimate strength. The consolidated layer is the main contributor to flexural strength, confirming, in general, the validity of the typical calculations which ignore the possible influence of the keel on ice strength. However, when the keel depth is significantly higher than the consolidated layer thickness, that is, for ratios above 7-8, increasing the freeze-bond strength can significantly increase the flexural strength of the ridge beam and in some cases the keel strength becomes the dominant factor in ice ridge strength.

This research achieved a significant milestone by linking experimental freeze-bond strength mechanisms with DEM simulations for broader applications. Expanding and validating this approach, particularly exploring how macroscopic behavior changes with variations in freeze-bond strength is recommended for future work. This enhances confidence in simulation tools for engineering design. While ice ridge simulations were not directly compared to experiments, the overall agreement with level ice and rubble failure experiments and field measurements supports the reliability of the DEM model. Direct comparison with medium-scale ice ridge field experiments, if feasible, would further boost confidence in the model.

6.8. References

Afzali, S., Taylor, R., Bailey, E., Sarracino, R., & Boroojerdi, M. T. (2021) 'Investigation of the Effect of Block Size, Shape, and Freeze Bond Strength on Flexural Failure of Freshwater Ice Rubble Using the Discrete Element Method', *Journal of Offshore Mechanics and Arctic Engineering*, 143(5).

Afzali, S., Taylor, R., Sarracino, R. (2023) 'Experimental investigation on the tensile strength of freshwater freeze-bonds', *Cold Regions Science and Technology*, 210, pp. 1-11.

Aly, M. *et al.* (2019) 'Scale Effect in Ice Flexural Strength', *Journal of Offshore Mechanics and Arctic Engineering*, 141(5), pp. 1–12, https://doi.org/10.1016/j.coldregions.2023.103823.

Astrup, O. S., Helgøy, H. and Høyland, K. V (2013) 'Laboratory work on freeze-bonds in ice rubble, Part III: Shear box experiments', *Proceedings of the International Conference on Port and Ocean Engineering under Arctic Conditions, POAC*.

Azarnejad, A. and Brown, T. G. (2001) 'Ice rubble behavior in punch tests', *Journal of Cold*

Regions Engineering, 15(3), pp. 135–153.

Bailey, E., Sammonds, P. R. and Feltham, D. L. (2012) 'The consolidation and bond strength of rafted sea ice', *Cold Regions Science and Technology*. Elsevier B.V., 83–84, pp. 37–48.

Bailey, E. *et al.* (2014) 'An Overview of the Development of Ice Ridge Keel Strengths Test Program', in *Society of Petroleum Engineers - Arctic Technology Conference 2014*.

Bailey, E., Taylor, R., & Croasdale, K. (2015) 'Mechanics of ice rubble over multiple scales', in *Proceedings of the ASME 2015 34th International Conference on Ocean, Offshore and Arctic Engineering OMAE2015*. St. John's, Canada.

Berg, M. van den and Lubbad, R. (2015) 'The application of a non-smooth discrete element method in ice rubble modeling', in *Proceedings of the 23rd International Conference on Port and Ocean Engineering under Arctic Conditions*.

Bjerkas, M., Albrektsen, A. and Guntner, A. (2010) 'Static And Dynamic Ice Actions In The Light Of New Design Codes', in *Proceedings of the ASME 29th International Conference on Ocean, Offshore and Arctic Engineering, 2010, Vol 4*. Three Park Avenue, New York, NY 10016-5990 Usa: Amer Soc Mechanical Engineers, Pp. 733–739.

Blanchet, D., Abdelnour, R. and Comfort, G. (1997) 'Mechanical properties of first-year sea ice at Tarsiut Island', *Journal of Cold Regions Engineering*, 11(1), pp. 59–83.

Boroojerdi, M. T. *et al.* (2016) 'Experimental Study on Shear Strength of Freeze Bonds in Freshwater Ice', in *Proceeding of Arctic Technology Conference 2016*. St. John's, Newfoundland and Labrador, pp. 1–9.

Boroojerdi, M. T., Bailey, E. and Taylor, R. (2019a) 'Experimental Investigation of Rate

Dependency of Freeze Bond Strength', *Cold Reg. Sci. Technol.*, Under Revi.

Boroojerdi, M. T., Bailey, E. and Taylor, R. (2019b) 'Experimental study of the effect of submersion time on the strength development of freeze bonds', *Cold Reg. Sci. Technol.*, Under Revi.

Bruneau, S. E. (1996) *Development of a first year ridge keel model*, *Doctor of Philosophy*. Memorial University of Newfoundland.

Bueide, I. M. and Høyland, K. V. (2015) 'Confined compression tests on saline and fresh freeze-bonds', in *Proceedings of the International Conference on Port and Ocean Engineering under Arctic Conditions, POAC*. Trondheim, Norway.

Croasdale & Associates Ltd., 1997. In-situ Ridge Strength Measurements. A study sponsored by NRC (PERD) and Exxon Production Research Co.

Croasdale & Associates Ltd., 1998. In-situ Ridge Strength Measurements. A study sponsored by NRC (PERD) and Exxon Production Research Co.

Ettema, R. and Schaefer, J. A. (1986) 'Experiments on freeze-bonding between ice blocks in floating ice rubble', *Journal of Glaciology*, 32(112), pp. 397–403.

Ettema, R. and Urroz, G. E. (1989) 'On internal friction and cohesion in unconsolidated ice rubble', *Cold Regions Science and Technology*, 16(3), pp. 237–247.

Frederking, R. M. W. and Timco, G. W. (1984) 'Measurement of shear strength of granular/discontinuous-columnar sea ice', *Cold Regions Science and Technology*, 9(3), pp. 215–220.

Ervik, Å. *et al.* (2019) 'Ice-ridge interactions with the Norströmsgrund lighthouse: Global forces

and interaction modes', *Cold Regions Science and Technology*. Elsevier, 158(February 2018), pp. 195–220.

Goldstein, R. *et al.* (2013) 'Grounded ice pile-up. 2D dem simulation', in *Proceedings of the 22nd International Conference on Port and Ocean Engineering under Arctic Conditions*.

Guzenko, R.B., et al. (2021). "Relationship between the consolidated layer thickness and other morphometric characteristics of first-year ice ridges," Proc 26th Int Conf on Port and Ocean Eng under Arctic Conditions (POAC), Moscow, Russia, 2021, POAC21-023.

Høyland, K. V and Møllegaard, A. (2014) 'Mechanical behaviour of laboratory made freeze-bonds as a function of submersion time, initial ice temperature and sample size', in *22nd IAHR International Symposium on Ice*. Singapore, pp. 265–273.

Jordaan, I. J. (2001) 'Mechanics of ice ± structure interaction', *Engineering Fracture Mechanics*, 68, pp. 1923–1960.

Kloss, C., Goniva, C., Hager, A., Amberger, S., and Pirker, S., (2012) "Models , algorithms and validation for opensource DEM and CFD-DEM Models , algorithms and validation for opensource DEM and CFD-DEM," *Prog. Comput. Fluid Dyn.*, vol. 12, no. 2/3, pp. 140–152, doi: 10.1504/PCFD.2012.047457.

Karulina, M. *et al.* (2019) 'Full-scale flexural strength of sea ice and freshwater ice in Spitsbergen Fjords and North-West Barents Sea', *Applied Ocean Research*. Elsevier, 90(April), p. 101853.

Leguillon, D., Martin, E., Lafarie-Frenot, M. C. 'Flexural vs. tensile strength in brittle materials', *Comptes Rendus Mécanique*, Volume 343, Issue 4, 2015, Pages 275-281, ISSN 1631-0721, https://doi.org/10.1016/j.crme.2015.02.003.

Lemee, E. and Brown, T. (2002) ‘Small-scale plane strain punch tests’, *Ice in the Environment: Proc. of the 16th IAHR International Symposium on Ice*, 2, pp. 1–7.

Lemee, E. and Brown, T. (2005) ‘Review of ridge failure against the confederation bridge’, *Cold Regions Science and Technology*, 42(1), pp. 1–15.

Leppäranta, M. and Hakala, R. (1992) ‘The structure and strength of first-year ice ridges in the Baltic Sea’, *Cold Regions Science and Technology*, 20(3), pp. 295–311.

Liferov, P. and Bonnemaire, B. (2005) ‘Ice rubble behaviour and strength: Part I. Review of testing and interpretation of results’, *Cold Regions Science and Technology*, 41(2), pp. 135–151.

Lilja, V.P., Polojärvi, A., Tuhkuri, J., Paavilainen, J. (2021), 'Finite-discrete element modelling of sea ice sheet fracture', *International Journal of Solids and Structures*, Volumes 217–218, 2021, Pages 228-258, ISSN 0020-7683, https://doi.org/10.1016/j.ijsolstr.2020.11.028.

Lishman, B. and Polojärvi, A. (2015) ‘2D DEM of ice rubble: The effect of rate-dependent friction’, in *Proceedings of the 23rd International Conference on Port and Ocean Engineering under Arctic Conditions*.

Liu, L. *et al.* (2015) ‘Numerical Simulation of Ice Ridge Gouging’, in *ASME 34th Int. Conf. on Ocean, Offshore and Arct. Eng.At: St. John’s, Canada*.

Løset, S. (1994a) ‘Discrete element modelling of a broken ice field - Part I: model development’, *Cold Regions Science and Technology*, 22(4), pp. 339–347.

Løset, S. (1994b) ‘Discrete element modelling of a broken ice field - Part II: simulation of ice loads on a boom’, *Cold Regions Science and Technology*, 22(4), pp. 349–360.

Lu, W. *et al.* (2016) ‘Fracture of an ice floe : Local out-of-plane flexural failures versus global in-

plane splitting failure', *Cold Regions Science and Technology*. Elsevier B.V., 123, pp. 1–13.

Marchenko, A. and Chenot, C. (2009) 'Regelation of ice blocks in the water and on the air', in *Proceedings of the International Conference on Port and Ocean Engineering under Arctic Conditions, POAC*. Luleå, Sweden, pp. 543–554.

Møllegaard, A. (2012) 'Experimental study on freeze-bonds in laboratory made saline ice.'

Palmer, A. and Croasdale, K. (2013) *Arctic offshore engineering*. Singapore: World Scientific Publishing Co. Pte. Ltd.

Morgan, D. *et al.* (2015) 'Simulations of Ice Rubbling Against Conical Structures Using 3D DEM', in *Proceedings of the 23rd International Conference on Port and Ocean Engineering under Arctic Conditions*.

Murdza, A., Polojärvi, A., Schulson, E. M., and Renshaw, C. E. 'The flexural strength of bonded ice' *The Cryosphere*, 15, 2957–2967, https://doi.org/10.5194/tc-15-2957-2021, 2021.

Paavilainen, J., Tuhkuri, J. and Polojärvi, A. (2009) '2D combined finite-discrete element method to model multi-fracture of beam structures', *Engineering Computations*, 26(2004), pp. 578–598.

Paavilainen, J., Tuhkuri, J. (2013) 'Pressure distributions and force chains during simulated ice rubbling against sloped structures', *Cold Regions Science and Technology*, Volume 85, 2013, Pages 157-174, ISSN 0165-232X, https://doi.org/10.1016/j.coldregions.2012.09.005.

Polojärvi, A. and Tuhkuri, J. (2013a) '2D FEM-DEM simulations of punch through tests: Effects of partly consolidated rubble deformation', in *Proceedings of the 22nd International Conference on Port and Ocean Engineering under Arctic Conditions*.

Polojärvi, A. and Tuhkuri, J. (2013b) 'On modeling cohesive ridge keel punch through tests with

a combined finite-discrete element method', *Cold Regions Science and Technology journal*, 85, pp. 191–205.

Polojärvi, A., Tuhkuri, J. and Pustogvar, A. (2015) 'DEM simulations of direct shear box experiments of ice rubble: Force chains and peak loads', *Cold Regions Science and Technology*. Elsevier B.V., 116, pp. 12–23.

Potyondy, D. O. and Cundall, P. A. (2004) "A bonded-particle model for rock," *Int. J. Rock Mech. Min. Sci.*, vol. 41, no. 8 SPEC.ISS., pp. 1329–1364, doi: 10.1016/j.ijrmms.2004.09.011.

Prasanna, M., Polojärvi, A. (2023) 'Breakage in quasi-static discrete element simulations of ice rubble', *International Journal of Mechanical Sciences*, Volume 259, 2023, 108595, ISSN 0020-7403, https://doi.org/10.1016/j.ijmecsci.2023.108595.

Ranta, J., Polojärvi, A. and Tuhkuri, J. (2015) 'Ice load estimation through combined finite-discrete element simulations', in *Proceedings of the 23rd International Conference on Port and Ocean Engineering under Arctic Conditions*.

Repetto-Llamazares, A. H. V., Høyland, K. V. and Kim, E. (2011) 'Experimental studies on shear failure of freeze-bonds in saline ice:. Part II: Ice-ice friction after failure and failure energy', *Cold Regions Science and Technology*. Elsevier B.V., 65(3), pp. 298–307.

Repetto-Llamazares, A. H. V., Høyland, K. V and Evers, K. U. (2011) 'Experimental studies on shear failure of freeze-bonds in saline ice: Part I. Set-up, failure mode and freeze-bond strength', *Cold Regions Science and Technology*. Elsevier B.V., 65(3), pp. 286–297.

Salganik, E., Høyland, V., Maus, S. (2020), Consolidation of fresh ice ridges for different scales, *Cold Regions Science and Technology*, 171, https://doi.org/10.1016/j.coldregions.2019.102959.

Sayed, M. and Frederking, R. (1986) ‘On Modelling of Ice Ridge Formation’, in *lAHR Ice Symposium 1986*. lowa City, USA, pp. 603–614.

Serré, N., Repetto-Llamazares, A. H. V. and Høyland, K. V. (2011) ‘Experiements on the relation between freeze-bond and ice rubble strength, Part I: Shear box experiments’, in *Proceedings of the International Conference on Port and Ocean Engineering under Arctic Conditions, POAC*.

Shafrova, S. and Høyland, K. V (2008) ‘The freeze-bond strength in first-year ice ridges. Small-scale field and laboratory experiments’, *Cold Regions Science and Technology*, 54(1), pp. 54–71.

Shayanfar, H. (2017) *An Experimental Investigation on the Strength and Failure Behavior of Freshwater Ice Rubble*. Memorial University of Newfoundland.

Shayanfar, H. *et al.* (2018) ‘The effects of consolidation time on the strength and failure behavior of freshwater ice rubble’, *International Journal of Naval Architecture and Ocean Engineering*. Elsevier Ltd, 10(3), pp. 403–412.

Sudom, D., Timco, G., Sand, B., Fransson, L., 2011. Analysis of first-year and old ice ridge characteristics. Proceedings of the 11th International Conference on Port and Ocean Engineering under Arctic Conditions, Montreal, Canada.

Sudom, D. Timco, G. (2013) ‘Knowledge gaps in sea ice ridge properties’, *Proceedings of the International Conference on Port and Ocean Engineering Under Arctic Conditions*, June 9-13, 2013, Espoo, Finland

Szabo, D. and Schneebeli, M. (2007) ‘Subsecond sintering of ice’, *Applied Physics Letters*, 90(15), pp. 1–4. doi: 10.1063/1.2721391.

Timco, G. W. and Frederking, R. M. W. (1982) ‘Comparative strengths of fresh water ice’, *Cold*

Regions Science and Technology, 6(1), pp. 21–27.

Timco, G. W. and O.'Brien, S. (1994) 'Flexural strength equation for sea ice', *Cold Regions Science and Technology*, 22(3), pp. 285–298.

Timco, G. W. and Cornett, A. M. (1999) "Is φ a constant for broken ice rubble?," in *Proc. of the 10th Workshop on River Ice Management with a Changing Climate.*, pp. 318–331.

Timco, G., Croasdale, K. R. and Wright, B. (2000) *An overview of first-year sea ice ridges*. National Research Council of Canada, Technical Report HYD-TR-047.

Vaudrey, K. D. (1977) 'Ice Engineering: Study of Related Properties of Floating Sea-Ice Sheets and Summary of Elastic and Viscoelastic Analyses', *Naval Facilities engineering Command*, pp. 1–85.

Weeks, W. and Assur, A. (1967) *MECHANICAL PROPERTIES OF SEA ICE, COLD REGIONS SCIENCE AND ENGINEERING*. Hanover, NH.

Yulmetov, R., Bailey, E. and Ralph, F. (2017) 'A Discrete Element Model of Ice Ridge Interaction with a Conical Structure', in *Proceedings of the 24th International Conference on Port and Ocean Engineering under Arctic Conditions*. Busan, Korea.

Zvyagin, P. and Ziemer, G. (2017) 'Study Of Local Ice Loads Measured At Norströmsgrund Lighthouse', in *Proceedings Of The Asme 36th International Conference On Ocean, Offshore And Arctic Engineering, 2017, VOL 8*. Three Park Avenue, New York, Ny 10016-5990 Usa: Amer Soc Mechanical Engineers.

7. CONCLUSION

7.1. Summary and Conclusions

Understanding the mechanical behavior and strength of the ice ridges, as the most prevalent type of deformed ice feature, under flexure is a crucial component for design and operation in the ice prone areas. In the absence on full-scale field data and laboratory experiments on the flexural failure of ice ridges, this research program aimed to provide an insight to the flexural behavior of ice ridges using Discrete Element Modeling technique. Given limited available data on the tensile strength of freeze-bonds as an important parameter for the numerical simulations, this property of the ice was experimentally investigated.

7.1.1. Ice Freeze-Bonds

The tensile strength of freeze-bonds is an essential mechanical property of ice rubble that has a significant impact on the strength and failure behavior of ice ridges and ice rubble. **This research has addressed critical data gap in knowledge available concerning the pure tensile strength of ice freeze-bonds**, particularly in relation to the specific confinement conditions relevant to naturally deformed ice features. To address this gap, **a novel apparatus and testing method to assess the tensile strength of freeze-bonds under submerged and confined conditions was developed**. A series of 30 experiments were conducted to examine the influence of normal confinement pressure and submersion time on the tensile strength of freeze-bonds in freshwater. The range of confinement pressure tested was between 25 kPa and 100 kPa, and freeze-bonds were formed within submersion times ranging from 5 minutes to 3 hours.

The experimental findings indicate that all tests conducted at strain rates of $3.6 \times 10^{-2}\ s^{-1}$ and $6 \times 10^{-2}\ s^{-1}$ resulted in a brittle failure mode. No observable degradation of the specimen gauge

section was noted before failure, with the specimens failing immediately after reaching their maximum force threshold. It was observed that the tensile strength of freeze-bonds increased proportionally with increasing the confinement pressure during freeze-bond formation. However, an increase in submersion time from 30 minutes to 3 hours led to a decrease of approximately 21% in the tensile strength of freeze-bonds. This weakening over time is attributed to the rising temperature of the freeze-bond around the center of the blocks, as well as potential effects on the microstructure of the freeze-bond.

In the initial stages of freeze-bond development, the mechanisms that contribute to tensile strength are expected to be similar to those observed in the development of shear strength in freeze-bonds. Upon submerging a confined specimen, thermal bonding is initially expected to be the predominant mechanism of freeze-bond development, potentially supplemented by localized crushing, pressure-melting, and refreezing of asperities due to the combined effects of confining pressure. The results from the present experiments, along with previous studies by Boroojerdi et al. (2020b), support this understanding.

7.1.2. Level Ice

The flexural failure of sea ice holds significant relevance across various applications, ranging from understanding the formation processes of rubble to modeling the bending failure of ice sheets against sloped structures and ship hulls. In-situ experiments conducted on side-loaded sea ice beam specimens in the ice fields near Storfjorden, Svalbard have provided valuable data for parameterizing a discrete element model that simulates ice fracture under flexural loading. **Utilizing a new material model within the open-source DEM code WooDEM, these experiments were simulated in three resolutions. The material model incorporates cohesive**

bonds in tension, shear, flexure, and torsion, based on a contact model featuring normal, shear, torsional, and flexural springs.

Based on the results of high-resolution simulations, it can be concluded that these simulations exhibit overall agreement with the results of field tests, especially considering the relatively small number of DEM particles used (13,000) compared to the number of grains in an ice beam (approximately five hundred thousand).

The experimental curve showed an initial phase of "settling in," attributed to local ice crushing at the platen-ice interface. Simulating ice crushing behavior is currently beyond the capabilities of existing DEM models and falls outside the scope of this study. **Despite the complexities introduced by these local phenomena, the simulations successfully captured the main features of beam failure reasonably well.**

The experimental curve exhibits linear elasticity until the onset of failure, after which it smoothly decreases with increased displacement. In contrast, the simulated curve remains linearly elastic until it reaches a critical load level, initiating bond breakage. Subsequently, the force continues to rise at a lower average slope until reaching peak load. Beyond the peak load, the material experiences "damage" due to continued bond breakage, resulting in apparent softening of the beam with increased displacement. The lack of smoothness in the simulated force-displacement curves, compared to the field test results, may be attributed to the coarseness of the discretization.

The damping coefficient significantly influences the post-peak behavior, as it affects the transmission of energy from individual bond breakage throughout the material, influencing subsequent bond breakage.

7.1.3. Ice Rubble

Using the DEM model described earlier, medium-scale freshwater ice rubble punch tests have been simulated. Rubble specimens were generated by "raining" individual DEM ice pieces into a rectangular form and compacting the rubble mass to achieve the target porosity. Before the compacting pressure was removed, bonds between contacting blocks were introduced with parameter values based on representative freeze-bond experiments. The rubble beam was then deformed by pushing a platen vertically downward through the center of the beam until failure occurred.

Two types of block shapes have been simulated: cuboid blocks generated based on the size distribution of the actual rubble, and **rubble blocks generated by image processing of actual blocks of broken ice via a custom code,** used in the comparison experiments. The mechanism of flexural rubble failure for both cuboid block simulations and empirical block simulations is in line with experimental results**. The findings indicate that the cuboid rubble simulations tend to overestimate the maximum load before flexural failure of the rubble beam, while simulations with empirically-based block shapes show better agreement with the experiments.** The overall agreement between simulation and experimental results suggests that the simplifications and assumptions employed in this approach provide a reasonable approximation of the physical rubble matrix observed in laboratory tests.

Two failure mechanisms of freeze-bonds are observed during the flexure of the rubble beam. In the initial loading stages, failure occurs through the development of a crack starting from the central bottom region of the beam and propagating to the top, primarily causing tension failure in the freeze-bonds. Subsequently, shear failures are observed along the entire length of the beam.

These simulation results align well with the observed failure behavior reported in experimental studies of ice rubble beam failure.

The results of this research program highlight the capabilities of DEM in simulating the macroscopic behavior of ice rubble masses based on block-block interaction mechanics and calibrated freeze-bond properties. DEM models offer advantages in accurately representing macroscale properties and strength by simulating freeze-bonds and post-failure friction between blocks, while maintaining reasonable computational costs for simulating larger domains relevant to ice features like ridges and rubble fields. Additionally, this approach allows for the consideration of breakable bonds for solid ice masses, which is crucial for simulating interactions involving ridges with consolidated layers and level ice, a topic that was explored in the next work.

7.1.4. Ice Ridges

There is limited data available on the flexural strength of ridges, and design loads are typically determined based on the thickness of the consolidated layer alone. This research introduces a mathematical model using the discrete element method (DEM) to investigate the flexural failure of ice ridges.

The ice rubble blocks, consisting of spherical DEM particles, were generated using the custom code LIGGGHTS and placed in the DEM domain under the influence of gravity and buoyancy forces. A consolidated layer was then bonded to the top of the blocks to create a simplified model of an ice ridge as a two-layer ice beam.

This research shows that when the keel to consolidated layer thickness ratio is less than around 7, the strength of the freeze-bond between the rubble blocks does not significantly affect the flexural

failure of ice ridges. The primary contributor to flexural strength is the thickness of the consolidated layer. When the keel depth exceeds the consolidated layer thickness by a significant margin, around 7 times or higher, increasing the freeze-bond strength can have a substantial impact on the flexural strength of the ridge beam and, in some cases, exceed the strength of the consolidated layer.

Changing the thickness of the rubble keel and consolidation also influence its mechanical behavior. In cases where the ice keels are weaker and thinner, the failure mechanism is mainly associated with sudden flexural failure of the consolidated layer. **Simulations indicate that as the keel depth increases, the strength of the keel becomes a more significant factor in failure**. In extreme cases, the onset of ice ridge failure can be predominantly influenced by the V-shaped failure of the thick bonded rubble keel.

This research provided a valuable insight to the strength and failure mechanism of the freshwater freeze-bond and demonstrated that the developed DEM model is an effective tool for understanding the behavior of ice ridges under flexure. This is also important in providing insights into seasonal variations in ice ridge behavior with different ice thickness, block proportion, and consolidated layer thickness.

7.2. Recommendations for Future Work

It was observed that the tensile strength of freeze-bond reduces with increasing the submersion time from 5 minutes to 3 hours. To further understand the time-dependent behavior, it is advisable to conduct additional experiments with a wider range of submersion times when assessing tensile strength.

It was found that both the tensile and shear strength of freeze-bonds increase significantly with an increase in confinement pressure, but the rate of increase is higher for tensile strength. It is recommended that thin sections of freeze-bonds be taken in future to study the microstructure of the bonds before and after failure to gain a better insight into the underpinning mechanisms associated with this behavior.

Comparing the data from Boroojerdi (2020), the ratio of shear strength to tensile strength for freeze-bonds in unseeded freshwater polycrystalline ice was determined to range between 0.4 and 0.9 under the considered conditions. Further experiments covering a broader range of submersion times and confinement pressure are recommended for future investigations. While tensile strength of ice does not exhibit strain rate dependency, it is recommended to conduct further research on the impact of strain rate on the tensile strength of freeze-bonds to verify this is also the case for freeze-bonds.

This research program investigated the tensile strength of freshwater freeze-bonds at freezing temperatures as a starting point. This type of ice was selected be in-line with the other tasks of the MIR and DIRKS project. This gave the authors the opportunity to validate, calibrate, and compare the results to the experiments conducted under the same conditions. It is recommended to examine the tensile strength of saline ice under various salinities and temperatures in future work.

While sensitivity of the DEM model of the level ice to the particle size in flexure was studied, further research is recommended to evaluate the sensitivity of simulation results to particle size. For example, it would be beneficial to consider a distribution of particle sizes instead of uniform particles, as that would reduce the void volume since smaller particles would fill gaps between larger ones. Exploring these aspects is advisable in future investigations.

It is acknowledged that, in addition to brittle fracture, other energy dissipation mechanisms such as crushing, spalling, damage, and creep phenomena may occur during ice-structure and ice-seabed interactions, depending on temperature, loading rate, and stress state of the ice. Incorporating appropriate models for these dissipative processes is recognized as an important long-term objective for extending this research.

A significant achievement of this research is the establishment of connections between experiments that characterize the physical mechanisms of freeze-bond strength and DEM simulations, which can utilize these test results for larger-scale simulations. Continued work to further expand and validate this approach, including investigating how the macroscopic behavior of simulated ice rubble masses changes with variations in freeze-bond strength due to applied confinement, submersion time, and loading rate is recommended. By establishing stronger correlations between the physics of freeze-bond formation and the overall behavior of macroscale ice rubble, this work ultimately enhanced confidence in simulation tools employed for engineering design.

While the DEM models were calibrated and verified against medium scale level ice and ice rubble experiments, the ice ridge simulations were not directly compared to experimental results. The overall good agreement between model results and level ice and rubble failure experiments as well as field measurements provides strong supporting confidence the DEM model provides a reasonable simulation of the full-scale process. However, if it should be possible to perform medium scale ice ridge field experiments on freshwater ice this would enable comparison of the results directly with the numerical simulations, and further enhance confidence in the model.

The simulations conducted in this study were ran on CPUs as the numerical solvers used in this study, WooDEM and LIGGGHTS, are CPU based solvers. With the advance of accelerated GPU

based simulation software, it may be possible to integrate the DEM model introduced here to a GPU based DEM simulation software in the future to accelerate the simulations. This could help the researchers to conduct a larger number of simulations to better understand and calibrate their simulations, and increase the resolution of the model to improve accuracy and smoothness.

In summary, this study was conducted using the 3D DEM ice model has yielded promising outcomes, demonstrating its value as a research tool for exploring and enhancing our understanding of ice sheet break-up caused by flexural failure. This research is particularly relevant to scenarios involving ice rubbling or interactions with ship-shaped or sloped structures. With ongoing development, this approach holds great potential for providing new insights into emerging failure phenomena and the associated loads resulting from the complex interplay between ice mechanical properties and the evolving geometry of ice edges and blocks. These advancements are crucial for reducing modeling uncertainties and establishing a solid foundation for developing advanced ice load models required to support offshore development in regions prone to ice.